TARGETING ROBO4-DEPENDENT SLIT SIGNALING

TO SURVIVE THE CYTOKINE STORM

IN SEPSIS AND INFLUENZA

by

Nyall R. London Jr.

A dissertation submitted to the faculty of
The University of Utah
in partial fulfillment of the requirements for the degree of

Doctor of Philosophy

Department of Oncological Sciences

The University of Utah

August 2011

The University of Utah Graduate School

STATEMENT OF DISSERTATION APPROVAL

The dissertation of **Nyall R. London Jr.**

has been approved by the following supervisory committee members:

Dean Y. Li	, Chair	**June 14, 2011** Date Approved
Guy A. Zimmerman	, Member	**June 14,2011** Date Approved
E. Dale Abel	, Member	**June 14, 2011** Date Approved
Alana L. Welm	, Member	**June 14, 2011** Date Approved
Matthew K. Topham	, Member	**June 14,2011** Date Approved

and by **Donald E. Ayer** , Chair of

the Department of **Oncological Sciences**

and by Charles A. Wight, Dean of The Graduate School.

ABSTRACT

The mature capillary network, comprised of a quiescent endothelial cell monolayer, utilizes tight cell-cell interactions to maintain vascular stability and limit vascular leak. An essential component of these intercellular contacts is the adherens junction protein vascular endothelial cadherin (VE-cadherin). In multiple disease settings such as macular degeneration, sepsis, and pandemic influenza, the endothelium is activated and destabilized by cytokines such as vascular endothelial growth factor (VEGF), interleukin-1β (IL-1β), and tumor necrosis factor-α (TNF-α). While an innate immune response is necessary to combat infection, an exuberant cytokine release can paradoxically injure the host endothelium, resulting in vascular damage, tissue edema, and death.

In this dissertation we demonstrate that an endogenous, endothelial-specific Roundabout (Robo), Robo4, maintains vascular stability and quiescence. Administration of Slit, an endogenous activator of Robo receptors, strengthens endothelial barrier function and limits vascular leak in a Robo4-dependent manner. Furthermore, Slit treatment enhanced survival during sepsis and avian flu infection, diseases both characterized by hypercytokinemia. We also discovered that Slit strengthens the vascular barrier by increasing VE-cadherin localization at the cell surface. Slit also increases p120-catenin localization at the cell surface and enhances the interaction of p120-catenin with VE-cadherin, preventing the internalization of VE-cadherin. Furthermore, Robo4 activation leads to the recruitment of a paxillin-GIT1 signaling module that inactivates

Arf6. Arf6 plays a known role in regulating endocytic recycling, thus perhaps defining Robo4-dependent Slit signaling as a paxillin-GIT1-Arf6-p120-catenin-VE-cadherin stabilization pathway.

Our studies fundamentally demonstrate that by specifically blunting the vascular response to hypercytokinemia, mortality can be reduced during severe experimental infections. Activation of a vascular stabilizing pathway such as Robo4 may therefore provide a platform for treating multiple infectious threats characterized by an exuberant cytokine response.

TABLE OF CONTENTS

ACKNOWLEDGMENTS

I am grateful for the many people who contributed to the success of the project described in this dissertation. These include: Dean Li, Weiquan Zhu, Fernando Bozza, Haoyu Chen, Chris Jones, Lise Sorensen, Dale Barnard, Matthew Smith, Diana Lim, and Naoyuki Nishiya.

CHAPTER 1

ENDOGENOUS ENDOTHELIAL CELL SIGNALING SYSTEMS MAINTAIN VASCULAR STABILITY

The following chapter is a reprint of a manuscript that Kevin Whitehead, Dean Li, and I co-authored for Angiogenesis. It was published in 2009, volume 12 (2), pages 149-158, Epub January 27, 2009.

Angiogenesis
DOI 10.1007/s10456-009-9130-z

ORIGINAL PAPER

Endogenous endothelial cell signaling systems maintain vascular stability

Nyall R. London · Kevin J. Whitehead · Dean Y. Li

Received: 19 December 2008 / Accepted: 6 January 2009

Abstract The function of the endothelium is to provide a network to allow delivery of oxygen and nutrients to tissues throughout the body. This network comprises adjacent endothelial cells that utilize adherens junction proteins such as vascular endothelial cadherin (VE-cadherin) to maintain the appropriate level of vascular permeability. The disruption of VE-cadherin interactions during pathologic settings can lead to excessive vascular leak with adverse effects. Endogenous cell signaling systems have been defined, which help to maintain the proper level of vascular stability. Perhaps the best described system is Angiopoietin-1 (Ang-1). Ang-1 acting through its receptor Tie2 generates a well-described set of signaling events ultimately leading to enhanced vascular stability. In this review, we will focus on what is known about additional endogenous cell signaling systems that stabilize the vasculature, and using Ang-1/Tie2 as a model, we will address where our understanding of these additional systems is lacking.

Keywords CCM · Permeability · Robo4 · Vascular stability · VE-cadherin

N. R. London · K. J. Whitehead · D. Y. Li (✉)
Department of Medicine, University of Utah, 15 N 2030 E, Salt Lake City, UT 84112-5330, USA
e-mail: dean.li@hmbg.utah.edu

D. Y. Li
Oncological Sciences, University of Utah, Salt Lake City, UT 84112, USA

N. R. London · K. J. Whitehead · D. Y. Li
Program in Molecular Medicine, University of Utah, Salt Lake City, UT 84112, USA

Introduction

The vascular system provides an essential network allowing blood to flow throughout the body. At the interface between the blood and various organs is the endothelial cell that lines all blood vessels. This endothelial cell barrier forms a semi-permeable membrane that regulates the passage of fluid, nutrients, and leukocytes out of the blood and into the interstitial space [1, 2]. In order to regulate barrier function, adjacent endothelial cells utilize adherens and tight junctions to maintain strong cell–cell contacts [3]. Further maturation and stabilization of the capillary occurs through tight endothelial associations with pericytes [4]. Under normal conditions, the endothelium of a mature capillary is quiescent, stable, and limits vascular leak. Many pathologic conditions cause a de-stabilization of the vascular network resulting in endothelial hyper-permeability, excessive vascular sprouting, and angiogenesis. These pathologic settings include tumor angiogenesis, proliferative diabetic retinopathy, age-related macular degeneration (AMD), and cerebral cavernous malformations (CCM) [5–7].

Destabilization of vascular barrier function occurs when interactions between inter-endothelial junction proteins are disrupted. In the endothelium, these critical vascular stabilizing interactions are provided by the adherens junction protein vascular endothelial cadherin (VE-cadherin; Fig. 1a) [2, 8]. This is supported by evidence that multiple antibodies directed to the extracellular domain of VE-cadherin can disrupt endothelial barrier function in vitro [9]. Furthermore, a VE-cadherin blocking antibody can cause a concentration and time-dependent increase in permeability in the lung and heart in vivo [10]. In the cell, breakdown of VE-cadherin interactions can be mediated by phosphorylation (Fig. 1b). Interestingly, phosphomimetic mutations at Y658 and Y731

Published online: 27 January 2009

were sufficient to cause decreased barrier function in CHO cells [11]. Furthermore, multiple permeability-inducing factors cause phosphorylation of VE-cadherin including histamine [12], lipopolysaccharides [13], and vascular endothelial growth factor (VEGF) [14]. Kinases are necessary to propagate these signals and phosphorylate the cytoplasmic tail of VE-cadherin. VEGF, for example, activates Src, a non-receptor kinase necessary for the permeability-inducing effects of VEGF. The necessity of Src has been demonstrated as VEGF-induced permeability in the dermis and brain was inhibited in $Src^{-/-}$ mice [15]. Phosphorylation of the cytoplasmic tail of VE-cadherin is also regulated by phosphatases such as vascular endothelial protein tyrosine phosphatase (VE-PTP). In fact, overexpression of VE-PTP-inhibited VEGF receptor 2 (VEGFR2)-mediated phosphorylation of VE-cadherin resulting in enhanced barrier integrity [16].

Phosphorylation of VE-cadherin not only disrupts homophilic interactions, but can also result in endocytosis of VE-cadherin and removal from the cell surface. For example, VEGF causes Src-dependent activation of the Rac pathway, ultimately resulting in phosphorylation of a serine residue on the cytoplasmic tail of VE-cadherin [17]. This phosphorylation recruits β-arrestin which then mediates VE-cadherin endocytosis in a clathrin-dependent manner. Cadherin endocytosis and turnover are also regulated through cytoplasmic-binding partners such as p120-catenin (Fig. 1c) [18]. This has been demonstrated as a direct p120-catenin interaction inhibits VE-cadherin endocytosis [19]. Furthermore, this interaction has been demonstrated to be necessary for maintaining endothelial barrier function [20].

In addition to breaking down vascular barrier function, pro-angiogenic cues such as VEGF de-stabilize the vascular network by causing sprouting of new blood vessels. This occurs by enhanced endothelial cell proliferation, breakdown of the endothelial barrier, and directional migration towards a signal gradient [21]. At the forefront of the vascular sprout is the endothelial tip cell. Tip cells utilize multiple filopodial extensions to sample the environment and follow chemotactic gradients, thus determining the direction the sprout will grow [22]. In contrast to tip cells, the endothelial cells that trail behind the tip cells, known as stalk cells, form the lumenized vascular network. These cells perform similar functions as the quiescent mature capillary. In this review, we will address newly identified endogenous endothelial cell signaling systems that enhance vascular stabilization.

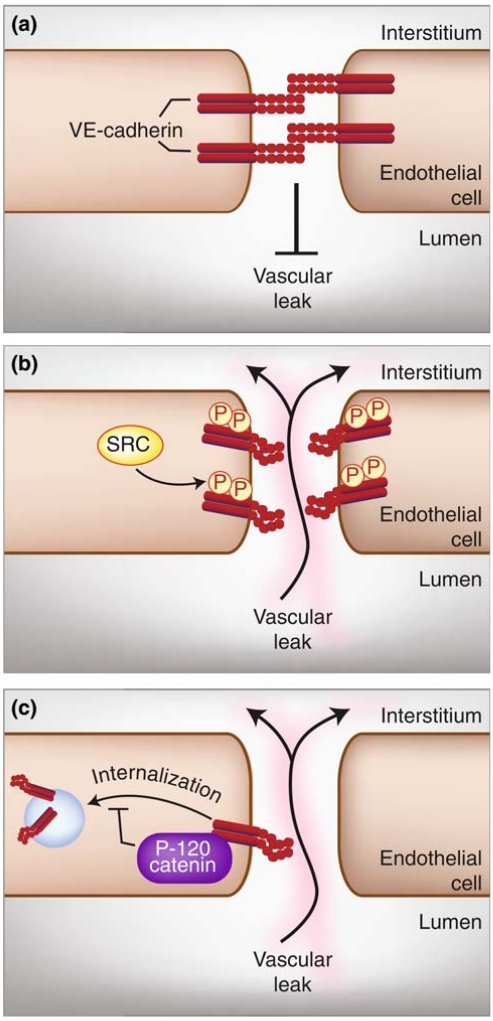

Fig. 1 VE-cadherin interactions are disrupted by phosphorylation and endocytosis. **a** Under normal conditions, VE-cadherin forms tight interactions that inhibit excessive vascular leak. **b** Kinases such as Src can phosphorylate the cytoplasmic tail of VE-cadherin, resulting in the disruption of VE-cadherin interactions and increased vascular permeability. **c** VE-cadherin interactions are also disrupted through endocytosis, resulting in increased vascular leak. The binding of p-120 catenin to the cytoplasmic tail of VE-cadherin inhibits internalization resulting in enhanced vascular stability

Ang-1–Tie2

Angiopoietin-1 (Ang-1) like VEGF is a potent pro-angiogenic factor, but conversely stabilizes the vasculature against vascular leak. The receptor for Ang-1 is the endothelial-specific receptor Tie2. When over-expressed in the dermis, Ang-1 induces enhanced neovascularization. When combined with VEGF over-expression, Ang-1 had an additive effect on neovascularization but stabilized these

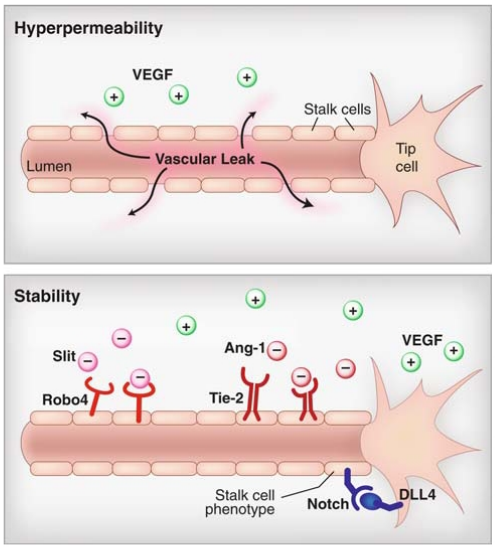

Fig. 2 Endogenous cell signaling systems decrease vascular hyperpermeability. VEGF disrupts the barrier function of the endothelium resulting in enhanced vascular leak (*top*). Cell signaling systems such as Slit–Robo4, Ang-1–Tie2, and Dll4–Notch stabilize the vasculature (*bottom*)

vessels as evidenced by decreased Evans Blue extravasation in the mouse ear (Fig. 2) [23]. Furthermore, Ang-1 can inhibit permeability induced by additional factors such as mustard oil [24].

How Ang-1 specifically inhibits the permeability-inducing effects of VEGF has recently been described. While Ang-1 administration did not affect VEGF-induced signaling events necessary for endothelial proliferation, Ang-1 inhibited VEGF-induced activation of Src [25]. Interestingly, Ang-1 activates Rho and both Rho siRNA knockdown and a Rho inhibitor blocked the ability of Ang-1 to inhibit VEGF-induced permeability in vitro. A Rho inhibitor also blocked Ang-1 in vivo as assessed by Evans Blue extravasation in the mouse dermis. This demonstrates that Ang-1 inhibits VEGF-induced permeability through a Rho-dependent mechanism. Furthermore, Ang-1 stimulates the dimerization of mDia1 and mDia2, downstream targets of Rho signaling. Ang-1 also stimulates the binding of mDia to Src, suggesting that Ang-1 inhibits VEGF-induced permeability through mDia-mediated sequestration of Src. Knockdown of either mDia1 or mDia2 using siRNA inhibited the activity of Ang-1; further demonstrating that mDia1 and mDia2 are indeed necessary for Ang-1-mediated signaling [25]. These data demonstrate that Ang-1 specifically stabilizes the endothelium against VEGF-induced permeability by inhibiting Src through a Rho/mDia-dependent pathway (Fig. 3a, b). Furthermore, defining these signaling events has linked the ligand and receptor to a central mechanism regulating VE-cadherin stability.

Vascular instability can also be manifest in the form of vascular malformations. Activating mutations in the kinase domain of Tie2 result in a rare hereditary form of mucocutaneous venous malformation [26], and somatic mutations of Tie2 have recently been described in a high percentage of sporadic venous malformations [27]. Recently, additional ligand receptor signaling pathways have been hypothesized to promote junctional stability of the endothelium, though a detailed understanding of their mechanistic pathway does not match that of Ang-Tie2.

Dll4–Notch

The necessity of Delta-like 4 (Dll4)–Notch1 signaling in the endothelium has been well established as loss of a single copy of Dll4 or deletion of Notch1 causes vascular defects and embryonic lethality [28, 29]. When Dll4 activates Notch1, a portion of the intracellular domain of Notch1 is cleaved through a γ-secretase-dependent mechanism. The resulting fragment known as the Notch1 intracellular domain (ICD) translocates to the nucleus where gene expression changes are enacted [30]. Notch signaling plays a well-defined role in cell fate decisions through a process known as lateral inhibition. A classic example in Drosophila is neural–epidermal determination where cells that have adopted a neural cell fate signal to adjacent cells to adopt an epidermal cell fate. When Notch signaling is removed, all cells adopt a pro-neural cell fate [31].

In the endothelium, VEGF induces endothelial cells to adopt a tip cell phenotype. However, the cell signaling systems that keep all endothelial cells from becoming tip cells have just recently been described. These studies have demonstrated that Dll4 from the endothelial tip cell signals through Notch on adjacent stalk cells to become stalk cells rather than tip cells. During vascular patterning, this allows for the correct number of endothelial tip cells and vascular sprouts. Using a γ-secretase inhibitor to inhibit Notch signaling, Hellstrom et al. [32] found increased filopodial protrusions in endothelial tip cells of the mouse retina. When given over an extended period of time, Notch inhibition resulted in increased vascular sprouting, density, and disrupted normal vascular patterning. In a separate experiment, inhibition of Notch1 signaling by endothelial-specific genetic deletion or using $Dll4^{+/-}$ mice also caused enhanced tip cell filopodial extensions and vascular sprouting. Furthermore, activation of Notch signaling reduced tip cell filopodia and vascular density [32].

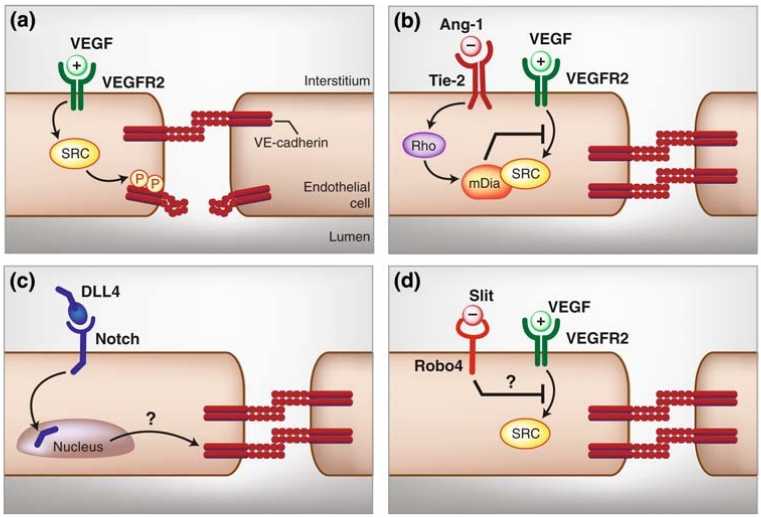

Fig. 3 Endogenous cell signaling systems enhance vascular stability. **a** VEGF disrupts VE-cadherin interactions through activation of Src resulting in the phosphorylation of the cytoplasmic tail of VE-cadherin. **b** Ang-1 through its receptor Tie2 activates Rho. This causes the activation of mDia, which sequesters Src resulting in the inhibition of Src and stabilization of VE-cadherin. **c** Dll4 binds Notch resulting in the cleavage of the NICD and its transfer to the nucleus. The resulting signaling events that affect endothelial cell junctional stability are unknown. **d** Slit through a Robo4-dependent mechanism inhibits VEGF-induced activation of Src. The signaling events from Robo4 to Src are unknown

The role of Dll4–Notch signaling applies not only to developmental angiogenesis, but also to pathologic neovascularization. Mice undergoing oxygen-induced retinopathy (OIR) and given a γ-secretase inhibitor displayed enhanced pathologic angiogenesis [32]. Additionally, in tumors over-expressing Dll4, a marked decrease in tumor angiogenesis was observed [33]. Interestingly, tumors over-expressing soluble Dll4, which acts as an inhibitor of Notch signaling, caused enhanced angiogenesis. Taken together, these studies demonstrate the importance of Dll4–Notch signaling in inducing a stalk cell fate decision and the effect this has on developmental and pathologic neovascularization (Fig. 2). In addition to its differentiation state, cell–cell contacts distinguish stalk cells from tip cells and play an important role in vascular stability. While the Dll4–Notch ligand receptor interaction appears to utilize the canonical Notch downstream signaling pathway, how the nuclear translocation of the Notch ICD distinguishes tip cell from stalk at the level of cell–cell interactions remains to be explored (Fig. 3c).

Slit–Robo4

After a decision has been made to be a stalk cell instead of a tip cell, there must be additional cues that help the stalk cells maintain a quiescent stabilized phenotype. Recent data have demonstrated that Slit–Robo4 signaling may be this signal. The Roundabout (Robo) family of single-pass transmembrane receptors comprises four members, Robo1–4, with members of the Slit family as ligands. Robo1–3 are expressed in the nervous system and have a well-established role in axon guidance [34]. Conversely, Robo4 expression is limited to the endothelium [35, 36]. Because the neural and vascular systems share similar patterning mechanisms, this suggests a role for Robo4 in vascular guidance. However, in studying this question in vivo, an unexpected role for Robo4 in vascular stability was uncovered.

Robo4$^{-/-}$ mice are viable, fertile, and show no vascular patterning defects in the cephalic or intersomitic vessels [37]. This demonstrates that Robo4 expression is not necessary for vascular guidance during mouse development. Interestingly, Robo4 expression in the mouse retina was found in the endothelial stalk cells but was often absent in the tip cells. As previously mentioned, endothelial tip cells are important for vascular guidance. The lack of Robo4 expression in the tip cell could perhaps explain why Robo4 does not play a role in vascular guidance in vivo. It would be interesting to see whether Dll4 from the tip cell was responsible for inducing stalk cell-specific expression of Robo4. While endothelial tip cells are important for

vascular guidance, stalk cells are similar to a mature, lumenized vascular tube that is important for regulating fluid leak and vascular stability. Vascular barrier function can be modeled in vitro by measuring flux of a reporter across an endothelial monolayer. By using mouse lung endothelial cells from *Robo4*$^{+/+}$ and *Robo4*$^{-/-}$ mice in this system, Jones et al. [37] found that Slit2 inhibited VEGF-induced permeability through a Robo4-dependent mechanism. Slit2 also inhibited VEGF-induced permeability in vivo in the mouse dermis and retina as measured by Evans Blue dye extravasation. The effect of Slit2 was lost in *Robo4*$^{-/-}$ mice, further demonstrating that Robo4 is necessary for the effect of Slit2 in vivo. As previously mentioned, VEGF acting through its receptor VEGFR2 activates Src that is necessary for VEGF-induced vascular destabilization. Although Slit2 did not inhibit VEGF-induced autophosphorylation of VEGFR2, Slit2 inhibited VEGF-induced Src activation. This demonstrates that Slit2 signaling acts downstream of VEGFR2 activation to inhibit Src signaling. Furthermore, Slit3 also inhibited VEGF-induced Src activation and retinal permeability in vivo, demonstrating that additional Slit family members also enhance vascular stability. Additionally, *Robo4*$^{-/-}$ mice demonstrated an increased level of permeability in the retina under basal conditions. Taken together, these data demonstrate a role for Slit–Robo4 signaling in inhibiting vascular permeability and enhancing vascular stability (Fig. 2).

A stabilized, quiescent phenotype not only applies to inhibiting excessive vascular hyperpermeability, but also is important in inhibiting new vascular sprouting and angiogenesis. This occurs during pathologic conditions such as proliferative diabetic retinopathy and AMD. These pathologic conditions can be modeled in the mouse by OIR and laser-induced choroidal neovascularization (CNV), respectively. Slit2 inhibited neovascularization in both these models, demonstrating that Slit2 can inhibit angiogenesis in a pathologic setting. Interestingly, the effect of Slit2 was lost in *Robo4*$^{-/-}$ mice, again demonstrating that Robo4 is necessary for the effect of Slit. Furthermore, *Robo4*$^{-/-}$ mice demonstrated enhanced angiogenesis in OIR, further exemplifying the importance of Robo4 in limiting excessive vascular destabilization in pathologic settings. Taken together, these data suggest that the role of Robo4 in vivo is to maintain vascular stability. Although vascular guidance may appear similar to neural guidance, it is important to remember that while an axon arises from a single cell, blood vessels are multi-cellular systems. This may explain why a neural repulsive cue such as Slit may translate into a vascular stability cue when applied to the multi-cellular blood vessel.

In contrast to studies demonstrating a repulsive effect of Slit [37–40], other studies suggest a pro-angiogenic role for Slit [41, 42]. These studies show that Slit increases endothelial cell migration and tube formation in vitro. One report suggests that the receptor responsible for this effect is Robo1 while the other proposes a heterodimer complex between Robo1 and Robo4 [41, 42]. Of special interest is data that Slit might stimulate migration of Robo1 expressing cells, in contradistinction to the original report that described many of the core reagents used in these subsequent studies and that demonstrated Slit-inhibited Robo1 expressing non-neural cells [42, 43]. Other studies have favored a Slit-independent role for Robo4 and suggested this role is proangiogenic [40, 44]. These studies propose that Robo4 plays no part in a receptor complex that mediates Slit signaling and either functions in a ligand-independent fashion similar to adhesion proteins or mediates the signaling of a yet unknown set of ligands. Clearly work is needed to reconcile these differences, with an emphasis on relating in vitro and cell culture findings to animal models lacking Robo receptors. Such an approach is important as consistent functional readouts that span cell biology and animal models are required to confirm the relevance of any potential downstream mechanism. Given that we are at such an early stage, we remain cautious of any strongly held convictions as the literature is replete with ligands having unexpected receptors [45], receptors having unexpected ligands [46], and transmembrane proteins participating as both adhesion proteins and ligand-mediated signaling complexes [47].

While the ligand-receptor system for Ang-1–Tie2 and Dll4–Notch has been well defined, little is known about how Slit might activate Robo4. Studies conducted in our laboratory using *Robo4*$^{-/-}$ mice, and lung endothelial cells derived from these mice, have demonstrated that Robo4 is necessary for the effect of Slit in vitro and in vivo. Our laboratory has also shown previously that Slit binds to the surface of Robo4 expressing but not control HEK cells [38]. A second recent report has corroborated this finding by demonstrating that Slit no longer binds to endothelial cells when endogenous Robo4 expression is knocked down by siRNA [40]. However, others have found using BiaCore that Slit1–3 do not interact with Robo4, suggesting that Slit does not directly bind to Robo4 [44]. One potential explanation is that Robo4 forms a complex with a co-receptor. Such a model has been suggested for other Robo receptors as heparan sulfate proteoglycans are necessary for repulsive guidance activities of Slit2 in vitro [48]. In this study, removal of cell surface heparan sulfate using heparinase III resulted in the loss of Slit2 repulsive activity for olfactory interneuron precursors and olfactory bulb axons.

Many questions about the mechanism of Robo4 signaling remain (Fig. 3d). To address these questions, the following experiments must be done. The cytoplasmic

domain necessary for Robo4 activity must be mapped and its binding partners determined. To confirm that this interaction is real, the domain of this binding partner necessary to bind Robo4 must also be mapped. Additionally, this interaction should be greatly enhanced upon stimulation with Slit and this interaction must also be shown to be necessary for Slit/Robo4 signaling. This could be achieved using siRNA to knockdown expression of the endogenous binding partner and reconstituting using a mutant that can no longer bind Robo4. In this setting, the functional in vitro effect of Slit should be lost. Furthermore, small molecules that target signaling effectors downstream of Robo4 might mimic the effect of Slit in vitro and in vivo. Such a broad-based approach utilizing biochemical, cell culture, and animal model studies would help to instill confidence that any mechanistic insights obtained have true biologic relevance and in the process might offer a new therapeutic approach for preventing pathologic angiogenesis or vascular leakage.

Cerebral cavernous malformations

Observations relating to the Ang-1/Tie2 pathway suggest that disruption of vascular stability pathways can lead to vascular malformation syndromes [26, 27]. Recent human genetic and developmental genetics studies of a different vascular malformation syndrome have led to a new signaling pathway promoting vascular stability. The *heart of glass* (*HEG*) cell surface receptor interacts with a complex of intracellular proteins identified on the basis of causal relationships with CCMs. Mutations in any one of three identified proteins result in cavernous angiomas. CCM is a common vascular malformation syndrome with a prevalence of 1 in 200 [49, 50]. Affected individuals develop vascular lesions of the central nervous system and systemic vasculature [51]. Lesions of the CNS are most commonly described and consist of dilated vascular caverns lined by endothelium and lacking supporting smooth muscle cells. Abnormal cell–cell junctions have been observed on ultrastructural studies [52]. The universal finding of hemosiderin (a blood break down product) in association with lesions, even in the absence of overt hemorrhage is further testament to the unstable, leaky endothelium of the cavernous angioma. Thus, one hypothesis for the basis of CCM is the presence of focally destabilized endothelium. These proteins act to promote stability of the endothelium.

A large proportion of CCM cases are familial, following an autosomal dominant inheritance pattern. Human genetics studies have identified mutations in three proteins from families with this disease. Mutations were first identified in *KREV1* (*RAP1A*) *interaction trapped-1* (*KRIT1* [53, 54], also known as *CCM1*). These studies were soon followed by identification of *CCM2* [55, 56] (also known as *Malcavernin* [56], or *Osmosensing scaffold for MEKK3* [57]) and *Programmed cell death 10* [58] (*PDCD10*, also known as *CCM3*) in families with cavernous angiomas. All three identified genes are intracellular proteins without identifiable enzymatic function and are thus predicted to be adaptor or scaffold proteins [59]. Studies with tagged overexpression constructs have found all three proteins to interact with each other and a large number of additional proteins [59, 60]. While there is a growing body of biochemical data regarding the complex of CCM proteins, prior to the human genetic studies linking these proteins to CCM there was little evidence to suggest a role in vascular stability.

Human genetic studies have provided the link between CCM disease and *KRIT1*, *CCM2*, and *PDCD10*, but developmental genetics and animal models have greatly expanded our understanding of the in vivo roles of these proteins and have highlighted additional proteins that function in a common genetic pathway to achieve vascular stability. An initial controversy regarding the in vivo function of these genes revolved around the cellular autonomy of protein function. The expression patterns of all three CCM proteins are similar [61], with ubiquitous expression in embryonic development and predominantly neural and epithelial expression in adult mice [62]. Although endothelial expression can be detected, the strong neural expression evoked the possibility of a neurally autonomous function for the CCM proteins. Such a mechanism is not without precedent as had been shown with *alpha-V integrin*-deficient mice [63]. Such mice die with vascular instability and brain hemorrhage with protein deficiency in neural rather than endothelial cells. Recent studies using mice with conditional mutations in *Ccm2* confirm an essential role for *Ccm2* in the endothelium for vascular development and vascular stability [64]. Profound angiogenesis defects result in failure of circulation and embryonic death in mice lacking *Ccm2* in the endothelium. This phenotype is shared with mice lacking *Krit1* [65]. In adult mice with heterozygous mutations of *Ccm2*, there is increased vascular permeability, whether such mutations are inherited through the germline, or induced by recombination only within the endothelium.

Forward genetic screening in zebrafish identified a phenotype characterized by an enlarged heart without circulation. Three separate mutants with this phenotype were termed *santa*, *valentine*, and *heart of glass* [66, 67]. As these genes were mapped, it was found that *santa* resulted from mutations in the zebrafish ortholog for *KRIT1* and *valentine* from *CCM2*. *Heart of glass* (*heg*) had not previously been associated with CCM. While no CCM patients have yet been found with mutations in *HEG*, mice lacking *Heg* die in late embryonic and perinatal stages [68].

Unlike zebrafish, this phenotype does not closely resemble *Krit1* or *Ccm2* mutants. However, heterozygosity for *Ccm2* on a *Heg* null background is sufficient to phenocopy *Ccm2* or *Krit1* null mouse embryos, confirming a genetic interaction between this cell surface protein and the CCM genes. Analogous experiments in zebrafish have used morpholino knockdown of gene expression to explore genetic interactions between *krit1* and putative interaction partners [67, 69]. Such studies also suggest that *rap1b* interacts genetically with the CCM proteins in vivo [69].

A number of studies in a variety of cell types have identified binding partners of the CCM proteins. Beginning with the initial identification of KRIT1 as a binding partner of KREV-1, this work began before the human genetics or developmental genetics studies, but has accelerated in pace recently as the human disease and in vivo functional links have been appreciated. Literally, hundreds of potential binding partners have been identified through a combination of yeast two-hybrid, co-immunoprecipitation, FRET, immunofluorescence, and proteomics approaches [57, 59, 60, 70–75]. The list includes such a dizzying array of different proteins, which is difficult to synthesize into an organized working model. While the role of each specific partner cannot easily be described, some general themes emerge. First, the three CCM proteins, KRIT1, CCM2 and PDCD10 interact with each other and appear to form a complex. Second, the complex is implicated in both GTPase and MAPK signaling. Third, interactions between the complex and cytoskeletal proteins have often been noted. When viewed in isolation, these protein interaction studies are limited by a lack of functional information from either in vitro or in vivo models.

While our understanding of the CCM proteins remains incomplete, four recent studies have provided much needed functional relevance to an emerging model of CCM signaling (Fig. 4). Concurrent with the genetic identification of mutations in *CCM2*, the same protein was identified by Uhlik et al. [57] in a screen of binding partners for MEKK3, an upstream kinase in the activation of p38 MAPK in response to osmotic stress. The authors named this protein Osmosensing scaffold for MEKK3 (or OSM). This work indicated a role for CCM2 (OSM) in mediating signaling from the GTPase Rac1 to MAP kinases with a stabilizing role in osmotically stressed cells. By demonstrating that CCM2 is able to mediate activation of MKK3 and p38 MAPK in a variety of non-endothelial cell types in response to osmotic stress, the authors provided initial evidence for the CCM protein complex in defending cell shape against environmental stress.

Further work by Glading et al. [74] has addressed CCM protein function in an endothelial context. Using a combination of siRNA and over-expression constructs of *KRIT1*, and by developing and validating a monoclonal

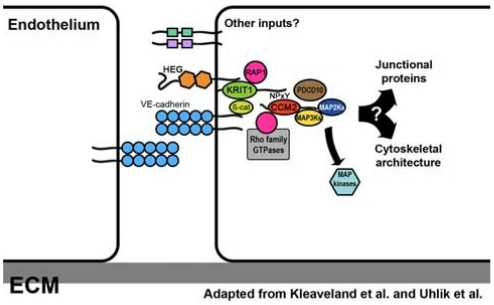

Fig. 4 The CCM genes define an intracellular protein complex promoting vascular stability. The three genes associated with cerebral cavernous malformations (KRIT1, CCM2, and PDCD10) interact with each other and a variety of other intracellular and cell surface proteins to enhance the stability of endothelial cell junctions and the cellular cytoskeleton. As described in the text, such interactions include the heart of glass (HEG) cell surface receptor, β-catenin (β-cat), small GTPases including RAP1 and Rho family GTPases and proteins of MAP kinase signaling cascades

antibody directed against KRIT1, the authors demonstrate that KRIT1 is an effector for the small GTPase RAP1. They show that KRIT1 binds to β-catenin under the control of RAP1 and that RAP1 stabilizes endothelial cell junctions in a KRIT1-dependent manner. The loss of KRIT1 leads to increased endothelial permeability. Endothelial cell junction stability is dependent upon KRIT1.

Recent work by Whitehead et al. [64] demonstrated the endothelial requirement for *Ccm2*. In the same work, the authors find that CCM2 binding to the small GTPase RHOA in endothelial cells leads to suppression of RHOA activity. Depletion of *CCM2* by siRNA leads to an increase in activated RHOA. These *CCM2* depleted cells have both increased actin stress fibers and greater monolayer permeability. These two papers show that when the CCM signaling complex is deficient, cell junctions are affected and the vasculature becomes more permeable.

Heterozygous mice are the genotype equivalent of CCM patients. While such mice are viable and fertile and do not spontaneously develop cavernous angiomas, defects in endothelial barrier function are demonstrated [64]. The permeability response to stressors such as VEGF is exaggerated. As with *CCM2*-deficient cells, these defects in permeability can be rescued by suppressing RhoA signaling. Thus, the vascular stability defects found in vitro are also observed in vivo and a potential therapeutic strategy begins to emerge for patients with CCM.

By interacting with small GTPases, MAP kinases, cell junctions, and the cytoskeleton, the CCM signaling complex is poised to mediate key aspects of vascular stability. For the CCM proteins to respond to external stressors, there must be communication with proteins at the cell surface.

The known interactions of CCM proteins point to a variety of possible candidates, including integrins [71, 73] and cadherins [74] among others [59]. The heart of glass (HEG) cell surface receptor is expressed by endothelium [68] and endocardium [66], shares a common mutant phenotype in zebrafish with *krit1* and *ccm2* [67], and interacts genetically with both [67]. Kleaveland et al. [68] recently characterized the interaction between the HEG and the CCM proteins. The authors show that HEG binds to KRIT1, which is required for binding with CCM2. Thus *CCM2* requires input from *HEG* via *KRIT1* in the endothelium.

Stability is achieved in endothelial cells by balancing a series of stabilizing signals in opposition to the wide variety destabilizing inputs. We have briefly reviewed several such stabilizing cell surface input pathways. In contrast to the Ang–Tie, Delta–Notch, and Slit–Robo systems of ligands and cell surface receptors, the CCM complex is not an extracellular ligand-receptor system with uncertain intracellular effectors, but rather an intracellular signaling complex that regulates cell surface events. In endothelial cells, this complex interacts with Heg at the cell surface, yet Heg deficiency cannot account for all CCM signaling. Thus, the CCM complex is expected to receive further inputs from different cell surface receptors. While CCM protein interactions may point to some of these inputs, it is possible that the CCM protein complex is involved in mediating the stabilizing signals from Tie, Notch, or Robo cell surface receptors. Future studies to define potential interactions between these receptors and the CCM signaling complex will be needed to determine whether they function in common pathways or diverse but parallel pathways.

Acknowledgments We thank D. Lim for expert graphical assistance. This work was funded by grants from the National Institutes of Health, Ruth L. Kirschstein National Research Service Award (N.R.L.); NHLBI (D.Y.L and K.J.W.); American Heart Association (K.J.W. and D.Y.L.); Juvenile Diabetes Research Foundation, HA and Edna Benning Foundation, and the Burroughs Wellcome Foundation (D.Y. L.).

References

1. Mehta D, Malik AB (2006) Signaling mechanisms regulating endothelial permeability. Physiol Rev 86:279–367. doi:10.1152/physrev.00012.2005
2. Vestweber D, Winderlich M, Cagna G, Nottebaum AF (2008) Cell adhesion dynamics at endothelial junctions: VE-cadherin as a major player. Trends Cell Biol
3. Wallez Y, Huber P (2008) Endothelial adherens and tight junctions in vascular homeostasis, inflammation and angiogenesis. Biochim Biophys Acta 1778:794–809. doi:10.1016/j.bbamem.2007.09.003
4. Lindahl P, Johansson BR, Leveen P, Betsholtz C (1997) Pericyte loss and microaneurysm formation in PDGF-B-deficient mice. Science 277:242–245. doi:10.1126/science.277.5323.242
5. Ferrara N, Alitalo K (1999) Clinical applications of angiogenic growth factors and their inhibitors. Nat Med 5:1359–1364. doi:10.1038/70928
6. Ferrara N (2002) Role of vascular endothelial growth factor in physiologic and pathologic angiogenesis: therapeutic implications. Semin Oncol 29:10–14
7. Gault J, Sarin H, Awadallah NA, Shenkar R, Awad IA (2004) Pathobiology of human cerebrovascular malformations: basic mechanisms and clinical relevance. Neurosurgery 55:1–16. doi:10.1227/01.NEU.0000126872.23715.E5 discussion 16–17
8. Dejana E, Orsenigo F, Lampugnani MG (2008) The role of adherens junctions and VE-cadherin in the control of vascular permeability. J Cell Sci 121:2115–2122. doi:10.1242/jcs.017897
9. Corada M, Liao F, Lindgren M, Lampugnani MG, Breviario F, Frank R, Muller WA, Hicklin DJ, Bohlen P, Dejana E (2001) Monoclonal antibodies directed to different regions of vascular endothelial cadherin extracellular domain affect adhesion and clustering of the protein and modulate endothelial permeability. Blood 97:1679–1684. doi:10.1182/blood.V97.6.1679
10. Corada M, Mariotti M, Thurston G, Smith K, Kunkel R, Brockhaus M, Lampugnani MG, Martin-Padura I, Stoppacciaro A, Ruco L, McDonald DM, Ward PA, Dejana E (1999) Vascular endothelial-cadherin is an important determinant of microvascular integrity in vivo. Proc Natl Acad Sci USA 96:9815–9820. doi:10.1073/pnas.96.17.9815
11. Potter MD, Barbero S, Cheresh DA (2005) Tyrosine phosphorylation of VE-cadherin prevents binding of p120- and beta-catenin and maintains the cellular mesenchymal state. J Biol Chem 280:31906–31912. doi:10.1074/jbc.M505568200
12. Andriopoulou P, Navarro P, Zanetti A, Lampugnani MG, Dejana E (1999) Histamine induces tyrosine phosphorylation of endothelial cell-to-cell adherens junctions. Arterioscler Thromb Vasc Biol 19:2286–2297
13. Gong P, Angelini DJ, Yang S, Xia G, Cross AS, Mann D, Bannerman DD, Vogel SN, Goldblum SE (2008) TLR4 signaling is coupled to SRC family kinase activation, tyrosine phosphorylation of zonula adherens proteins, and opening of the paracellular pathway in human lung microvascular endothelia. J Biol Chem 283:13437–13449. doi:10.1074/jbc.M707986200
14. Esser S, Lampugnani MG, Corada M, Dejana E, Risau W (1998) Vascular endothelial growth factor induces VE-cadherin tyrosine phosphorylation in endothelial cells. J Cell Sci 111(Pt 13):1853–1865
15. Eliceiri BP, Paul R, Schwartzberg PL, Hood JD, Leng J, Cheresh DA (1999) Selective requirement for Src kinases during VEGF-induced angiogenesis and vascular permeability. Mol Cell 4:915–924. doi:10.1016/S1097-2765(00)80221-X
16. Nawroth R, Poell G, Ranft A, Kloep S, Samulowitz U, Fachinger G, Golding M, Shima DT, Deutsch U, Vestweber D (2002) VE-PTP and VE-cadherin ectodomains interact to facilitate regulation of phosphorylation and cell contacts. EMBO J 21:4885–4895. doi:10.1093/emboj/cdf497
17. Gavard J, Gutkind JS (2006) VEGF controls endothelial-cell permeability by promoting the beta-arrestin-dependent endocytosis of VE-cadherin. Nat Cell Biol 8:1223–1234. doi:10.1038/ncb1486
18. Davis MA, Ireton RC, Reynolds AB (2003) A core function for p120-catenin in cadherin turnover. J Cell Biol 163:525–534. doi:10.1083/jcb.200307111
19. Xiao K, Garner J, Buckley KM, Vincent PA, Chiasson CM, Dejana E, Faundez V, Kowalczyk AP (2005) p120-Catenin regulates clathrin-dependent endocytosis of VE-cadherin. Mol Biol Cell 16:5141–5151. doi:10.1091/mbc.E05-05-0440
20. Iyer S, Ferreri DM, DeCocco NC, Minnear FL, Vincent PA (2004) VE-cadherin-p120 interaction is required for maintenance

of endothelial barrier function. Am J Physiol Lung Cell Mol Physiol 286:L1143–L1153. doi:10.1152/ajplung.00305.2003
21. Nagy JA, Dvorak AM, Dvorak HF (2007) VEGF-A and the induction of pathological angiogenesis. Annu Rev Pathol 2:251–275. doi:10.1146/annurev.pathol.2.010506.134925
22. Gerhardt H, Golding M, Fruttiger M, Ruhrberg C, Lundkvist A, Abramsson A, Jeltsch M, Mitchell C, Alitalo K, Shima D, Betsholtz C (2003) VEGF guides angiogenic sprouting utilizing endothelial tip cell filopodia. J Cell Biol 161:1163–1177. doi:10.1083/jcb.200302047
23. Thurston G, Suri C, Smith K, McClain J, Sato TN, Yancopoulos GD, McDonald DM (1999) Leakage-resistant blood vessels in mice transgenically overexpressing angiopoietin-1. Science 286:2511–2514. doi:10.1126/science.286.5449.2511
24. Thurston G, Rudge JS, Ioffe E, Zhou H, Ross L, Croll SD, Glazer N, Holash J, McDonald DM, Yancopoulos GD (2000) Angiopoietin-1 protects the adult vasculature against plasma leakage. Nat Med 6:460–463. doi:10.1038/74725
25. Gavard J, Patel V, Gutkind JS (2008) Angiopoietin-1 prevents VEGF-induced endothelial permeability by sequestering Src through mDia. Dev Cell 14:25–36. doi:10.1016/j.devcel.2007.10.019
26. Vikkula M, Boon LM, Carraway KL 3rd, Calvert JT, Diamonti AJ, Goumnerov B, Pasyk KA, Marchuk DA, Warman ML, Cantley LC, Mulliken JB, Olsen BR (1996) Vascular dysmorphogenesis caused by an activating mutation in the receptor tyrosine kinase TIE2. Cell 87:1181–1190. doi:10.1016/S0092-8674(00)81814-0
27. Limaye N, Wouters V, Uebelhoer M, Tuominen M, Wirkkala R, Mulliken JB, Eklund L, Boon LM, Vikkula M (2009) Somatic mutations in angiopoietin receptor gene TEK cause solitary and multiple sporadic venous malformations. Nat Genet 41:118–124. doi:10.1038/ng.272
28. Gale NW, Dominguez MG, Noguera I, Pan L, Hughes V, Valenzuela DM, Murphy AJ, Adams NC, Lin HC, Holash J, Thurston G, Yancopoulos GD (2004) Haploinsufficiency of delta-like 4 ligand results in embryonic lethality due to major defects in arterial and vascular development. Proc Natl Acad Sci USA 101:15949–15954. doi:10.1073/pnas.0407290101
29. Limbourg FP, Takeshita K, Radtke F, Bronson RT, Chin MT, Liao JK (2005) Essential role of endothelial Notch1 in angiogenesis. Circulation 111:1826–1832. doi:10.1161/01.CIR.0000160870.93058.DD
30. Ehebauer M, Hayward P, Martinez-Arias A (2006) Notch signaling pathway. Sci STKE 2006:cm7. doi:10.1126/stke.3642006cm7
31. Lai EC (2004) Notch signaling: control of cell communication and cell fate. Development 131:965–973. doi:10.1242/dev.01074
32. Hellstrom M, Phng LK, Hofmann JJ, Wallgard E, Coultas L, Lindblom P, Alva J, Nilsson AK, Karlsson L, Gaiano N, Yoon K, Rossant J, Iruela-Arispe ML, Kalen M, Gerhardt H, Betsholtz C (2007) Dll4 signalling through Notch1 regulates formation of tip cells during angiogenesis. Nature 445:776–780. doi:10.1038/nature05571
33. Noguera-Troise I, Daly C, Papadopoulos NJ, Coetzee S, Boland P, Gale NW, Lin HC, Yancopoulos GD, Thurston G (2006) Blockade of Dll4 inhibits tumour growth by promoting non-productive angiogenesis. Nature 444:1032–1037. doi:10.1038/nature05355
34. Dickson BJ, Gilestro GF (2006) Regulation of commissural axon pathfinding by slit and its Robo receptors. Annu Rev Cell Dev Biol 22:651–675. doi:10.1146/annurev.cellbio.21.090704.151234
35. Huminiecki L, Gorn M, Suchting S, Poulsom R, Bicknell R (2002) Magic roundabout is a new member of the roundabout receptor family that is endothelial specific and expressed at sites of active angiogenesis. Genomics 79:547–552. doi:10.1006/geno.2002.6745
36. Okada Y, Jin E, Nikolova-Krstevski V, Yano K, Liu J, Beeler D, Spokes K, Kitayama M, Funahashi N, Doi T, Janes L, Minami T, Oettgen P, Aird WC (2008) A GABP-binding element in the Robo4 promoter is necessary for endothelial expression in vivo. Blood 112:2336–2339. doi:10.1182/blood-2008-01-135079
37. Jones CA, London NR, Chen H, Park KW, Sauvaget D, Stockton RA, Wythe JD, Suh W, Larrieu-Lahargue F, Mukouyama YS, Lindblom P, Seth P, Frias A, Nishiya N, Ginsberg MH, Gerhardt H, Zhang K, Li DY (2008) Robo4 stabilizes the vascular network by inhibiting pathologic angiogenesis and endothelial hyperpermeability. Nat Med 14:448–453. doi:10.1038/nm1742
38. Park KW, Morrison CM, Sorensen LK, Jones CA, Rao Y, Chien CB, Wu JY, Urness LD, Li DY (2003) Robo4 is a vascular-specific receptor that inhibits endothelial migration. Dev Biol 261:251–267. doi:10.1016/S0012-1606(03)00258-6
39. Seth P, Lin Y, Hanai J, Shivalingappa V, Duyao MP, Sukhatme VP (2005) Magic roundabout, a tumor endothelial marker: expression and signaling. Biochem Biophys Res Commun 332:533–541. doi:10.1016/j.bbrc.2005.03.250
40. Kaur S, Samant GV, Pramanik K, Loscombe PW, Pendrak ML, Roberts DD, Ramchandran R (2008) Silencing of directional migration in Roundabout4 knockdown endothelial cells. BMC Cell Biol 9:61. doi:10.1186/1471-2121-9-61
41. Sheldon H, Andre M, Legg JA, Heal P, Herbert JM, Sainson R, Sharma AS, Kitajewski JK, Heath VL, Bicknell R (2008) Active involvement of Robo1 and Robo4 in filopodia formation and endothelial cell motility mediated via WASP and other actin nucleation-promoting factors. FASEB J
42. Wang B, Xiao Y, Ding BB, Zhang N, Yuan X, Gui L, Qian KX, Duan S, Chen Z, Rao Y, Geng JG (2003) Induction of tumor angiogenesis by Slit-Robo signaling and inhibition of cancer growth by blocking Robo activity. Cancer Cell 4:19–29. doi:10.1016/S1535-6108(03)00164-8
43. Wu JY, Feng L, Park HT, Havlioglu N, Wen L, Tang H, Bacon KB, Jiang Z, Zhang X, Rao Y (2001) The neuronal repellent Slit inhibits leukocyte chemotaxis induced by chemotactic factors. Nature 410:948–952. doi:10.1038/35073616
44. Suchting S, Heal P, Tahtis K, Stewart LM, Bicknell R (2005) Soluble Robo4 receptor inhibits in vivo angiogenesis and endothelial cell migration. FASEB J 19:121–123
45. Ly A, Nikolaev A, Suresh G, Zheng Y, Tessier-Lavigne M, Stein E (2008) DSCAM is a netrin receptor that collaborates with DCC in mediating turning responses to netrin-1. Cell 133:1241–1254. doi:10.1016/j.cell.2008.05.030
46. Soker S, Takashima S, Miao HQ, Neufeld G, Klagsbrun M (1998) Neuropilin-1 is expressed by endothelial and tumor cells as an isoform-specific receptor for vascular endothelial growth factor. Cell 92:735–745. doi:10.1016/S0092-8674(00)81402-6
47. Paratcha G, Ledda F, Ibanez CF (2003) The neural cell adhesion molecule NCAM is an alternative signaling receptor for GDNF family ligands. Cell 113:867–879. doi:10.1016/S0092-8674(03)00435-5
48. Hu H (2001) Cell-surface heparan sulfate is involved in the repulsive guidance activities of Slit2 protein. Nat Neurosci 4:695–701. doi:10.1038/89482
49. Otten P, Pizzolato GP, Rilliet B, Berney J (1989) A propos de 131 cas d'angiomes caverneux (cavernomes) du S.N.C. repérés par l'analyse rétrospective de 24 535 autopsies. Neurochirurgie 35(82–83):128–131
50. Robinson JR, Awad IA, Little JR (1991) Natural history of the cavernous angioma. J Neurosurg 75:709–714
51. Toldo I, Drigo P, Mammi I, Marini V, Carollo C (2008) Vertebral and spinal cavernous angiomas associated with familial cerebral cavernous malformation. Surg Neurol

52. Clatterbuck RE, Eberhart CG, Crain BJ, Rigamonti D (2001) Ultrastructural and immunocytochemical evidence that an incompetent blood-brain barrier is related to the pathophysiology of cavernous malformations. J Neurol Neurosurg Psychiatry 71:188–192. doi:10.1136/jnnp.71.2.188
53. Sahoo T, Johnson EW, Thomas JW, Kuehl PM, Jones TL, Dokken CG, Touchman JW, Gallione CJ, Lee-Lin SQ, Kosofsky B, Kurth JH, Louis DN, Mettler G, Morrison L, Gil-Nagel A, Rich SS, Zabramski JM, Boguski MS, Green ED, Marchuk DA (1999) Mutations in the gene encoding KRIT1, a Krev-1/rap1a binding protein, cause cerebral cavernous malformations (CCM1). Hum Mol Genet 8:2325–2333. doi:10.1093/hmg/8.12.2325
54. Laberge-le Couteulx S, Jung HH, Labauge P, Houtteville JP, Lescoat C, Cecillon M, Marechal E, Joutel A, Bach JF, Tournier-Lasserve E (1999) Truncating mutations in CCM1, encoding KRIT1, cause hereditary cavernous angiomas. Nat Genet 23:189–193. doi:10.1038/13815
55. Denier C, Goutagny S, Labauge P, Krivosic V, Arnoult M, Cousin A, Benabid AL, Comoy J, Frerebeau P, Gilbert B, Houtteville JP, Jan M, Lapierre F, Loiseau H, Menei P, Mercier P, Moreau JJ, Nivelon-Chevallier A, Parker F, Redondo AM, Scarabin JM, Tremoulet M, Zerah M, Maciazek J, Tournier-Lasserve E (2004) Mutations within the MGC4607 gene cause cerebral cavernous malformations. Am J Hum Genet 74:326–337. doi:10.1086/381718
56. Liquori CL, Berg MJ, Siegel AM, Huang E, Zawistowski JS, Stoffer T, Verlaan D, Balogun F, Hughes L, Leedom TP, Plummer NW, Cannella M, Maglione V, Squitieri F, Johnson EW, Rouleau GA, Ptacek L, Marchuk DA (2003) Mutations in a gene encoding a novel protein containing a phosphotyrosine-binding domain cause type 2 cerebral cavernous malformations. Am J Hum Genet 73:1459–1464. doi:10.1086/380314
57. Uhlik MT, Abell AN, Johnson NL, Sun W, Cuevas BD, Lobel-Rice KE, Horne EA, Dell'Acqua ML, Johnson GL (2003) Rac-MEKK3-MKK3 scaffolding for p38 MAPK activation during hyperosmotic shock. Nat Cell Biol 5:1104–1110. doi:10.1038/ncb1071
58. Bergametti F, Denier C, Labauge P, Arnoult M, Boetto S, Clanet M, Coubes P, Echenne B, Ibrahim R, Irthum B, Jacquet G, Lonjon M, Moreau JJ, Neau JP, Parker F, Tremoulet M, Tournier-Lasserve E (2005) Mutations within the programmed cell death 10 gene cause cerebral cavernous malformations. Am J Hum Genet 76:42–51. doi:10.1086/426952
59. Hilder TL, Malone MH, Bencharit S, Colicelli J, Haystead TA, Johnson GL, Wu CC (2007) Proteomic identification of the cerebral cavernous malformation signaling complex. J Proteome Res 6:4343–4355. doi:10.1021/pr0704276
60. Zawistowski JS, Stalheim L, Uhlik MT, Abell AN, Ancrile BB, Johnson GL, Marchuk DA (2005) CCM1 and CCM2 protein interactions in cell signaling: implications for cerebral cavernous malformations pathogenesis. Hum Mol Genet 14:2521–2531. doi:10.1093/hmg/ddi256
61. Petit N, Blecon A, Denier C, Tournier-Lasserve E (2006) Patterns of expression of the three cerebral cavernous malformation (CCM) genes during embryonic and postnatal brain development. Gene Expr Patterns 6:495–503. doi:10.1016/j.modgep.2005.11.001
62. Denier C, Gasc J, Chapon F, Domenga V, Lescoat C, Joutel A, Tournier-Lasserve E (2002) Krit1/cerebral cavernous malformation 1 mRNA is preferentially expressed in neurons and epithelial cells in embryo and adult. Mech Dev 117:363. doi:10.1016/S0925-4773(02)00209-5
63. McCarty JH, Lacy-Hulbert A, Charest A, Bronson RT, Crowley D, Housman D, Savill J, Roes J, Hynes RO (2005) Selective ablation of {alpha}v integrins in the central nervous system leads to cerebral hemorrhage, seizures, axonal degeneration and premature death. Development 132:165–176. doi:10.1242/dev.01551
64. Whitehead KJ, Chan AC, Navankasattusas S, Wonshill K, London NR, Jing L, Mayo AH, Drakos SG, Marchuk DA, Davis GE, Li DY (2009) The *Cerebral Cavernous Malformation* signaling pathway promotes vascular integrity via Rho GTPases. Nat Med. doi:10.1038/nm.1911
65. Whitehead KJ, Plummer NW, Adams JA, Marchuk DA, Li DY (2004) Ccm1 is required for arterial morphogenesis: implications for the etiology of human cavernous malformations. Development 131:1437–1448. doi:10.1242/dev.01036
66. Mably JD, Mohideen MA, Burns CG, Chen JN, Fishman MC (2003) Heart of glass regulates the concentric growth of the heart in zebrafish. Curr Biol 13:2138–2147. doi:10.1016/j.cub.2003.11.055
67. Mably JD, Chuang LP, Serluca FC, Mohideen MA, Chen JN, Fishman MC (2006) Santa and valentine pattern concentric growth of cardiac myocardium in the zebrafish. Development 133:3139–3146. doi:10.1242/dev.02469
68. Kleaveland B, Zheng X, Liu JJ, Blum Y, Tung JJ, Zou Z, Chen M, Guo L, Lu MM, Zhou D, Kitajewski J, Affolter M, Ginsberg MH, Kahn ML (2009) Regulation of cardiovascular development and integrity by the heart of glass-cerebral cavernous malformation pathway. Nat Med. doi:10.1038/nm.1918
69. Gore AV, Lampugnani MG, Dye L, Dejana E, Weinstein BM (2008) Combinatorial interaction between CCM pathway genes precipitates hemorrhagic stroke. Dis Model Mech 1:275–281. doi:10.1242/dmm.000513
70. Serebriiskii I, Estojak J, Sonoda G, Testa JR, Golemis EA (1997) Association of Krev-1/rap1a with Krit1, a novel ankyrin repeat-containing protein encoded by a gene mapping to 7q21–22. Oncogene 15:1043–1049. doi:10.1038/sj.onc.1201268
71. Zhang J, Clatterbuck RE, Rigamonti D, Chang DD, Dietz HC (2001) Interaction between krit1 and icap1alpha infers perturbation of integrin beta1-mediated angiogenesis in the pathogenesis of cerebral cavernous malformation. Hum Mol Genet 10:2953–2960. doi:10.1093/hmg/10.25.2953
72. Gunel M, Laurans MS, Shin D, DiLuna ML, Voorhees J, Choate K, Nelson-Williams C, Lifton RP (2002) KRIT1, a gene mutated in cerebral cavernous malformation, encodes a microtubule-associated protein. Proc Natl Acad Sci USA 99:10677–10682. doi:10.1073/pnas.122354499
73. Zawistowski JS, Serebriiskii IG, Lee MF, Golemis EA, Marchuk DA (2002) KRIT1 association with the integrin-binding protein ICAP-1: a new direction in the elucidation of cerebral cavernous malformations (CCM1) pathogenesis. Hum Mol Genet 11:389–396. doi:10.1093/hmg/11.4.389
74. Glading A, Han J, Stockton RA, Ginsberg MH (2007) KRIT-1/CCM1 is a Rap1 effector that regulates endothelial cell cell junctions. J Cell Biol 179:247–254. doi:10.1083/jcb.200705175
75. Goudreault M, D'Ambrosio LM, Kean MJ, Mullin M, Larsen BG, Sanchez A, Chaudhry S, Chen GI, Sicheri F, Nesvizhskii AI, Aebersold R, Raught B, Gingras AC (2009) A PP2A phosphatase high-density interaction network identifies a novel striatin-interacting phosphatase and kinase complex linked to the cerebral cavernous malformation 3 (CCM3) protein. Mol Cell Proteomics 8:157–171

CHAPTER 2

TARGETING ROBO4-DEPENDENT SLIT SIGNALING TO SURVIVE THE CYTOKINE STORM IN SEPSIS AND INFLUENZA

The following chapter is a reprint of a manuscript published in Science Translational Medicine. It was published March 17, 2010, volume 2 (23), 23ra19, DOI: 10.1126/scitranslmed.3000678. In addition to myself, the other authors were Weiquan Zhu, Fernando Bozza, Matthew Smith, Dan Greif, Lise Sorensen, Luming Chen, Yuuki Kaminoh, Aubrey Chan, Samuel Passi, Craig Day, Dale Barnard, Guy Zimmerman, Mark Krasnow, and Dean Li. I participated in the design, execution, interpretation of data, and preparation of the manuscript.

Targeting Robo4-Dependent Slit Signaling to Survive the Cytokine Storm in Sepsis and Influenza
Nyall R. London, *et al.*
Sci Transl Med **2**, 23ra19 (2010);
DOI: 10.1126/scitranslmed.3000678

RESEARCH ARTICLE

SEPSIS

Targeting Robo4-Dependent Slit Signaling to Survive the Cytokine Storm in Sepsis and Influenza

Nyall R. London,[1,2,3]* Weiquan Zhu,[1,2,3]* Fernando A. Bozza,[4] Matthew C. P. Smith,[1,2,3] Daniel M. Greif,[5,6] Lise K. Sorensen,[1,2,3] Luming Chen,[1,2,3] Yuuki Kaminoh,[1,2,3] Aubrey C. Chan,[1,2,3] Samuel F. Passi,[1,2,3] Craig W. Day,[7] Dale L. Barnard,[7] Guy A. Zimmerman,[2] Mark A. Krasnow,[5] Dean Y. Li[1,2,3]†

(Published 17 March 2010; Volume 2 Issue 23 23ra19)

The innate immune system provides a first line of defense against invading pathogens by releasing multiple inflammatory cytokines, such as interleukin-1β and tumor necrosis factor–α, which directly combat the infectious agent and recruit additional immune responses. This exuberant cytokine release paradoxically injures the host by triggering leakage from capillaries, tissue edema, organ failure, and shock. Current medical therapies target individual pathogens with antimicrobial agents or directly either blunt or boost the host's immune system. We explored a third approach: activating with the soluble ligand Slit an endothelium-specific, Robo4-dependent signaling pathway that strengthens the vascular barrier, diminishing deleterious aspects of the host's response to the pathogen-induced cytokine storm. This approach reduced vascular permeability in the lung and other organs and increased survival in animal models of bacterial endotoxin exposure, polymicrobial sepsis, and H5N1 influenza. Thus, enhancing the resilience of the host vascular system to the host's innate immune response may provide a therapeutic strategy for treating multiple infectious agents.

INTRODUCTION

The devastating consequences of influenza epidemics, the poor medical outcome after sepsis, and the emergence of new infectious pandemic and biowarfare threats have kindled interest in the development of broad-spectrum strategies that can be rapidly implemented by public health and military defense agencies (*1*, *2*). There are now two main ways to address these infectious threats. The first is to target specific pathogens with antimicrobials. With this approach, time is required to identify the specific pathogen once a pandemic has emerged. In addition, pathogens often mutate, developing resistance to antibiotics and antiviral agents (*3*, *4*). The recent emergence of a pandemic influenza strain highlights these limitations (*5*).

A second approach is to modulate the host's innate immune system (*6*). Innate immunity provides the host with immediate protection against a broad and unforeseen spectrum of pathogens. When activated by endotoxin [lipopolysaccharide (LPS)] or other microbial components, this system, which is composed of neutrophils, monocytes, macrophages, Langerhans cells, dendritic cells, and natural killer cells, releases multiple cytokines with broad antibacterial and antiviral properties as well as regulatory effects on subsequent adaptive immune responses. The marked and abrupt release of multiple cytokines by the immune system, often referred to as hypercytokinemia or cytokine storm, itself has disruptive effects on the host's physiology. In many infections, components of the resulting cytokine-induced secondary inflammatory injury can be more toxic than the invading microbes themselves (*7*). Inflammatory cytokines, such as tumor necrosis factor (TNF) and interleukin-1β (IL-1β), destabilize endothelial cell-cell interactions and cripple vascular barrier function, resulting in capillary leakage, tissue edema, organ failure, and death (*5*, *8*, *9*). These phenomena occur in septic shock, acute lung injury, and acute respiratory distress syndrome—all common endpoints in patients exposed to serious infections (for example, the 1918 influenza pandemic). The prominent role of cytokines in these pathologies has led to the testing of agents that reduce cytokine signaling as possible therapeutics (*10*). This clinical strategy has, however, been disappointing, often resulting in increased mortality (*11*–*13*). The converse strategy of boosting the immune system with infusion of inflammatory cytokines has also been advocated, but its clinical use has been limited because of undesirable outcomes (*6*). For example, delivery of ILs to treat melanoma precipitates aseptic vasogenic shock in patients (*14*). Thus, for survival of the infected patient or animal, a balance must be struck between a protective innate immune response that eliminates the pathogen and an excessive immune response that injures the host.

Here, we have explored a third approach: maximizing the host's endogenous ability to overcome infectious challenge by limiting the disruptive effects of proinflammatory mediators on the vasculature. By augmenting the resilience of the host's vascular system to cytokines, we sought to enable the body to endure an excessive innate immune response. We identified the Slit-induced signaling pathway as a modulator of vascular stability that can strengthen endothelial cell-cell interactions. Activation of this pathway is effective in reducing capillary leak, multiorgan edema, and death in multiple animal models of infections, including H5N1 influenza.

[1]Department of Oncological Sciences, University of Utah, Salt Lake City, UT 84112, USA. [2]Department of Medicine, University of Utah, Salt Lake City, UT 84112, USA. [3]Program in Molecular Medicine, University of Utah, Salt Lake City, UT 84112, USA. [4]Intensive Care Unit, Instituto de Pesquisa Clínica Evandro Chagas, and Laboratório de Imunofarmacologia, Fundação Oswaldo Cruz, Rio de Janeiro 21045-900, Brazil. [5]Department of Biochemistry and Howard Hughes Medical Institute, Stanford University School of Medicine, Stanford, CA 94305, USA. [6]Department of Medicine, Division of Cardiovascular Medicine, Stanford University School of Medicine, Stanford, CA 94305, USA. [7]Institute for Antiviral Research, Utah State University, Logan, UT 84322, USA.

*These authors contributed equally to this work.

†To whom correspondence should be addressed. E-mail: dean.li@u2m2.utah.edu

RESULTS

Slit regulates vascular endothelial cadherin localization

Because the vascular system is exposed to ischemic, infectious, and inflammatory stresses, the endothelium is continuously challenged by angiogenic factors, inflammatory mediators, and permeability agents. All of these molecules disrupt the endothelial barrier of the mature vascular system and contribute to the classic findings of calor (heat), dolor (pain), rubor (redness), and tumor (swelling) on inflammation. Members of the Slit family of neurovascular guidance cues inhibit vascular endothelial growth factor (VEGF)–induced vascular hyperpermeability in a process dependent on the endothelial-specific receptor Robo4 (*15*). This inhibition of VEGF signaling by Slit protein is mediated through the small intracellular guanosine triphosphatase, Arf6 (*16*). Because Robo4 messenger RNA concentrations increase in response to a diverse repertoire of angiogenic (*15*, *17*, *18*) and inflammatory exposures, we hypothesized that Robo4 may be part of a vascular stability signaling program. We tested this hypothesis by examining whether Robo4-dependent Slit signaling reduces the endothelial hyperpermeability induced by endotoxin (LPS), TNF-α, and IL-1β, all important mediators of inflammation (*19*). To study barrier function in vitro, we assessed the ability of a human endothelial cell monolayer to act as a barrier to diffusion of a horseradish peroxidase reporter. We used the N-terminal fragment (Slit2N), which is the active fragment of Slit that is released by proteolytic cleavage (*20*). Slit2N at 10 nM substantially reduced LPS-induced, TNF-α–induced, and IL-1β–induced permeability (Fig. 1A) but did not significantly affect basal permeability (fig. S1A). Furthermore, the inhibitory effect of Slit2N was lost in cells exposed to small interfering RNA (siRNA) directed against Robo4 but not in those exposed to control scrambled siRNA (Fig. 1B and fig. S1B).

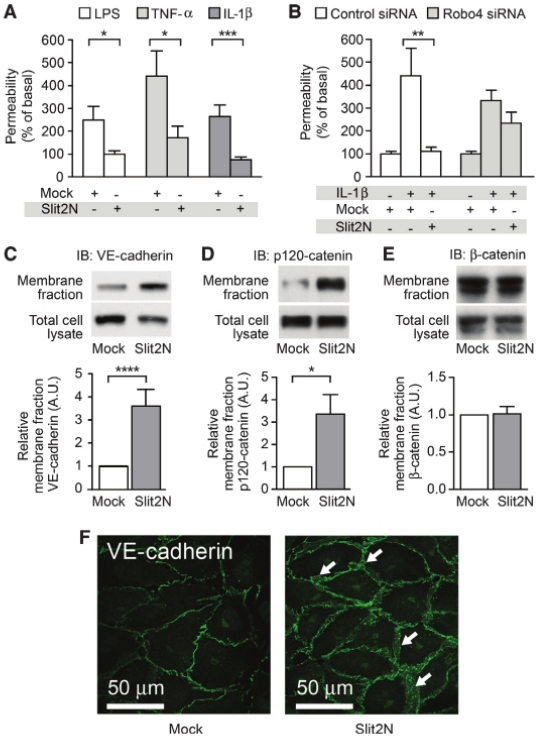

Fig. 1. Slit2N stabilizes the endothelium in vitro by enhancing VE-cadherin localization at the cell surface. (**A**) In vitro permeability was measured in HMVEC-lung cells stimulated with LPS, TNF-α, or IL-1β in the presence of Mock (see Materials and Methods) or Slit2N. (**B**) Robo4 or control siRNA knockdown-treated HMVEC-lung cells were stimulated with IL-1β in the presence of Mock or Slit2N to assess permeability in vitro. (**C** to **E**) HMVEC-lung cells were treated with Mock or Slit2N and subjected to membrane fractionation and subsequent immunoblotting for VE-cadherin (C), p120-catenin (D), or β-catenin (E). (**F**) HMVEC-lung cells were stimulated with Mock or Slit2N and subjected to immunofluorescence for VE-cadherin (green). White arrows, areas of enhanced VE-cadherin cell surface localization. For all experiments, $n \geq 3$, and error bars represent SEM. $^{*}P < 0.05$, $^{**}P < 0.01$, $^{***}P < 0.005$, $^{****}P < 0.001$.

Because Robo4-dependent Slit2N signaling tempers the effects of such a range of angiogenic and inflammatory cytokines (Fig. 1A), we tested whether this pathway promotes vascular stability by directly enhancing the molecular machinery responsible for cell-cell interactions. In the endothelium, critical intercellular interactions are mediated by the adherens junction protein vascular endothelial cadherin (VE-cadherin) (*21*, *22*). When we treated human microvascular lung endothelial (HMVEC-lung) cells with Slit2N, VE-cadherin abundance was significantly increased at the cell surface junctions (Fig. 1, C and F, and fig. S1C). VE-cadherin presence on the cell surface is regulated by the association of p120-catenin with VE-cadherin, an association that inhibits VE-cadherin internalization from the cell surface and promotes vascular stability (*23*, *24*). Slit2N also increased the cell surface abundance of p120-catenin (Fig. 1D) but had no effect on β-catenin (Fig. 1E).

Next, we determined whether Slit2N affected VE-cadherin at the cell surface after exposure to IL-1β. IL-1β reduced VE-cadherin at the cell surface, and Slit2N negated this effect (Fig. 2A). IL-1β stimulation decreased p120-catenin at the cell surface, and Slit2N reversed this effect (Fig. 2A). IL-1β induced dissociation of VE-cadherin from p120-catenin and internalization of VE-cadherin (Fig. 2, B and C). Slit2N restored the association of VE-cadherin and p120-catenin and blocked internalization of VE-cadherin (Fig. 2, B and C). VE-cadherin internalization experiments were performed in the presence of primaquine to prevent endocytic recycling (*25*). In the absence of primaquine, we were unable to detect IL-1β–induced VE-cadherin internalization (fig. S1D). It has been proposed that phosphorylation of VE-cadherin at Tyr^{658} disrupts its binding to p120-catenin and results in the endocytosis of VE-cadherin (*23*). Our experiments indicate that Slit2N stabilized the interaction between VE-cadherin and p120-catenin by inhibiting IL-1β–induced phosphorylation of VE-cadherin at Tyr^{658} (fig. S1E).

Next, we investigated whether the effect of Slit2N on VE-cadherin localization is necessary for its ability to enhance vascular stability. Because VE-cadherin siRNA had a potent disruptive effect on the endothelial monolayer at baseline (fig. S1, F and G), we used an antibody to VE-cadherin to block the effect of Slit2N on permeability in vitro. Slit2N inhibited IL-1β–induced permeability in vitro in the presence of a nonspecific immunoglobulin G (IgG); however, the effect of Slit2N was lost in the presence of an antibody to VE-cadherin (Fig. 2D). Together, these data suggest that Slit2N preserves the association of p120-catenin with VE-cadherin in the face of IL-1β stimulation and thereby promotes vascular integrity by reducing cytokine-induced VE-cadherin endocytosis.

Slit enhances vascular stability in vivo

To examine whether Slit reduces permeability under conditions of cytokine storm in vivo, we used a bacterial endotoxin model of pulmonary inflammation. In this model, LPS is administered to the lungs of mice through intratracheal instillation, simulating a Gram-negative infection (*26*). LPS administration triggers a massive inflammatory reaction and release of cytokines, resulting in a large increase in alveolar capillary permeability. Using Evans blue albumin (EBA) as a tracer, we found that Slit2N significantly reduced vascular leak in the lungs of LPS-treated *Robo4*$^{+/+}$ mice (Fig. 3A). The effect of Slit2N was lost in *Robo4*-null (*Robo4*$^{AP/AP}$) mice, showing that Robo4 is necessary for the effect of Slit2N in vivo (Fig. 3A). This result also indicates that this activity is endothelial-specific, as Robo4 is only detected in the endothelium (*17*, *18*). LPS instillation in the lung also induces accumulation of protein exudates and leukocytes in the alveolar space, inflammatory responses that can be quantified in bronchoalveolar lavage fluid (BALF) (*26*). Slit2N reduced protein exudate, a key marker of acute lung injury and indicator of vascular barrier disruption (*10*), and inflammatory cell accumulation in the BALF of *Robo4*$^{+/+}$ mice in a dose-dependent manner (Fig. 3, B to D, and fig. S2, A and B). The Slit2N-induced inhibition of protein and leukocyte accumulation in BALF was lost in *Robo4*$^{AP/AP}$ mice, indicating again that Slit2N acts directly on the vasculature to decrease protein exudates and inflammatory cell accumulation in the alveoli (Fig. 3, B to D). Finally, histological examination of the lung confirmed that Slit2N acts in a Robo4-dependent manner by reducing LPS-induced lung inflammation in *Robo4*$^{+/+}$ but not *Robo4*$^{AP/AP}$ mice (Fig. 3E and fig. S2C). Because neutrophils are a predominant cell type in bacterial pneumonia and LPS challenge models (*26*), we tested whether Slit2N had a direct effect on neutrophil migration. Primary human polymorphonuclear leukocytes (hPMNs) did not respond to Slit2N, consistent with the fact that they do not express Robo receptors (fig. S3, A and B).

One might anticipate that the loss of Robo4 would make mice more sensitive to LPS exposure, but in initial studies, we did not detect enhanced sensitivity in the lungs of *Robo4*$^{AP/AP}$ mice relative to *Robo4*$^{+/+}$ mice (Fig. 3, B to D). We reasoned that if the amount of LPS administered was too large, it could cause such severe damage that any difference between the two genotypes would be masked. Thus, we lowered the dose of LPS used to challenge the mice and, under these conditions, found that *Robo4*$^{AP/AP}$ mice exhibited signifi-

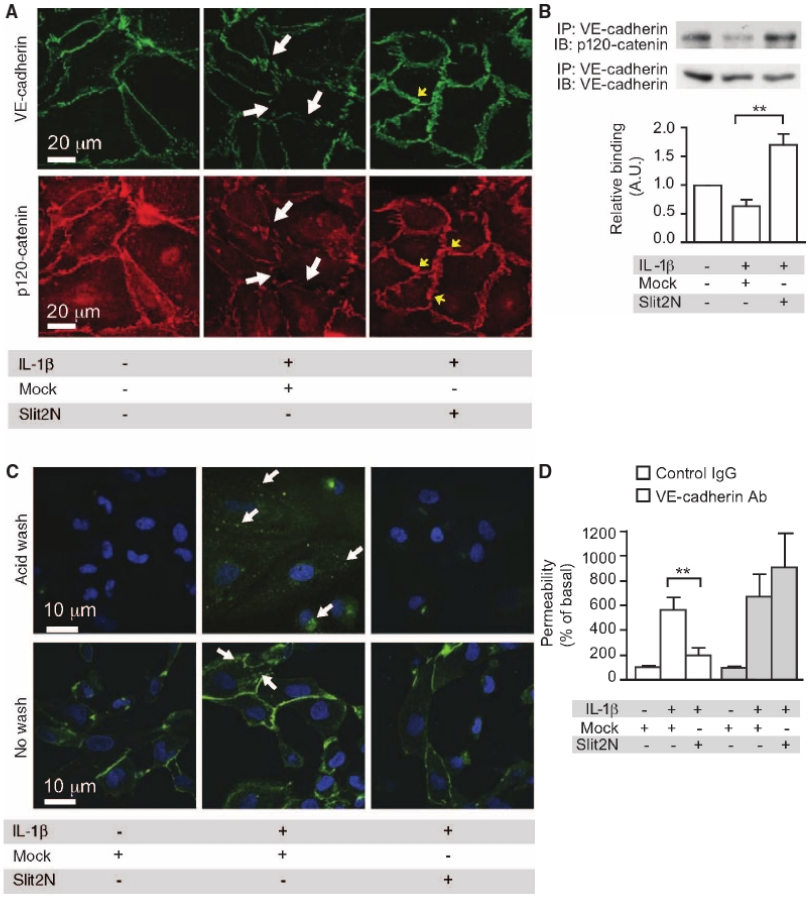

Fig. 2. Slit2N enhances a VE-cadherin–p120-catenin interaction in vitro. (**A**) HMVEC-lung cells were stimulated with IL-1β in the presence of Mock or Slit2N and immunostained for VE-cadherin and p120-catenin. White arrows, cell surface areas lacking VE-cadherin or p120-catenin in Mock-treated cells; yellow arrows, areas of enhanced cell surface localization of VE-cadherin or p120-catenin in Slit2N-treated cells. (**B**) HMVEC-lung cells were stimulated with IL-1β in the presence of Mock or Slit2N. Lysates were subjected to immunoprecipitation for VE-cadherin followed by immunoblot for p120-catenin and VE-cadherin. (**C**) HMVEC-lung cells were labeled with an antibody to VE-cadherin and stimulated with IL-1β in the presence of Mock or Slit2N. Cells were acid-washed to strip the surface-bound VE-cadherin (top row). VE-cadherin internalization (green) was assessed. White arrows, areas of internalization. (**D**) In vitro permeability was measured in the presence of a control IgG or VE-cadherin antibody (Ab). For all experiments, $n \geq 3$, and error bars represent SEM. $^{**}P < 0.01$.

cantly higher protein concentrations in BALF than did littermate *Robo4*$^{+/+}$ mice (Fig. 3F). This increased sensitivity of *Robo4*$^{AP/AP}$ mice to LPS suggests that endogenous Robo4-dependent Slit signaling normally dampens the effects of cytokines on the vasculature. Consistent with this suggestion, Slit2 protein is expressed throughout the lung and in close proximity to the endothelium (fig. S4).

To determine whether Slit acts via a VE-cadherin–dependent mechanism in vivo, we blocked VE-cadherin with a specific antibody that prevents homophilic interactions between VE-cadherin expressed on adjacent endothelial cells (*27*). Slit2N reduced protein exudates and inflammatory cell infiltration in the presence of a control IgG antibody but not in the presence of a VE-cadherin–blocking antibody (Fig. 3, G to I). Thus, as in our cell culture experiments, our in vivo experimental results support the idea that Slit2N promotes VE-cadherin expression at the cell surface, which blunts cytokine-mediated endothelial hyperpermeability.

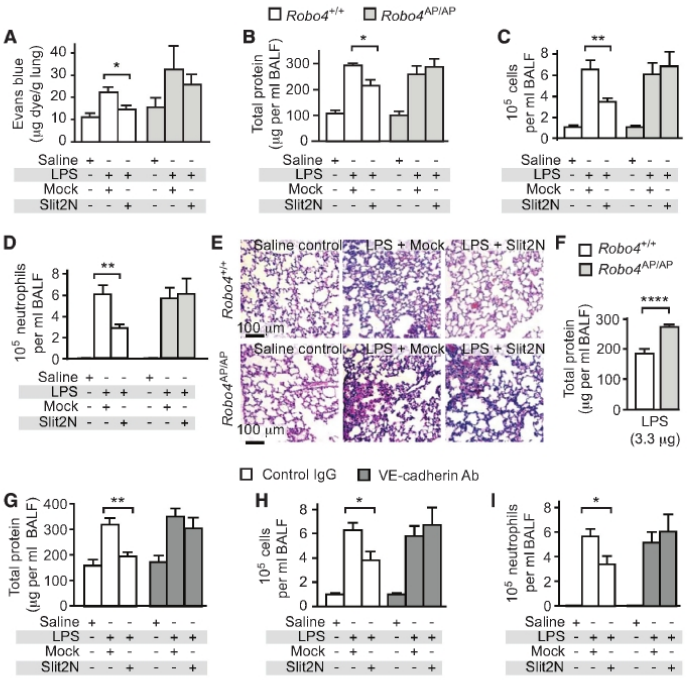

Fig. 3. Slit2N inhibits LPS-induced permeability, protein exudates, and cell infiltrates in vivo. (**A**) *Robo4*$^{+/+}$ and *Robo4*$^{AP/AP}$ mice were given an intravenous injection of Mock or Slit2N followed by intratracheal instillation of LPS (10 μg). Mice later received an intravenous injection of EBA, and EBA accumulation in the lungs was used to assess vascular permeability ($n \geq 4$). (**B** to **D**) Twenty-four hours after LPS administration, bronchoalveolar lavages were obtained and assessed for protein content (B), total inflammatory cell accumulation (C), or neutrophil accumulation (saline value is too low to be visible) (D) ($n \geq 5$). (**E**) H&E staining was performed on lung sections from mice exposed to LPS in the presence of Mock or Slit2N. (**F**) Protein exudates measured in mice treated with 3.3 μg of LPS ($n = 5$). (**G** to **I**) Mice were given an intravenous injection of Mock or Slit2N with control or VE-cadherin–blocking antibody followed by intratracheal instillation of LPS. Bronchoalveolar lavages were obtained and assessed for protein content (G), total inflammatory cell accumulation (H), or neutrophil accumulation (I) ($n \geq 5$). Error bars represent SEM. *$P < 0.05$, **$P < 0.01$, ****$P < 0.001$.

Enhancing vascular stability during polymicrobial sepsis

To evaluate whether Slit2N can reduce mortality in the setting of systemic vascular instability, and whether the effect of Slit2N is limited to the lung, we used a model of polymicrobial sepsis known as cecal ligation and puncture (CLP) (*28*). Slit2N significantly reduced vascular permeability in the kidney and spleen (Fig. 4, A and B) and improved the survival of mice exposed to CLP-induced sepsis from 33 to ~80% (Fig. 4C). Under the conditions of these experiments, CLP did not cause significant damage to the lung (fig. S5, A to C). Because a hyperinflammatory response contributes to the pathogenesis of sepsis, we also tested whether Slit2N could affect cytokine and chemokine concentrations in the plasma of septic mice (*19*). Slit2N did not alter plasma concentrations of a panel of cytokines and chemokines, demonstrating that the therapeutic effect of Slit2N is not secondary to a reduction in inflammatory cytokine and chemokines (Fig. 4, D and E). The effect of Slit2N on mortality after CLP treatment was lost in *Robo4*$^{AP/AP}$ mice (Fig. 4F), hence Robo4 is necessary for this activity of Slit2N. Additionally, the loss of Robo4 did not alter cytokine receptor levels, nor does Slit2N inhibit cytokine receptor activation or induce Robo4 expression in endothelial cells (fig. S6, A and B). Together, these data demonstrate that Slit can enhance survival by specifically enhancing vascular stability during the systemic inflammatory response triggered by sepsis.

Stabilizing the vasculature reduces mortality after H5N1 infection

LPS instillation and CLP mimic the vascular instability and dysregulated inflammation induced by bacterial pathogens. To determine whether a therapeutic strategy of vascular stabilization can be productively applied to viral infections, we examined the effects of Robo4-dependent Slit2N treatment in a model of H5N1 influenza. Pandemic influenzas such as avian flu (H5N1) provide extreme examples of infection-induced lung injury characterized by large increases in cytokine concentrations and excessive inflammation (*29*–*31*). Slit2N significantly inhibited endothelial hyperpermeability in the lung 3 days after H5N1 infection of mice (Fig. 5A) and also reduced mortality (Fig. 5B). The lung pathology in Slit2N-treated mice was less severe than it was in mock-treated mice (Fig. 5C). To exclude the possibility that Slit2N has direct antiviral activity, we measured lung viral titers and found that Slit2N did not alter viral load (Fig. 5D); further, Slit2N did not significantly reduce the amount of inflammatory cytokine released in the lung after H5N1 infection (Fig. 5, E and F). These results are consistent with our LPS and CLP studies and indicate that limiting the vascular response to hypercytokinemia is sufficient to reduce mortality and morbidity in animal models of serious infection.

DISCUSSION

Pandemic influenza and bacterial sepsis are infections that have sizable mortality rates and substantially affect public health (*32*). New ways to address these constantly evolving biological threats are needed (*33*). Here, using rodent models of infection, we have demonstrated that cytokine storm and capillary leakage contribute to the poor outcome of endotoxin-induced acute lung injury, polymicrobial sepsis, and pandemic influenza. We further show that administration of the exogenous ligand Slit2N strengthens the endothelial barrier and blunts vascular leak in response to cytokine storm (Fig. 6). Exogenously applied Slit2N stabilizes cell surface VE-cadherin, a primary molecular determinant of intact barrier function in the endothelium, and this strengthened barrier can protect mice from the lethal effects of sepsis or influenza infection. Furthermore, in genetically modified mice lacking Robo4, Slit2N cannot prevent vascular leakage in infection or sepsis, indicating that Robo4 is a critical mediator of Slit-promoted vascular stability.

We and others have long assumed that Robo4 played an essential role in development based on a number of observations, including the role of Slit-Robo signaling in neuronal guidance (*34*) and the lethality of mutations in genes of this signaling pathway (*35*–*37*). Yet, unexpectedly, mice homozygous for null mutations of *Robo4* are viable (*15*). Similarly, in a detailed characterization of lung development, we could find no structural differences between $Robo4^{AP/AP}$ (null) mice and their wild-type sibling controls (figs. S7 and S8).

Our results suggest an alternative function for Robo4: This receptor may be important for modulating the vascular response to inflammatory cytokines but not for development. As with other pathways that maintain adult homeostasis, including many involved in the immune response, one cannot a priori expect that these pathways are also essential for development. Genetic alterations in these pathways might only manifest after exposure to physiologic or environmental stress (*38*).

In our experiments, we tested one way that signaling via Robo4 could modulate critical host inflammatory responses. Because Slit2 affects migration of dimethyl sulfoxide (DMSO)–treated HL-60 cells, a promyelocytic leukemia cell line often used as a surrogate for primary neutrophils (*39*), we asked whether Slit2 inhibits migration of neutrophils, which could account for the reduced numbers of inflammatory cells in the lungs of LPS-treated mice (*40*). Although in our hands Slit2 also inhibited migration of DMSO-treated HL-60 cells, we found no evidence that primary hPMNs respond to Slit2N, nor do they express Robo receptors (fig. S3, A and B).

Rather, our data demonstrate that Robo4 is required for the effect of Slit2N on VE-cadherin–mediated vascular barrier function. Similarly, expression of either Robo4 or Robo1 is necessary and sufficient to make cells sensitive to Slit (*15*, *16*, *18*, *39*, *41*). The simplest interpretation of these data would be that Slit2 acts as a direct ligand for Robo4. This may not be the case, however. Others have postulated that co-receptors such as syndecans are required for the function of Robo receptors in neural guidance (*42*–*45*). Western blot and immunoprecipitation studies in the presence of non-denaturing detergents (0.5% NP-40) reveal specific binding of Slit2 to Robo4 (*18*), but the use of harsher conditions using ionic denaturing detergents (1% Triton X-100–0.5% deoxycholate) fails to preserve this interaction (*46*). To reconcile this variable and detergent-dependent binding between Slit2 and cell surface Robo4, the absence of strong interaction between Slit and Robo4 in an in vitro Biacore assay (*46*), and the strong signaling and functional response of Robo4 to Slit, Sheldon *et al.* (*42*) and Suchting *et al.* (*46*) propose that Robo4 and Robo1 receptors form a heterodimeric complex in human vein endothelial cells and show that the Robo1 and Robo4 receptors bind to one another. Consistent with their model, we find that knockdown of either Robo4 or Robo1 abrogates the ability of Slit to inhibit migration of human vein endothelial cells (fig. S9). Further investigation of the roles of Robo1 and syndecans as co-receptors for Robo4 is needed.

The endothelial cell monolayer provides a critical semipermeable barrier between the blood and tissue that regulates the passage of nutrients, fluid, and leukocytes into the interstitial space (*47*). The integrity of this barrier is determined by homophilic interactions between the cell surface adherens junction protein VE-cadherin on adjacent endothelial cells (*48*). In states of active angiogenesis or acute inflammation, cytokines induce rapid endocytosis of VE-cadherin, disrupting the transcellular homophilic binding of VE-cadherins, deconstructing paracellular adherens junctions, and resulting

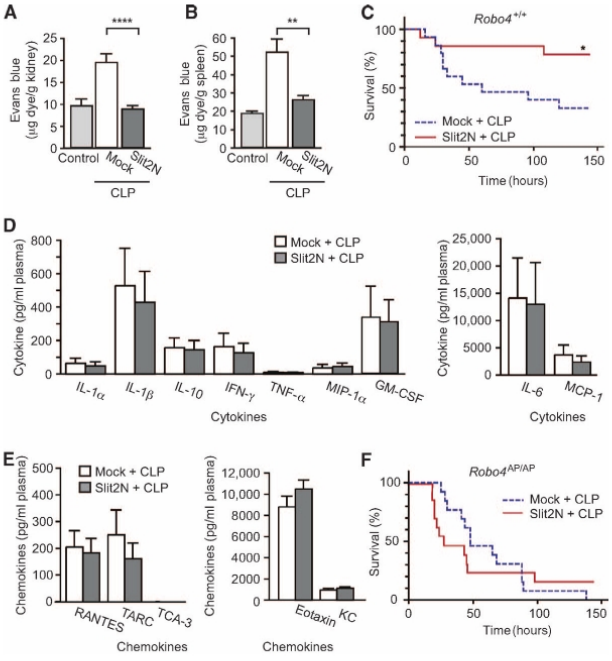

Fig. 4. Slit2N reduces permeability and mortality in a CLP model of sepsis. (**A** and **B**) Mice were subjected to CLP or sham operation and then given an intravenous injection of EBA. EBA accumulation was measured in the kidney (A) or spleen (B) to assess vascular permeability ($n = 5$). (**C**) $Robo4^{+/+}$ mice were subjected to CLP and treated with Mock or Slit2N, and survival was assessed (Mock-treated, $n = 15$; Slit2N-treated, $n = 14$). (**D** and **E**) Cytokine (D) and chemokine (E) concentrations in the serum of Mock- or Slit2N-treated CLP mice ($n = 6$). (**F**) $Robo4^{AP/AP}$ mice were subjected to CLP and treated with Mock or Slit2N, and survival was assessed (Mock-treated, $n = 13$; Slit2N-treated, $n = 13$). Error bars represent SEM. $^*P < 0.05$, $^{**}P < 0.01$, $^{****}P < 0.001$.

in hyperpermeability (*21*, *49*–*51*). Our study suggests that the destabilizing effects of angiogenic and inflammatory cytokines are opposed by extracellular cues that promote vascular stability. Although two stabilizing regulators of the vascular barrier, Tie2-dependent angiopoietin signaling and Robo4-dependent Slit signaling, use different immediate downstream signaling cascades, both ultimately blunt cytokine-mediated endocytosis of cell surface VE-cadherin (*15*, *16*, *52*). Thus, the strength of the endothelial barrier may be a product of a constant tug-of-war between opposing stabilizing and destabilizing signals that control VE-cadherin trafficking, allowing the vascular system the necessary plasticity to respond to changing physiologic needs.

The innate immune system provides the first line of defense of the body against pathogens and must be rapid, broad-spectrum, and toxic to the offending pathogen. There is a fine line between overwhelming the invaders and inflicting severe collateral damage to the host. Boosting the innate immune system with cytokines increases the risk of vasogenic shock, yet efforts to reduce secondary damage by suppressing the innate immune response with glucocorticoids can worsen the outcomes from severe infection. Thus, pharmacologic modulation of the innate immune response has a narrow therapeutic window.

The specific cytokines elaborated and their temporal secretion profile may differ for each pathogen. Nevertheless, the cumulative effects of hypercytokinemia on vascular leakage and noncardiogenic shock are common among severe infections characterized by septic shock (*29*, *30*, *53*). Our data suggest that an alternative approach to combating these infections is to strengthen the vascular barrier. The pharmacologic promotion of vascular stability was sufficient to mute the vascular hyperpermeability induced by multiple different cytokines and the subsequent mortality in rodent models of severe bacterial and viral infections. Enhancing stability offers practical advantages over a more complicated approach aimed at blocking each individual cytokine contributing to cytokine storm. The practical success of targeting the vascular response to cytokines may require a careful characterization of the temporal sequence involving infection, hypercytokinemia, vascular leakage, organ failure, and eventual death (*9*, *29*, *30*, *54*). A likely limitation is that this therapeutic approach may need to be used before the vascular damage is too grave to repair. Even so, targeting the host and not the pathogen offers a stratagem that could offer sufficient flexibility to successfully combat ever-changing biologic threats from drug-resistant, mutating, and emerging infectious agents (*55*).

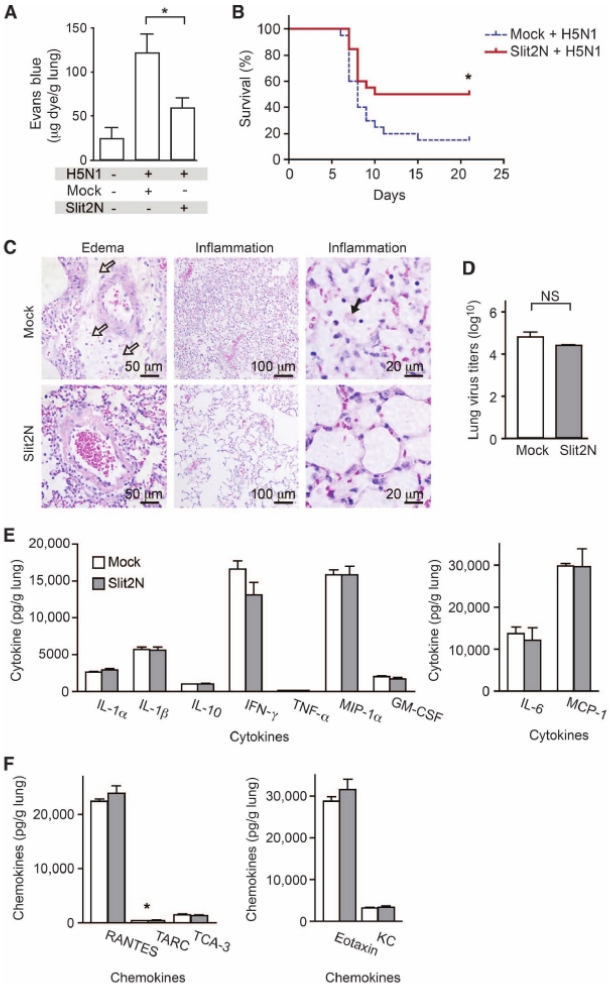

Fig. 5. Slit2N reduces mortality in models of H5N1 infection. (**A**) BALB/c mice were infected intranasally with H5N1 virus. Mice were given an intravenous injection of EBA, and EBA accumulation was measured in the lungs to assess vascular permeability (n = 5). (**B**) Mouse survival after H5N1 infection (Mock-treated, n = 20; Slit2N-treated, n = 20). (**C**) H&E staining was performed on lung sections from H5N1-infected mice 6 days after infection. White arrows in the top left panel show accumulation of edema fluid around a pulmonary arteriole. The top middle panel demonstrates exuberant alveolar inflammation. The black arrow in the top right panel shows the presence of foamy macrophages. (**D**) H5N1 viral titers were measured 6 days after infection (n = 3 groups of pooled mice). (**E** and **F**) Cytokine (E) or chemokine (F) concentrations measured in lung homogenates 6 days after infection (n = 3 groups of pooled mice). *P < 0.05. NS, not significant.

MATERIALS AND METHODS

Preparation of recombinant Slit2N

293T cells plated onto poly-L-lysine (Sigma)–coated dishes were transiently transfected with empty vector pSecTagB or pSecTagB::hSlit2N. For each 15-cm dish of cells, 60 μg of DNA and 100 μl of Lipofectamine (Invitrogen) in serum-free Opti-MEM were used. Slit2N protein was salt-extracted as described (*15*). Using this protocol, we obtained Slit2N concentrations of 0.5 to 1.5 mg/ml. We performed the same salt extraction procedure on cells transfected with empty vector pSecTagB. This preparation is referred to as Mock and was used as a control for Slit2N in all experiments. In vitro studies were conducted with 10 nM Slit2N.

In vitro permeability assay

In vitro permeability testing was performed as described (*15*) with LPS (100 ng/ml; serotype 0111:B4; Sigma) for 3 hours, TNF-α (10 ng/ml; R&D Systems) for 6 hours, or IL-1β (10 ng/ml; R&D Systems) for 2 hours. As indicated, this was repeated in the presence of control rabbit IgG (25 μg/ml; Jackson ImmunoResearch) or antibody to human VE-cadherin (25 μg/ml; RDI Fitzgerald). Basal permeability for unstimulated monolayers was set at 100%. Data are presented as mean ± SEM of at least three independent experiments performed in triplicate.

Robo4 siRNA knockdown

huRobo4 siRNA duplex (Hs_Robo4_1_HP; Qiagen) or equimolar All-Stars Negative Control siRNA (Qiagen) transfection complexes were formed according to standard protocol and added to the upper chamber of Transwell filters. Twenty-four hours later, cells were transfected a second time with huRobo4 or control siRNA. After an additional 24 hours, in vitro permeability was assessed as described. Data are presented as mean ± SEM of at least three independent experiments performed in triplicate. Successful knockdown of Robo4 protein expression was confirmed by Western blot with antibodies against Robo4 (N-17) or β-tubulin (Santa Cruz Biotechnology).

Subcellular fractionation

HMVEC-lung cells were treated with Slit2N or Mock in 0.1% fetal bovine serum (FBS) EBM-2 for 1.5 hours. Cells were then washed twice with ice-cold phosphate-buffered saline (PBS) containing Ca^{2+}-Mg^{2+} and once with HLB buffer [10 mM tris-HCl (pH 7.4), 5 mM KCl, and 1 mM $MgCl_2$] and collected in HLB buffer supplemented with protease inhibitors (Roche), phosphatase inhibitors (Sigma), and 1 mM dithiothreitol (DTT). Cells were then homogenized in a Dounce homogenizer (20 strokes). The homogenate was centrifuged at 400*g* for 10 min at 4°C to pellet cell debris. The resulting supernatant was centrifuged again at 16,000*g* for 30 min at 4°C. The pellet was washed once with HLB and resuspended in radioimmunoprecipitation assay (RIPA) buffer for 30 min at 4°C. The resuspended pellet was centrifuged (16,000*g* for 15 min at 4°C), and the resulting supernatant was saved as a soluble membrane fraction. To obtain the total cell lysate, we saved an aliquot before Dounce homogenization. RIPA buffer was added to this aliquot and centrifuged at 13,000*g* for 10 min at 4°C. The supernatant was saved and used as total cell lysate. Antibodies to VE-cadherin were obtained from Cell Signaling, and p120-catenin and β-catenin were from BD Biosciences. Densitometry was performed on at least three independent experiments and data are presented as mean ± SEM.

Immunofluorescence

Immunofluorescence was performed as described (*15*). Cells were pretreated with Slit2N or Mock for 30 min followed by stimulation with IL-1β (10 ng/ml) for 3 hours. Primary antibodies to VE-cadherin (BD Biosciences) or p120-catenin (Santa Cruz Biotechnology) were applied at 4°C overnight. Images are representative of three independent experiments.

Immunoprecipitation

HMVEC-lung cells (Lonza) were treated with Slit2N or Mock in 0.1% FBS EBM-2 for 30 min. Cells were then stimulated with IL-1β (10 ng/ml) for 10 min. HMVEC-lung cells were then washed with ice-cold PBS and lysed with ice-cold lysis buffer [10 mM tris-HCl (pH 7.4), 50 mM NaCl, 1% NP-40, and 10% glycerol] supplemented with protease inhibitors, phosphatase inhibitors, and 1 mM DTT. Cell lysates were incubated on ice for 30 min and centrifuged at 13,000*g* for 15 min to pellet cell debris. Protein concentrations were determined by BCA assay (Pierce), and 0.5 mg of lysate was incubated with 8 μg of VE-cadherin antibody (Cell Signaling) and protein A/G–Sepharose (Santa Cruz Biotechnology) for 1 hour at 4°C. Complexes were washed three times with lysis buffer. The immunoprecipitates were subjected to Western blot analysis using a 95% fraction of the immunoprecipitate for the p120-catenin blots and the remaining 5% fraction for the VE-cadherin blots (Fig. 2B). Densitometry was performed on three independent experiments, and data as a ratio of immunoprecipitated p120-catenin to loaded VE-cadherin are presented as mean ± SEM.

Internalization assay

VE-cadherin internalization was performed as described (*24*). In brief, HMVEC-lung cells were seeded onto chamber slides and cultured for 72 hours. The media were then removed, and the cells were labeled for 30 min at 4°C with an antibody to VE-cadherin (clone BV6; RDI Fitzgerald). Cells were then pretreated with Slit2N or Mock for 30 min. Excess antibody was removed by washing twice on ice with ice-cold media. Chamber slides were moved to 37°C and incubated for 1 hour with IL-1β (10 ng/ml) and 0.6 mM primaquine in the presence of 10 nM Slit2N or Mock. Cells were acid-washed to strip the surface-bound VE-cadherin. Monolayers were washed, fixed, and permeabilized. Internalized VE-cadherin antibody was detected with Alexa 488–conjugated donkey antibody to mouse IgG (Molecular Probes). Images are representative of four independent experiments.

Animals

The Institutional Animal Care and Use Committee at the University of Utah or at Utah State University approved the following animal protocols. *Robo4*$^{AP/AP}$ mice have been described (*15*).

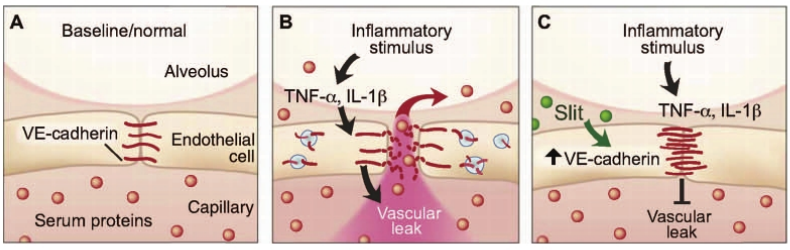

Fig. 6. Slit reduces vascular leak caused by multiple inflammatory stimuli through enhancing VE-cadherin at the cell surface. (**A**) Under normal conditions, alveolar capillaries are semipermeable. (**B**) Inflammatory stimuli cause a large release of cytokines, leading to internalization of VE-cadherin and disruption of barrier function. This results in vascular leak and accumulation of protein-rich edema fluid in the alveolar space. (**C**) Slit enhances vascular barrier function against multiple cytokines by enhancing VE-cadherin at the cell surface.

LPS-induced acute lung injury

Eight- to 12-week-old C57BL/6 mice were injected intravenously with saline alone or 3.5 μg of Slit2N or Mock in saline. Alternatively, the intravenous injection also contained 20 μg of control IgG or 20 μg of VE-cadherin–blocking antibody (clone BV13; eBiosciences). Animals were anesthetized with Avertin before surgical exposure of the trachea. LPS (10 μg; serotype 0111:B4) in 100 μl of saline or saline alone was administered intratracheally. Twenty-four hours later, the trachea was reexposed and catheterized. BALF was obtained by injection of saline (1 ml) followed by aspiration repeated three times. BALF was centrifuged at 300*g* for 5 min to recover inflammatory cells. The pellet was treated with ACK buffer for 3 min to remove red blood cells. Cells were centrifuged at 300*g* for 5 min and resuspended in 1 ml of PBS containing 1% FBS. Cell counts were then determined by hemocytometer. Neutrophil counts were determined by cell differential counts. A white blood cell differential was achieved by staining an aliquot of cells followed by microscopic examination to determine the percentage of the cell population that were neutrophils. BALF protein was assessed by protein assay (Bio-Rad). Data are presented as SEM of at least five mice per condition.

CLP sepsis model

Seven- to 11-week-old male C57BL/6 mice were given an intraperitoneal injection of 5 μg of Slit2N or Mock. One hour later, mice were anesthetized with isoflurane, and CLP was performed as described (*56*). Mice continued to receive an intraperitoneal injection of 5 μg of Slit2N or Mock once a day. Mice in the sham operation group were subjected to identical procedures, except that ligation and puncture of the cecum were omitted. Survival rate of mice subjected to CLP was determined for 6 days, with $n = 14$ for Slit2N treatment and $n = 15$ for Mock treatment for *Robo4*$^{+/+}$ mice. For *Robo4*$^{AP/AP}$ mice, $n = 13$ for Slit2N treatment and $n = 13$ for Mock treatment.

H5N1 infection

Female, 18 to 20 g, BALB/c mice (Charles River Laboratories) were anesthetized and infected with H5N1 virus (Influenza A, Duck/MN/1525/81) intranasally. Mice were given an intravenous injection of 1.56 μg of Slit2N or Mock daily for 5 days. Survival rate of mice subjected to H5N1 lung infection was determined for 21 days with 20 mice per condition.

Evans blue permeability

Vascular permeability in the lung was assessed with EBA as described (*57*). Five hours after intratracheal instillation of LPS, 4 hours after CLP, and 3 days after H5N1 infection, mice were given an intravenous injection of EBA (20 mg/kg). EBA was allowed to circulate for 1 hour, and mice were deeply anesthetized and perfused with saline plus 5 mM EDTA. Lungs were excised, weighed, and homogenized in 2 ml of PBS. Formamide (4 ml; Invitrogen) was added, and the samples were incubated overnight at 60°C to extract Evans blue dye. The samples were then centrifuged, and supernatants were analyzed by spectrophotometry at both 620 and 740 nm. CLP-treated mice were perfused, and their kidneys and spleen were removed, weighed, and placed in formamide for 48 hours at 60°C. The absorbances were normalized as described (*57*) and converted to microgram Evans blue dye per gram wet weight of lungs, kidneys, or spleen, respectively. Data are presented as SEM of at least four mice per condition.

Histology

Twenty-four hours after LPS exposure or CLP, mice were killed by CO_2 asphyxiation. Chest cavities were opened, and lungs were inflated with $ZnSO_4$-buffered 10% formalin. Formalin-fixed tissues were processed routinely, embedded in paraffin, sectioned at 6 μm, and stained with hematoxylin and eosin (H&E). Histologic quantification was modified from methods described (*58*). For H5N1 samples, 6 days after infection, the right lobes of the lungs from two animals were harvested and fixed in 10% neutral-buffered formalin. Formalin-fixed tissues were processed routinely, embedded in paraffin, sectioned at 5 μm, stained with H&E, and evaluated for microscopic lesions by a board-certified veterinary pathologist.

Lung immunofluorescence

Adult *Robo4*$^{+/AP}$ mice were killed by CO_2 asphyxiation. Chest cavities were opened, and lungs were inflated with optimum cutting temperature (OCT) embedding compound and frozen quickly in OCT on dry ice. Lung sections were stained for alkaline phosphatase activity, denoting areas of Robo4 expression as described (*15*). Sections were then stained with primary antibodies against Slit2 (E-20; Santa Cruz Biotechnology) or CD31 (BD Pharmingen) followed by fluorescent secondary antibody staining.

Cytokine or chemokine array

Six hours after CLP, mice were heavily anesthetized. Whole blood was drawn into acid-citrate-dextrose solution (ACD) (~1:9 volume) from the carotid artery. Plasma was isolated by centrifugation of blood at 4000*g* for 10 min. Plasma was analyzed by Quansys Biosciences to quantify cytokine and chemokine levels. Data are presented as mean ± SEM of six mice per condition. For H5N1 samples, 6 days after infection, clarified mouse lung homogenates were prepared and inflammatory cytokine and chemokine profiles were determined with mouse cytokine and chemokine arrays (Quansys Biosciences). Data are presented as mean ± SEM of three groups of pooled mice.

Lung virus titer determination

These assays were performed as described (*59*).

Lung development

Embryos were dissected, fixed, and rehydrated as described (*60*). Lungs were serially immunostained with primary antibody to platelet endothelial cell adhesion molecule (clone MEC 13.3; BD Pharmingen) and primary antibody to E-cadherin (clone ECCD-2; Zymed) with a variation of the described method (*60*).

Neutrophil migration

HL-60 cells were grown under standard conditions with RPMI 1640 supplemented with 10% FBS and 1% penicillin–streptomycin. Cells induced with 1.2% DMSO were obtained by seeding HL-60 cells at 3×10^6 per milliliter in growth media and culturing for 4 to 6 days (*61*). Human PMNs were isolated from healthy adult donor whole blood with ACD using techniques previously described (*62*). The leukocyte chemoattractant *N*-formyl-Met-Leu-Phe (*f*MLP) (10 μM), along with Slit2 or Mock, was placed in the lower wells of a 48-well chemotaxis chamber (Neuroprobe). A fibronectin-coated (overnight at 4°C) polycarbonate membrane (5 μm; Neuroprobe) was placed between the chemoattractant and the cells. HL-60 cells induced with DMSO or hPMNs (50 μl, 50,000 cells) were added to the upper wells. After incubating at 37°C for 2 hours, cells on the top surface of the filter were removed and cells that had migrated through the filter onto the undersurface were fixed and stained using Diff-Quik stain set (Dade Behring). Migrated cells in five

high-power fields were counted and migration was expressed as the percent of cells migrated relative to cells migrated toward *f*MLP in the absence of Slit2 or Mock. Data are presented as SEM of at least three independent experiments.

Quantitative polymerase chain reaction

For hPMN studies, RNA was isolated using Trizol (Invitrogen) and quantitative polymerase chain reaction was performed with TaqMan assays (Applied Biosystems) for human *GAPDH* and *ROBO1* to *ROBO4*.

Endothelial cell migration

Equimolar huRobo1 siRNA (Hs_Robo1_11_HP; Qiagen), huRobo4 siRNA (Hs_Robo4_1_HP), or AllStars Negative Control siRNA transfection complexes were formed according to standard protocol and added to human umbilical vein endothelial cells (Lonza). Companion dishes were prepared to assess knockdown of gene expression. Forty-eight hours later, cells were serum-starved, and 30,000 cells were seeded per fibronectin-coated 6.5-mm Transwell filters with an 8-μm pore size (Costar). Cells were allowed to migrate to 2 nM VEGF in the presence of 10 nM Slit2N or Mock for 20 hours. Filters were removed, migrated cells were counterstained, and eight high-power fields per filter were counted. Relative migration over unstimulated was determined, and data are presented as mean ± SEM of at least three independent experiments performed in at least triplicate.

Statistical analysis

The Student's *t* test, log rank test, or analysis of variance with post hoc tests, where appropriate, was used to assess statistical significance. A P value of <0.05 was considered statistically significant.

SUPPLEMENTARY MATERIAL

www.sciencetranslationalmedicine.org/cgi/content/full/2/23/23ra19/DC1
Fig. S1. Slit2N stabilizes VE-cadherin at the cell surface.
Fig. S2. Slit2N inhibits LPS-induced cell infiltrates in a dose-dependent manner.
Fig. S3. Slit does not reduce migration of primary human PMNs.
Fig. S4. Slit2 protein is expressed throughout the lung in close proximity to the endothelium.
Fig. S5. Significant lung injury is absent during CLP.
Fig. S6. Loss of *Robo4* does not significantly change cytokine receptor expression in vivo.
Fig. S7. Loss of Robo4 does not affect patterning of the vascular endothelium in the early developing lung.
Fig. S8. Loss of Robo4 does not affect patterning of the vascular endothelium in the developing lung.
Fig. S9. Robo1 and Robo4 are necessary for Slit2N-mediated inhibition of VEGF-induced HUVEC migration.

REFERENCES AND NOTES

1. M. L. Perdue, D. E. Swayne, Public health risk from avian influenza viruses. *Avian Dis.* **49**, 317–327 (2005).
2. P. Bossi, D. Garin, A. Guihot, F. Gay, J. M. Crance, T. Debord, B. Autran, F. Bricaire, Bioterrorism: Management of major biological agents. *Cell. Mol. Life Sci.* **63**, 2196–2212 (2006).
3. J. C. De Jong, G. F. Rimmelzwaan, R. A. Fouchier, A. D. Osterhaus, Influenza virus: A master of metamorphosis. *J. Infect.* **40**, 218–228 (2000).
4. S. S. Morse, R. L. Garwin, P. J. Olsiewski, Public health. Next flu pandemic: What to do until the vaccine arrives? *Science* **314**, 929 (2006).
5. Y. C. Hsieh, T. Z. Wu, D. P. Liu, P. L. Shao, L. Y. Chang, C. Y. Lu, C. Y. Lee, F. Y. Huang, L. M. Huang, Influenza pandemics: Past, present and future. *J. Formos. Med. Assoc.* **105**, 1–6 (2006).
6. C. J. Hackett, Innate immune activation as a broad-spectrum biodefense strategy: Prospects and research challenges. *J. Allergy Clin. Immunol.* **112**, 686–694 (2003).
7. C. Nathan, Points of control in inflammation. *Nature* **420**, 846–852 (2002).
8. W. C. Aird, The role of the endothelium in severe sepsis and multiple organ dysfunction syndrome. *Blood* **101**, 3765–3777 (2003).
9. D. M. Morens, A. S. Fauci, Dengue and hemorrhagic fever: A potential threat to public health in the United States. *JAMA* **299**, 214–216 (2008).
10. L. B. Ware, M. A. Matthay, The acute respiratory distress syndrome. *N. Engl. J. Med.* **342**, 1334–1349 (2000).
11. E. Abraham, P. F. Laterre, J. Garbino, S. Pingleton, T. Butler, T. Dugernier, B. Margolis, K. Kudsk, W. Zimmerli, P. Anderson, M. Reynaert, D. Lew, W. Lesslauer, S. Passe, P. Cooper, A. Burdeska, M. Modi, A. Leighton, M. Salgo, P. Van der Auwera; Lenercept Study Group, Lenercept (p55 tumor necrosis factor receptor fusion protein) in severe sepsis and early septic shock: A randomized, double-blind, placebo-controlled, multicenter phase III trial with 1,342 patients. *Crit. Care Med.* **29**, 503–510 (2001).
12. N. F. Crum, E. R. Lederman, M. R. Wallace, Infections associated with tumor necrosis factor-α antagonists. *Medicine* **84**, 291–302 (2005).
13. L. Cronin, D. J. Cook, J. Carlet, D. K. Heyland, D. King, M. A. Lansang, C. J. Fisher Jr., Corticosteroid treatment for sepsis: A critical appraisal and meta-analysis of the literature. *Crit. Care Med.* **23**, 1430–1439 (1995).
14. M. B. Atkins, M. T. Lotze, J. P. Dutcher, R. I. Fisher, G. Weiss, K. Margolin, J. Abrams, M. Sznol, D. Parkinson, M. Hawkins, C. Paradise, L. Kunkel, S. A. Rosenberg, High-dose recombinant interleukin 2 therapy for patients with metastatic melanoma: Analysis of 270 patients treated between 1985 and 1993. *J. Clin. Oncol.* **17**, 2105–2116 (1999).
15. C. A. Jones, N. R. London, H. Chen, K. W. Park, D. Sauvaget, R. A. Stockton, J. D. Wythe, W. Suh, F. Larrieu-Lahargue, Y. S. Mukouyama, P. Lindblom, P. Seth, A. Frias, N. Nishiya, M. H. Ginsberg, H. Gerhardt, K. Zhang, D. Y. Li, Robo4 stabilizes the vascular network by inhibiting pathologic angiogenesis and endothelial hyperpermeability. *Nat. Med.* **14**, 448–453 (2008).
16. C. A. Jones, N. Nishiya, N. R. London, W. Zhu, L. K. Sorensen, A. C. Chan, C. J. Lim, H. Chen, Q. Zhang, P. G. Schultz, A. M. Hayallah, K. R. Thomas, M. Famulok, K. Zhang, M. H. Ginsberg, D. Y. Li, Slit2–Robo4 signalling promotes vascular stability by blocking Arf6 activity. *Nat. Cell Biol.* **11**, 1325–1331 (2009).
17. L. Huminiecki, M. Gorn, S. Suchting, R. Poulsom, R. Bicknell, Magic roundabout is a new member of the roundabout receptor family that is endothelial specific and expressed at sites of active angiogenesis. *Genomics* **79**, 547–552 (2002).
18. K. W. Park, C. M. Morrison, L. K. Sorensen, C. A. Jones, Y. Rao, C. B. Chien, J. Y. Wu, L. D. Urness, D. Y. Li, Robo4 is a vascular-specific receptor that inhibits endothelial migration. *Dev. Biol.* **261**, 251–267 (2003).
19. C. A. Dinarello, Proinflammatory and anti-inflammatory cytokines as mediators in the pathogenesis of septic shock. *Chest* **112**, 321S–329S (1997).
20. A. Chédotal, Slits and their receptors. *Adv. Exp. Med. Biol.* **621**, 65–80 (2007).
21. E. Dejana, F. Orsenigo, M. G. Lampugnani, The role of adherens junctions and VE-cadherin in the control of vascular permeability. *J. Cell Sci.* **121**, 2115–2122 (2008).
22. D. Vestweber, VE-cadherin: The major endothelial adhesion molecule controlling cellular junctions and blood vessel formation. *Arterioscler. Thromb. Vasc. Biol.* **28**, 223–232 (2008).
23. M. D. Potter, S. Barbero, D. A. Cheresh, Tyrosine phosphorylation of VE-cadherin prevents binding of p120- and β-catenin and maintains the cellular mesenchymal state. *J. Biol. Chem.* **280**, 31906–31912 (2005).
24. K. Xiao, J. Garner, K. M. Buckley, P. A. Vincent, C. M. Chiasson, E. Dejana, V. Faundez, A. P. Kowalczyk, p120-catenin regulates clathrin-dependent endocytosis of VE-cadherin. *Mol. Biol. Cell* **16**, 5141–5151 (2005).
25. A. Gampel, L. Moss, M. C. Jones, V. Brunton, J. C. Norman, H. Mellor, VEGF regulates the mobilization of VEGFR2/KDR from an intracellular endothelial storage compartment. *Blood* **108**, 2624–2631 (2006).
26. G. Matute-Bello, C. W. Frevert, T. R. Martin, Animal models of acute lung injury. *Am. J. Physiol. Lung Cell. Mol. Physiol.* **295**, L379–L399 (2008).
27. M. Corada, F. Liao, M. Lindgren, M. G. Lampugnani, F. Breviario, R. Frank, W. A. Muller, D. J. Hicklin, P. Bohlen, E. Dejana, Monoclonal antibodies directed to different regions of vascular endothelial cadherin extracellular domain affect adhesion and clustering of the protein and modulate endothelial permeability. *Blood* **97**, 1679–1684 (2001).
28. W. J. Hubbard, M. Choudhry, M. G. Schwacha, J. D. Kerby, L. W. Rue III, K. I. Bland, I. H. Chaudry, Cecal ligation and puncture. *Shock* **24**, 52–57 (2005).
29. M. D. de Jong, C. P. Simmons, T. T. Thanh, V. M. Hien, G. J. Smith, T. N. Chau, D. M. Hoang, N. V. Chau, T. H. Khanh, V. C. Dong, P. T. Qui, B. V. Cam, Q. Ha do, Y. Guan, J. S. Peiris, N. T. Chinh, T. T. Hien, J. Farrar, Fatal outcome of human influenza A (H5N1) is associated with high viral load and hypercytokinemia. *Nat. Med.* **12**, 1203–1207 (2006).
30. D. Kobasa, S. M. Jones, K. Shinya, J. C. Kash, J. Copps, H. Ebihara, H. Ebihara, Y. Hatta, J. H. Kim, P. Halfmann, M. Hatta, F. Feldmann, J. B. Alimonti, L. Fernando, Y. Li, M. G. Katze, H. Feldmann, Y. Kawaoka, Aberrant innate immune response in lethal infection of macaques with the 1918 influenza virus. *Nature* **445**, 319–323 (2007).
31. Writing Committee of the Second World Health Organization Consultation on Clinical Aspects of Human Infection with Avian Influenza A (H5N1) Virus; A. N. Abdel-Ghafar, T. Chotpitayasunondh, Z. Gao, F. G. Hayden, D. H. Nguyen, M. D. de Jong, A. Naghdaliyev, J. S. Peiris, N. Shindo, S. Soeroso, T. M. Uyeki, Update on avian influenza A (H5N1) virus infection in humans. *N. Engl. J. Med.* **358**, 261–273 (2008).

32. K. A. Sepkowitz, Forever unprepared—The predictable unpredictability of pathogens. *N. Engl. J. Med.* **361**, 120–121 (2009).
33. S. P. Layne, A. S. Monto, J. K. Taubenberger, Pandemic influenza: An inconvenient mutation. *Science* **323**, 1560–1561 (2009).
34. M. Seeger, G. Tear, D. Ferres-Marco, C. S. Goodman, Mutations affecting growth cone guidance in *Drosophila*: Genes necessary for guidance toward or away from the midline. *Neuron* **10**, 409–426 (1993).
35. J. Xian, K. J. Clark, R. Fordham, R. Pannell, T. H. Rabbitts, P. H. Rabbitts, Inadequate lung development and bronchial hyperplasia in mice with a targeted deletion in the *Dutt1/Robo1* gene. *Proc. Natl. Acad. Sci. U.S.A.* **98**, 15062–15066 (2001).
36. U. Grieshammer, M. Le, A. S. Plump, F. Wang, M. Tessier-Lavigne, G. R. Martin, SLIT2-mediated ROBO2 signaling restricts kidney induction to a single site. *Dev. Cell* **6**, 709–717 (2004).
37. C. Sabatier, A. S. Plump, M. Le, K. Brose, A. Tamada, F. Murakami, E. Y. Leem, M. Tessier-Lavigne, The divergent Robo family protein Rig-1/Robo3 is a negative regulator of Slit responsiveness required for midline crossing by commissural axons. *Cell* **117**, 157–169 (2004).
38. S. T. Qureshi, R. Medzhitov, Toll-like receptors and their role in experimental models of microbial infection. *Genes Immun.* **4**, 87–94 (2003).
39. J. Y. Wu, L. Feng, H. T. Park, N. Havlioglu, L. Wen, H. Tang, K. B. Bacon, Z. Jiang, X. Zhang, Y. Rao, The neuronal repellent Slit inhibits leukocyte chemotaxis induced by chemotactic factors. *Nature* **410**, 948–952 (2001).
40. S. H. Mei, S. D. McCarter, Y. Deng, C. H. Parker, W. C. Liles, D. J. Stewart, Prevention of LPS-induced acute lung injury in mice by mesenchymal stem cells overexpressing angiopoietin 1. *PLoS Med.* **4**, e269 (2007).
41. P. Seth, Y. Lin, J. Hanai, V. Shivalingappa, M. P. Duyao, V. P. Sukhatme, Magic roundabout, a tumor endothelial marker: Expression and signaling. *Biochem. Biophys. Res. Commun.* **332**, 533–541 (2005).
42. H. Sheldon, M. Andre, J. A. Legg, P. Heal, J. M. Herbert, R. Sainson, A. S. Sharma, J. K. Kitajewski, V. L. Heath, R. Bicknell, Active involvement of Robo1 and Robo4 in filopodia formation and endothelial cell motility mediated via WASP and other actin nucleation-promoting factors. *FASEB J.* **23**, 513–522 (2009).
43. H. Hu, Cell-surface heparan sulfate is involved in the repulsive guidance activities of Slit2 protein. *Nat. Neurosci.* **4**, 695–701 (2001).
44. E. Hohenester, S. Hussain, J. A. Howitt, Interaction of the guidance molecule Slit with cellular receptors. *Biochem. Soc. Trans.* **34**, 418–421 (2006).
45. P. Steigemann, A. Molitor, S. Fellert, H. Jäckle, G. Vorbrüggen, Heparan sulfate proteoglycan syndecan promotes axonal and myotube guidance by Slit/Robo signaling. *Curr. Biol.* **14**, 225–230 (2004).
46. S. Suchting, P. Heal, K. Tahtis, L. M. Stewart, R. Bicknell, Soluble Robo4 receptor inhibits in vivo angiogenesis and endothelial cell migration. *FASEB J.* **19**, 121–123 (2005).
47. D. Vestweber, M. Winderlich, G. Cagna, A. F. Nottebaum, Cell adhesion dynamics at endothelial junctions: VE-cadherin as a major player. *Trends Cell Biol.* **19**, 8–15 (2009).
48. Y. Wallez, P. Huber, Endothelial adherens and tight junctions in vascular homeostasis, inflammation and angiogenesis. *Biochim. Biophys. Acta* **1778**, 794–809 (2008).
49. J. Gavard, J. S. Gutkind, VEGF controls endothelial-cell permeability by promoting the β-arrestin-dependent endocytosis of VE-cadherin. *Nat. Cell Biol.* **8**, 1223–1234 (2006).
50. A. M. Ferreira, C. J. McNeil, K. M. Stallaert, K. A. Rogers, M. Sandig, Interleukin-1β reduces transcellular monocyte diapedesis and compromises endothelial adherens junction integrity. *Microcirculation* **12**, 563–579 (2005).
51. D. J. Angelini, S. W. Hyun, D. N. Grigoryev, P. Garg, P. Gong, I. S. Singh, A. Passaniti, J. D. Hasday, S. E. Goldblum, TNF-α increases tyrosine phosphorylation of vascular endothelial cadherin and opens the paracellular pathway through fyn activation in human lung endothelia. *Am. J. Physiol. Lung Cell. Mol. Physiol.* **291**, L1232–L1245 (2006).
52. J. Gavard, V. Patel, J. S. Gutkind, Angiopoietin-1 prevents VEGF-induced endothelial permeability by sequestering Src through mDia. *Dev. Cell* **14**, 25–36 (2008).
53. P. Villa, G. Sartor, M. Angelini, M. Sironi, M. Conni, P. Gnocchi, A. M. Isetta, G. Grau, W. Buurman, L. J. van Tits, Pattern of cytokines and pharmacomodulation in sepsis induced by cecal ligation and puncture compared with that induced by endotoxin. *Clin. Diagn. Lab. Immunol.* **2**, 549–553 (1995).
54. N. Coltel, V. Combes, N. H. Hunt, G. E. Grau, Cerebral malaria—A neurovascular pathology with many riddles still to be solved. *Curr. Neurovasc. Res.* **1**, 91–110 (2004).
55. N. R. London, K. J. Whitehead, D.Y. Li, Endogenous endothelial cell signaling systems maintain vascular stability. *Angiogenesis* **12**, 149–158 (2009).
56. R. N. Gomes, R. T. Figueiredo, F. A. Bozza, P. Pacheco, R. T. Amâncio, A. P. Laranjeira, H. C. Castro-Faria-Neto, P. T. Bozza, M. T. Bozza, Increased susceptibility to septic and endotoxic shock in monocyte chemoattractant protein 1/cc chemokine ligand 2-deficient mice correlates with reduced interleukin 10 and enhanced macrophage migration inhibitory factor production. *Shock* **26**, 457–463 (2006).
57. J. Moitra, S. Sammani, J. G. Garcia, Re-evaluation of Evans Blue dye as a marker of albumin clearance in murine models of acute lung injury. *Transl. Res.* **150**, 253–265 (2007).
58. N. Gupta, X. Su, B. Popov, J. W. Lee, V. Serikov, M. A. Matthay, Intrapulmonary delivery of bone marrow-derived mesenchymal stem cells improves survival and attenuates endotoxin-induced acute lung injury in mice. *J. Immunol.* **179**, 1855–1863 (2007).
59. R. W. Sidwell, K. W. Bailey, M. H. Wong, D. L. Barnard, D. F. Smee, In vitro and in vivo influenza virus-inhibitory effects of viramidine. *Antiviral Res.* **68**, 10–17 (2005).
60. R. J. Metzger, O. D. Klein, G. R. Martin, M. A. Krasnow, The branching programme of mouse lung development. *Nature* **453**, 745–750 (2008).
61. S. J. Collins, F. W. Ruscetti, R. E. Gallagher, R. C. Gallo, Terminal differentiation of human promyelocytic leukemia cells induced by dimethyl sulfoxide and other polar compounds. *Proc. Natl. Acad. Sci. U.S.A.* **75**, 2458–2462 (1978).
62. G. A. Zimmerman, T. M. McIntyre, S. M. Prescott, Thrombin stimulates the adherence of neutrophils to human endothelial cells in vitro. *J. Clin. Invest.* **76**, 2235–2246 (1985).

63. Acknowledgments: We thank D. Lim for graphical assistance and K. Thomas, M. Sanguinetti, A. Welm, C. Murtaugh, S. Odelberg, and S. Stanley for critical reading of this manuscript.
Funding: National Heart, Lung, and Blood Institute (NHLBI); National Institute of Allergy and Infectious Diseases (NIAID); Rocky Mountain Regional Center of Excellence in Biodefense and Emerging Infectious Disease; Juvenile Diabetes Research Foundation; HA and Edna Benning Foundation; American Asthma Foundation; National Center for Research Resources Public Health Services research grant UL1-RR025764; and Department of Defense. D.Y.L. is a Burroughs Wellcome Foundation Clinical Scientist in Translational Research and an Established Investigator of the American Heart Association. N.R.L., M.C.P.S., and A.C.C. were supported, respectively, by the Ruth L. Kirschstein National Research Service Award, T-32 Hematology Training Grant, and training grant T32-GM007464. This work was also supported by NIAID contract NO1-AI-15435 (C.W.D. and D.L.B.); a NIH Merit Award 5R37 HL44525-20 (G.A.Z.); and the Sarnoff Cardiovascular Research Foundation Scholar Award, NIH-NHLBI (K08), and the Pulmonary Hypertension Association (D.M.G.). F.A.B. is a research scholar supported by Conselho Nacional de Desenvolvimento Cientifico e Tecnológico (CNPq, Brazil).
Author contributions: N.R.L., W.Z., and D.Y.L. were responsible for project conceptualization, experimental design, and data analysis. N.R.L., G.A.Z., and D.Y.L. were responsible for manuscript preparation. N.R.L., W.Z., and F.A.B. were responsible for performing all experiments or coordinating experimental design and work of others. M.C.P.S., D.M.G., L.K.S., L.C., Y.K., A.C.C., and S.F.P. performed necessary experiments for the manuscript or in response to reviewers. C.W.D., D.L.B., G.A.Z, and M.A.K. provided important expertise, reagents, technical personnel and advice.
Competing interests: N.R.L., W.Z., M.C.P.S., L.K.S., L.C., Y.K., S.F.P., G.A.Z., and D.Y.L. are or were previously employed by the University of Utah, which has filed intellectual property surrounding the therapeutic uses of targeting Robo4 and with the intent to license this body of intellectual property for commercialization. The University of Utah has licensed Robo4 technology to Navigen, a biotechnology company owned in part by the University of Utah Research Foundation. N.R.L. and W.Z. are paid consultants for Navigen, and D.Y.L. is a founder of and is on the Board of Directors of Navigen.

Submitted 25 November 2009
Accepted 26 February 2010
Published 17 March 2010
10.1126/scitranslmed.3000678

Citation: N. R. London, W. Zhu, F. A. Bozza, M. C. P. Smith, D. M. Greif, L. K. Sorensen, L. Chen, Y. Kaminoh, A. C. Chan, S. F. Passi, C. W. Day, D. L. Barnard, G. A. Zimmerman, M. A. Krasnow, D. Y. Li, Targeting Robo4-dependent slit signaling to survive the cytokine storm in sepsis and influenza. *Sci. Transl. Med.* **2**, 23ra19 (2010).

www.sciencetranslationalmedicine.org/cgi/content/full/2/23/23ra19/DC1

Supplementary Materials for

Targeting Robo4-Dependent Slit Signaling to Survive the Cytokine Storm in Sepsis and Influenza

Nyall R. London, Weiquan Zhu, Fernando A. Bozza, Matthew C. P. Smith, Daniel M. Greif, Lise K. Sorensen, Luming Chen, Yuuki Kaminoh, Aubrey C. Chan, Samuel F. Passi, Craig W. Day, Dale L. Barnard, Guy A. Zimmerman, Mark A. Krasnow, Dean Y. Li*

*To whom correspondence should be addressed. E-mail: dean.li@u2m2.utah.edu

Published 17 March 2010, *Sci. Transl. Med.* **2**, 23ra19 (2010)
DOI: 10.1126/scitranslmed.3000678

This PDF file includes:

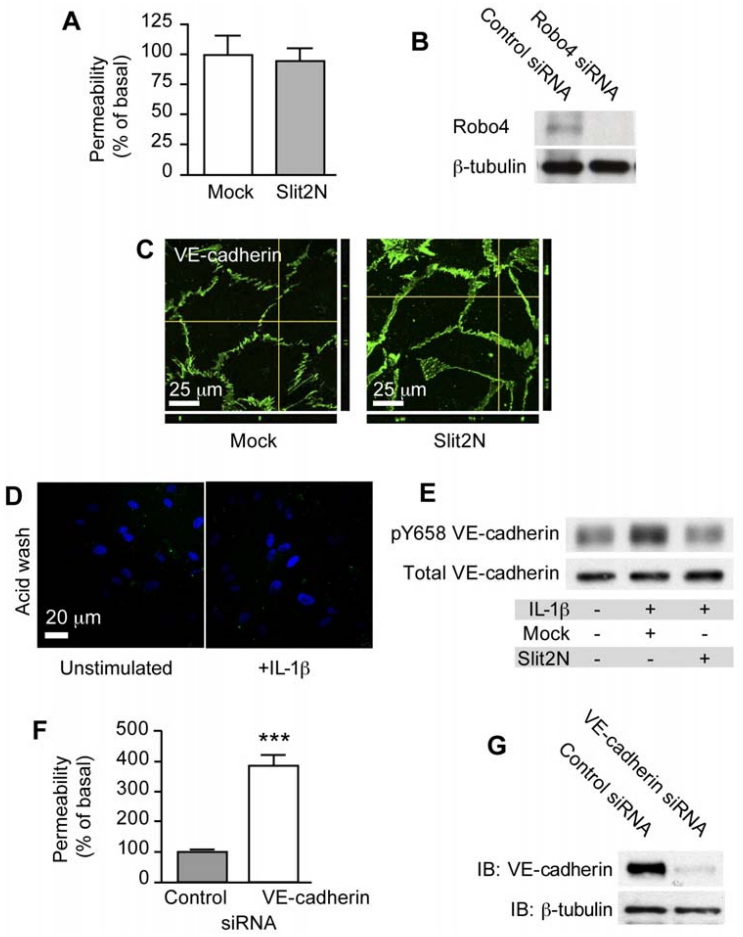

Fig. S1. Slit2N stabilizes VE-cadherin at the cell surface. (**A**) HMVEC-lung were treated with Mock or Slit2N and basal permeability was assessed. (**B**) Robo4 or control siRNA knockdown HMVEC-lung were assessed for Robo4 expression by immunoblot. (**C**) Confocal images of the Z-axis are shown below and to the side as indicated by yellow lines. Enhanced junctional thickness is observed in Slit2N treated cells. (**D**) In the absence of primaquine, detection of IL-1β-induced VE-cadherin internalization is compromised. **(E)** HMVEC-lung were exposed to IL-1β in the presence or absence of Mock or Slit2N followed by immunoblot using a phosphorylation specific antibody against VE-cadherin Y658. (**F**) HMVEC-lung were subjected to control or VE-cadherin siRNA knockdown and barrier function assessed by *in vitro* permeability. (**G**) Western blot analysis confirmed knockdown of VE-cadherin expression. ***P<0.005.

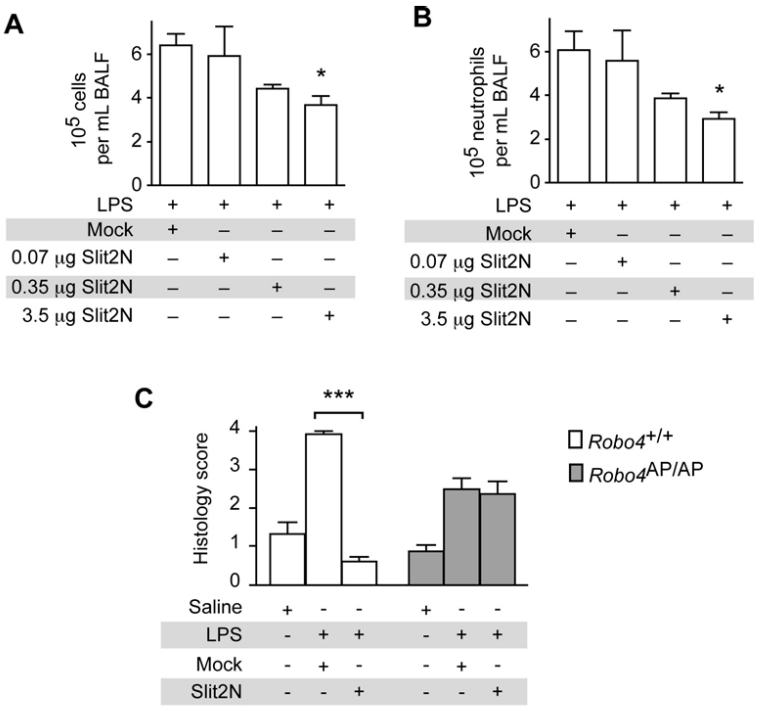

Fig. S2. Slit2N inhibits LPS-induced cell infiltrates in a dose-dependent manner. (**A-B**) Mice were subjected to LPS-induced ALI in the presence of increasing levels of Slit2N. Cell infiltrate and neutrophil counts are shown. N≥4, * P<0.05. (**C**) *Robo4*$^{+/+}$ and *Robo4*$^{AP/AP}$ mice were subjected to LPS-induced ALI in the presence of Mock or Slit2N. Lung sections from these mice were stained for H&E and quantitative histology to assess the degree of lung injury was performed by blinded investigators. N=3, *** P<0.005.

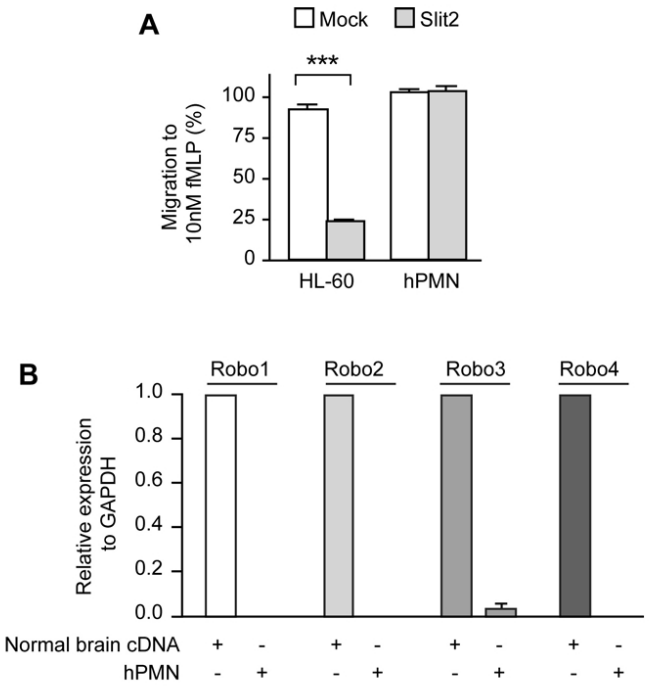

Fig. S3. Slit does not reduce migration of primary human PMNs. (**A**) Cells were subjected to migration to the leukocyte chemoattractant fMLP in the presence of Mock or Slit2. (**B**) RNA was isolated from hPMNs and subjected to quantitative PCR. Brain cDNA was used as a positive control. N=3, *** P<0.005, error bars represent s.e.m.

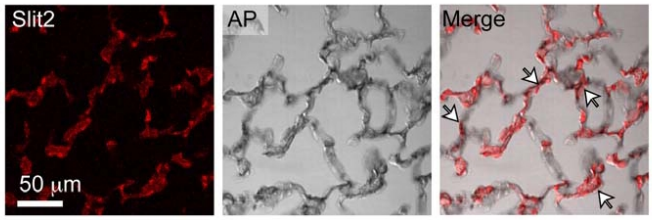

Fig. S4. Slit2 protein is expressed throughout the lung in close proximity to the endothelium. Slit2 (red) co-localizes with Robo4 alkaline phosphatase (AP) expression (black) indicated by white arrows.

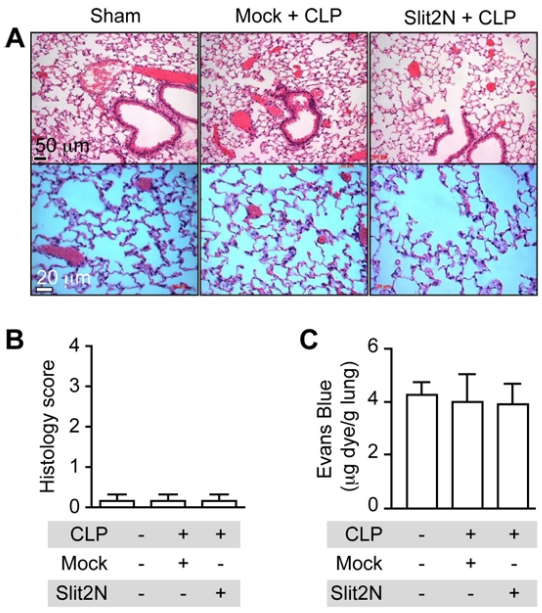

Fig. S5. Significant lung injury is absent during CLP. (**A-C**) Mice were subjected to CLP and treated with Mock or Slit2N. Lung sections were stained with H&E (**A**) and quantitative histology to assess the degree of lung injury performed (**B**) N=3. (**C**) Permeability in the lungs of mice was assessed using Evans Blue Albumin. N=5.

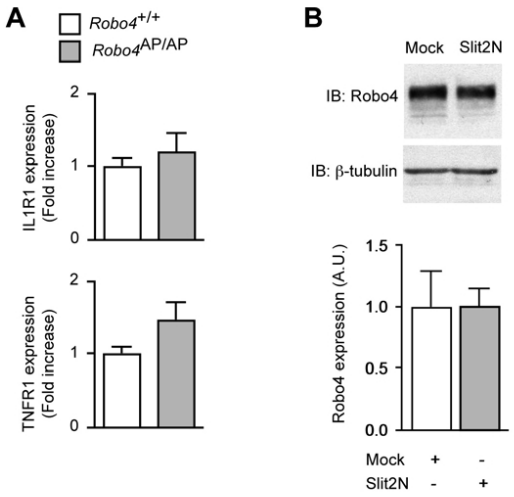

Fig. S6. Loss of *Robo4* does not significantly change cytokine receptor expression *in vivo.* (**A**) RNA from *Robo4*$^{+/+}$ or *Robo4*$^{AP/AP}$ mice was isolated and subjected to qPCR for IL1R1 or TNFR1. N=9 per genotype. (**B**) HMVEC-lung were exposed to Mock or Slit2N treatment and subjected to Western Blot analysis. Densitometric analysis is presented below representative blots.

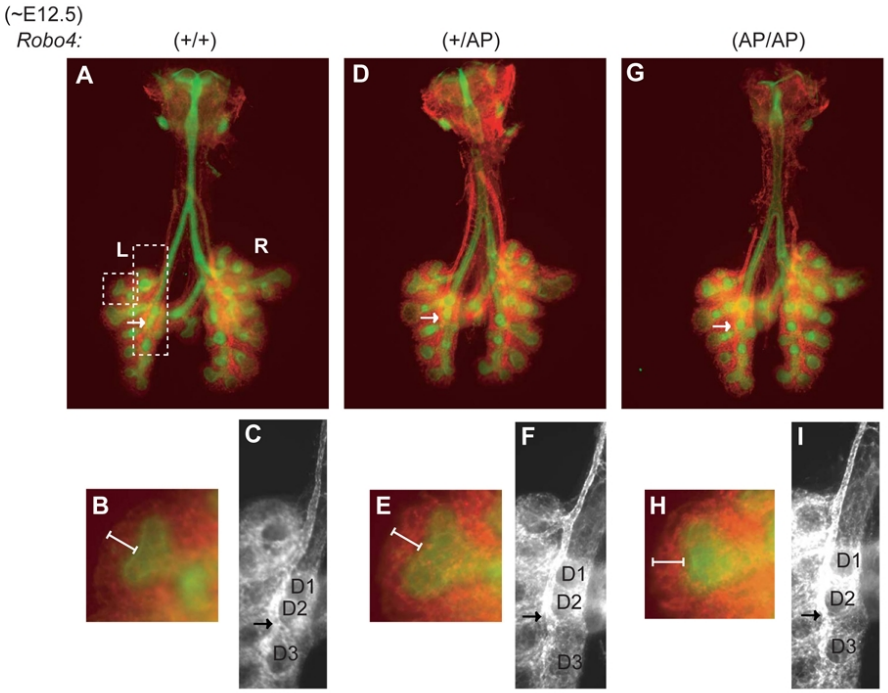

Fig. S7. Loss of Robo4 does not affect patterning of the vascular endothelium in the early developing lung. **A-C, D-F** and **G-I** show $Robo4^{+/+}$, $Robo4^{+/AP}$ and $Robo4^{AP/AP}$ ~E12.5 lungs, respectively, stained for epithelium (E-cadherin, green) and vasculature (CD31, red). Arrows indicate the distal extent of the left pulmonary artery EC tube. **B**, **E**, and **H** are magnified views of the distal branches of the first left lateral secondary airway branch with the white crossbar denoting the thickness of the CD31+ plexus compartment extending linearly outward from the vertex of the distal branches. **C, F**, and **I** show magnified views of the distal left pulmonary artery EC tube regions stained with an antibody directed against CD31. The locations of the first, second and third left dorsal secondary airway buds are denoted by D1, D2 and D3.

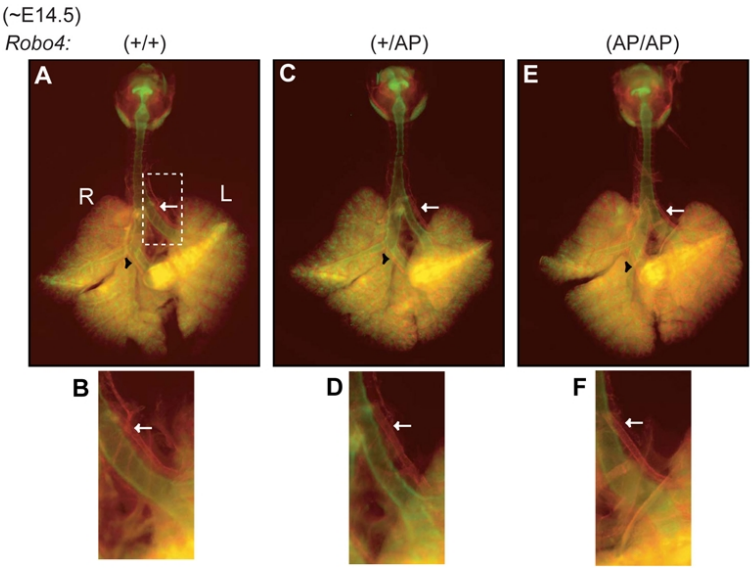

Fig. S8. Loss of Robo4 does not affect patterning of the vascular endothelium in the developing lung. **A-B, C-D** and **E-F** show *Robo4*$^{+/+}$, *Robo4*$^{+/AP}$ and *Robo4*$^{AP/AP}$ ~E14.5 lungs, respectively, stained for lung epithelium (E-cadherin, green) and vascular development (CD31, red). Arrows denote the left pulmonary artery located lateral to the left primary bronchus. The black arrowheads in **A, C,** and **E** mark the branch of the right pulmonary artery supplying the right accessory lobe and located posterior to the right secondary airway branch to the accessory lobe.

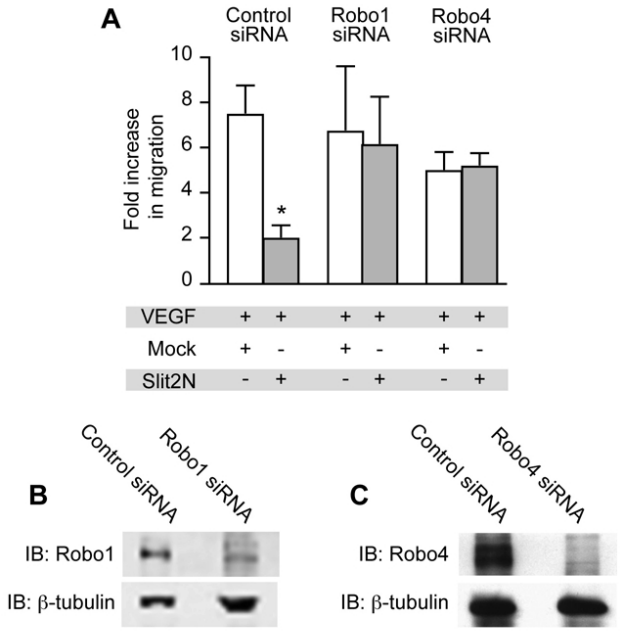

Fig. S9. Robo1 and Robo4 are necessary for Slit2N-mediated inhibition of VEGF-induced HUVEC migration. (**A**) Human umbilical vein endothelial cells were subjected to control, Robo1, or Robo4 siRNA and migrated to VEGF in the presence of Mock or Slit2N. N=3, * $P<0.05$. Western blot analysis confirmed knockdown of Robo1 (**B**) or Robo4 (**C**) expression.

CHAPTER 3

SLIT2-ROBO4 SIGNALLING PROMOTES VASCULAR STABILITY BY BLOCKING ARF6 ACTIVITY

The following chapter is a reprint of a manuscript published in Nature Cell Biology. It was published November 2009, volume 11 (11): pages 1325-1331. Epub October 18, 2009. In addition to myself, the other authors were Chris Jones, Nayouki Nishiya, Weiquan Zhu, Lise Sorensen, Aubrey Chan, C. James Lim, Hayou Chen, Qisheng Zhang, Peter Schultz, Alaa Hayallah, Kirk Thomas, Michael Famulok, Kang Zhang, Mark Ginsberg, and Dean Li. I participated predominantly in the design, execution, and interpretation of the *in vivo* data.

LETTERS

nature cell biology

Slit2–Robo4 signalling promotes vascular stability by blocking Arf6 activity

Christopher A. Jones[1,2,14], Naoyuki Nishiya[3,10,14], Nyall R. London[1,2,14], Weiquan Zhu[1,2], Lise K. Sorensen[2], Aubrey C. Chan[1,2], Chinten J. Lim[3], Haoyu Chen[4,11], Qisheng Zhang[5], Peter G. Schultz[6], Alaa M. Hayallah[7,12], Kirk R. Thomas[2,8], Michael Famulok[7], Kang Zhang[4,13], Mark H. Ginsberg[3,15] and Dean Y. Li[1,2,9,15]

Slit–Roundabout (Robo) signalling has a well-understood role in axon guidance[1–5]. Unlike in the nervous system, however, Slit-dependent activation of an endothelial-specific Robo, Robo4, does not initiate a guidance program. Instead, Robo4 maintains the barrier function of the mature vascular network by inhibiting neovascular tuft formation and endothelial hyperpermeability induced by pro-angiogenic factors[6]. In this study, we used cell biological and biochemical techniques to elucidate the molecular mechanism underlying the maintenance of vascular stability by Robo4. Here, we demonstrate that Robo4 mediates Slit2-dependent suppression of cellular protrusive activity through direct interaction with the intracellular adaptor protein paxillin and its paralogue, Hic-5. Formation of a Robo4–paxillin complex at the cell surface blocks activation of the small GTPase Arf6 and, consequently, Rac by recruitment of Arf-GAPs (ADP-ribosylation factor- directed GTPase-activating proteins) such as GIT1. Consistent with these *in vitro* studies, inhibition of Arf6 activity *in vivo* phenocopies Robo4 activation by reducing pathologic angiogenesis in choroidal and retinal vascular disease and VEGF-165 (vascular endothelial growth factor-165)-induced retinal hyperpermeability. These data reveal that a Slit2–Robo4–paxillin–GIT1 network inhibits the cellular protrusive activity underlying neovascularization and vascular leak, and identify a new therapeutic target for ameliorating diseases involving the vascular system.

In both developmental and pathologic settings, cells migrate by orienting protrusive events in response to attractive and repulsive cues. Slit2–Robo4 signalling has been shown previously to inhibit migration of cells towards a soluble chemoattractant gradient[7,8]. In addition to chemoattractants, immobilized extracellular matrix proteins, such as fibronectin, have a critical role in regulating cellular motility during development and disease[9], and gradients of fibronectin direct migration in a process called haptotaxis. We determined whether Slit2–Robo4 signalling modulates extracellular matrix-driven motility, using HEK 293 cells expressing full-length Robo4 or a cytoplasmic tail-domain deletion mutant containing only the ectodomain and the transmembrane domain (Robo4 ED–TM; Fig. 1a). We induced these cells to migrate to fibronectin in the absence (mock) and presence of Slit2, and found that Slit2 inhibited the motility of cells expressing Robo4, but not Robo4 ED–TM (Fig. 1b).

Migrating cells protrude in the forward direction and form new attachments to the extracellular matrix[9]. These newly formed attachments lead to adhesion-induced activation of the small GTPase Rac, which creates broad protrusive structures called lamellipodia through localized actin polymerization[10]. When detached cells adhere, adhesion-induced Rac activation leads to unpolarized lamellipodial extension, resulting in spreading[11]. As cell spreading is an integral part of migration on the extracellular matrix, we assessed whether Slit2–Robo4 signalling inhibits this process. We found that although cells expressing Robo4 adhered normally to fibronectin and Slit2 (data not shown), they spread significantly less in the presence of Slit2 than cells expressing Robo4 ED–TM or LacZ (Fig. 1c, d).

The inability of Robo4 ED–TM to inhibit spreading showed that the cytoplasmic tail is required for this activity. To test whether it is also sufficient for inhibition of spreading, we generated an αIIb integrin–Robo4 chimaeric protein (Fig. 1a), which enabled initiation of Robo4 signalling with fibrinogen, a ligand for αIIb:β3 integrin. Cells expressing αIIb:β3

[1]Department of Oncological Sciences, University of Utah, Salt Lake City, UT 84112, USA. [2]Molecular Medicine Program, University of Utah, Salt Lake City, UT 84112, USA. [3]Department of Medicine, University of California San Diego, La Jolla, CA 92093-0726, USA. [4]Department of Ophthalmology, University of Utah, Salt Lake City, UT 84112, USA. [5]School of Pharmacy, University of North Carolina at Chapel Hill, NC 27599, USA. [6]Department of Chemistry and The Skaggs Institute for Chemical Biology, The Scripps Research Institute, La Jolla, CA 92037, USA. [7]LIMES Program Unit Chemical Biology & Medicinal Chemistry, c/o Kekulé Institut für Organische Chemie und Biochemie, University of Bonn, Gerhard-Domagk-Strae 1, 53121 Bonn, Germany. [8]Division of Haematology, Department of Medicine, University of Utah, Salt Lake City, UT 84112, USA. [9]Division of Cardiology, Department of Medicine, University of Utah, Salt Lake City, UT 84112, USA. [10]Current address: Department of Microbial Chemical Biology and Drug Discovery, Iwate Medical University School of Pharmaceutical Sciences, 2-1-1 Nishitokuta, Yahaba, Shiwa-gun, Iwate 028-3694, Japan. [11]Current address: Joint Shantou International Eye Centre, Shantou University and Chinese University Hong Kong, Shantou, China. [12]Current address: Department of Pharmaceutical Organic Chemistry, Faculty of Pharmacy, Assiut University, Assiut 71526, Egypt. [13]Current address: University of California at San Diego School of Medicine and VASDHS Centre for Human Genetics and Genomics, La Jolla, CA 92093-0838, USA.
[14]These authors contributed equally to this work
[15]Correspondence should be addressed to D.Y. L. or M.H.G. (e-mails: dean.li@hmbg.utah.edu; mhginsberg@ucsd.edu).

Received 22 May 2009; accepted 28 July 2009; published online 18 October 2009; DOI: 10.1038/ncb1976

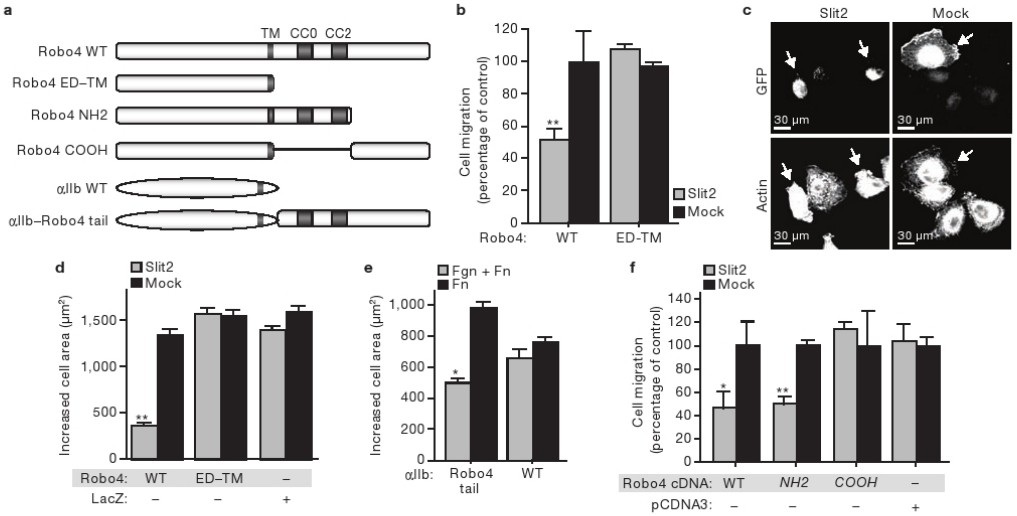

Figure 1 The Robo4 cytoplasmic tail suppresses fibronectin-induced protrusive activity. (**a**) Schematic representation of cDNA constructs used in migration and spreading assays. TM, transmembrane domain. CC0 and CC2 are conserved cytoplasmic signalling motifs found in Robo family members. (**b–d**, **f**) HEK 293 cells expressing GFP and the indicated constructs were subjected to haptotaxis migration assays (**b**, **f**) or spreading assays (**c**, **d**) on fibronectin and mock or Slit2. Arrows indicate GFP-positive cells. (**e**) CHO-K1 cells stably expressing αIIb integrin or αIIb integrin–Robo4 cytoplasmic tail were subjected to spreading assays on fibronectin (Fn) or fibronectin and fibrinogen (Fn + Fgn). Cell area was determined using ImageJ software. For migration assays, GFP-positive cells on the underside of the filter were counted and migration on fibronectin or mock membranes was set at 100% ($n = 3$, in triplicate). For spreading assays, the area of GFP-positive cells was determined using ImageJ ($n = 3$, 150 cells per experiment). Expression of Robo4 constructs was verified by immunoblotting (data not shown). $^{*}P < 0.05$; $^{**}P < 0.005$. Error bars indicate the mean ± s.e.m. WT, wild type. Mock, a sham preparation of Slit2. αIIb–Robo4, αIIb integrin–Robo4. pCDNA3, empty vector.

integrin spread equivalently on fibronectin alone, and a mixture of fibronectin and fibrinogen, whereas αIIb integrin–Robo4:β3-expressing cells spread significantly less in the presence of fibrinogen (Fig. 1e).

To define the region of the Robo4 cytoplasmic tail that is required for inhibition of fibronectin-induced protrusive activity, cells expressing Robo4 deletion constructs (Fig. 1a) were subjected to haptotaxis assays. Migration of cells expressing Robo4 NH2, but not Robo4 COOH, was inhibited by Slit2 (Fig. 1f), indicating the necessity and sufficiency of the amino-terminal half of the Robo4 tail for suppressing cell motility elicited by the extracellular matrix.

Identification of the region of the Robo4 cytoplasmic tail that confers functional activity allowed us to search for cytoplasmic components that might regulate Robo4 signal transduction. Using the N-terminal half of the Robo4 tail as bait, a yeast two-hybrid screen of a human aortic cDNA library identified a member of the paxillin family of adaptor proteins, Hic-5, as a potential Robo4-interacting protein (Supplementary Information, Fig. S1).

Hic-5 and its paralogue, paxillin, show cell-type-specific expression[12,13]. Western blotting of CHO-K1, HEK 293 and NIH3T3 cell lysates with antibodies against Hic-5 and paxillin detected paxillin in each cell line, whereas Hic-5 was only found in CHO-K1 and NIH3T3 cells (Supplementary Information, Fig. S1d). As functional studies used HEK 293 cells, this result suggested that paxillin interacts with Robo4 to regulate cell migration. As observed with Hic-5 (Supplementary Information, Fig. S1c), paxillin was identified in Robo4 immunoprecipitates of cells expressing paxillin and the Robo4 cytoplasmic tail, but not paxillin alone (Fig. 2a).

As Slit2 activates Robo4 (refs 7, 8, 14, 15), we asked whether Slit2 stimulation regulates the interaction between Robo4 and paxillin. Full-length Robo4 was immunoprecipitated from cell lysates after incubation in the absence and presence of Slit2, and endogenous paxillin was only detected in Robo4 immunoprecipitates after Slit2 treatment (Fig. 2b).

We defined the region of Robo4 that is required for interaction with paxillin by generating GST–Robo4 fusion proteins spanning the cytoplasmic tail (Supplementary Information, Fig. S2a, b), and performing *in vitro* binding assays with purified recombinant paxillin (Supplementary Information, Fig. S2c, d). We identified a 70-amino-acid fragment of the N-terminal half of the Robo4 tail as the region that mediates interaction with paxillin (Supplementary Information, Fig. S2d). Deletion of this region prevented interaction with paxillin, as well as the known Robo family-binding protein Mena (murine enabled; data not shown)[7,16]. As Mena interacts with Robo through the Robo CC2 motif, which lies outside the deleted region, these binding data suggested that elimination of amino acids 604–674 affects conformation of the Robo4 tail. We then created smaller deletions within this 70-amino-acid stretch and performed additional *in vitro* binding assays (data not shown). Using this approach we identified a mutant GST–Robo4 fusion protein lacking 35 amino acids (604–639) that failed to bind paxillin, but retained interaction with Mena (Fig. 2c). This region of Robo4 is subsequently referred to as the paxillin interaction motif (PIM; Supplementary Information, Fig. S2e). We confirmed the importance of this region in promoting interaction with endogenous paxillin using co-immunoprecipitation from cells expressing wild-type Robo4 cytoplasmic tail or Robo4ΔPIM (Fig. 2d).

We next determined whether the PIM is important for receptor activity by performing functional assays with cells expressing Robo4ΔPIM. This mutant form of the receptor failed to inhibit fibronectin-induced

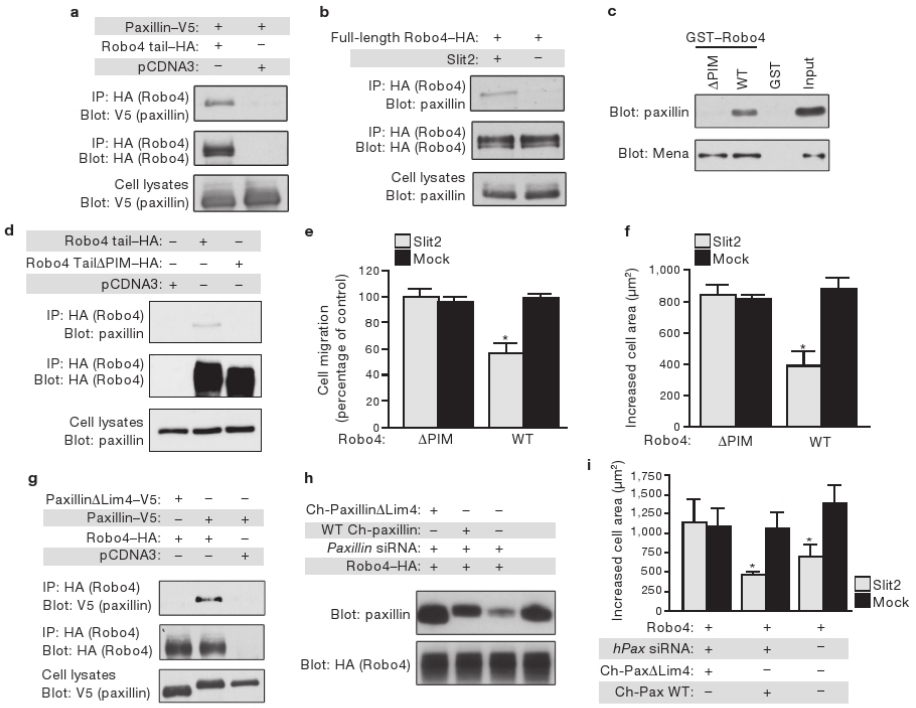

Figure 2 Robo4–paxillin interaction is required for Slit2-dependent inhibition of protrusive activity. (**a**) Lysates from HEK 293 cells expressing paxillin–V5 and Robo4 cytoplasmic tail–HA or empty vector (pcDNA3) were immunoprecipitated with HA antibodies and immunoblotted with V5 antibodies. (**b**) Lysates from Slit2-stimulated HEK 293 cells expressing full-length Robo4–HA were immunoprecipitated with HA antibodies and immunoblotted with paxillin antibodies. (**c**) Purified GST–Robo4 wild type or GST–Robo4ΔPIM were incubated with recombinant purified paxillin or *in vitro* transcribed/translated Mena–V5, precipitated with glutathione agarose, and immunoblotted with paxillin or V5 antibodies. (**d**) Lysates from HEK 293 cells expressing wild-type Robo4 cytoplasmic tail–HA, Robo4ΔPIM cytoplasmic tail–HA or empty vector (pcDNA3) were immunoprecipitated with HA antibodies and immunoblotted with paxillin antibodies. (**e**, **f**) HEK 293 cells expressing GFP and the indicated constructs were subjected to haptotaxis migration assays **(e)** or spreading assays (**f**) on fibronectin and mock or Slit2. (**g**) Lysates from HEK 293 cells expressing Robo4 cytoplasmic tail–HA and either wild-type paxillin-V5 or paxillinΔLim4–V5 were immunoprecipitated with HA antibodies and immunoblotted with V5 antibodies. (**h**) Endogenous paxillin was depleted in HEK 293 cells using siRNA and reconstituted with wild-type chicken (Ch-) paxillin or Ch-paxillinΔLim4. Lysates were immunoblotted with paxillin antibodies. (**i**) Depleted/reconstituted HEK 293 cells were subjected to spreading assays on fibronectin and mock or Slit2. In migration assays, GFP-positive cells on the underside of the filter were counted and migration on fibronectin/mock membranes was set at 100% ($n = 3$, in triplicate). In spreading assays, the area of GFP-positive cells was determined using ImageJ software ($n = 3$, 150 cells per experiment). Expression of Robo4 constructs was verified by immunoblotting (data not shown). $^*P < 0.05$. Error bars indicate the mean ± s.e.m. Full scans of blots are shown in Supplementary Information, Fig. S6. WT, wild type. Mock, sham preparation of Slit2.

cell migration and spreading in the presence of Slit2 (Fig. 2e, f), demonstrating that the region of the Robo4 tail necessary for paxillin binding is also required for inhibition of protrusive activity.

Although Robo4ΔPIM maintained its interaction with Mena (Fig. 2c), it remained possible that the mutation perturbed interactions between Robo4 and proteins other than paxillin. To investigate this, we generated paxillin mutants that disrupt its association with Robo4. Paxillin is a modular protein composed of N-terminal leucine/aspartic acid (LD) repeats and C-terminal Lim domains[17] (Supplementary Information, Fig. S2f). Analysis of clones recovered from the yeast two-hybrid screen (Supplementary Information, Fig. S1a) suggested that the Lim domains, particularly Lim3 and Lim4, are important for interaction with Robo4. We performed co-immunoprecipitation experiments using cells expressing the Robo4 tail and either paxillin-LD or paxillin-Lim, and found Paxillin-Lim, but not paxillin-LD, was in Robo4 immunoprecipitates (Supplementary Information, Fig. S2g). To clarify which Lim domain is required for binding to Robo4, we made serial deletions from the C terminus of paxillin, co-transfected these with the Robo4 cytoplasmic tail into cells and performed co-immunoprecipitation experiments. Deletion of Lim4 completely abrogated binding between paxillin and Robo4 (Fig. 2g).

Delineation of the Robo4 binding site on paxillin allowed us to evaluate the role of paxillin in Robo4-dependent processes. If paxillin were required for receptor activity, the paxillinΔLim4 mutant, which is unable to interact with Robo4, should fail to inhibit fibronectin-induced spreading in the presence of Slit2. Endogenous paxillin was depleted in Robo4-expressing cells using short interfering RNA (siRNA) and then reconstituted with wild-type chicken paxillin (Ch-paxillin) or Ch-paxillinΔLim4, both of which are resistant to siRNA targeting the endogenous gene (Fig. 2h).

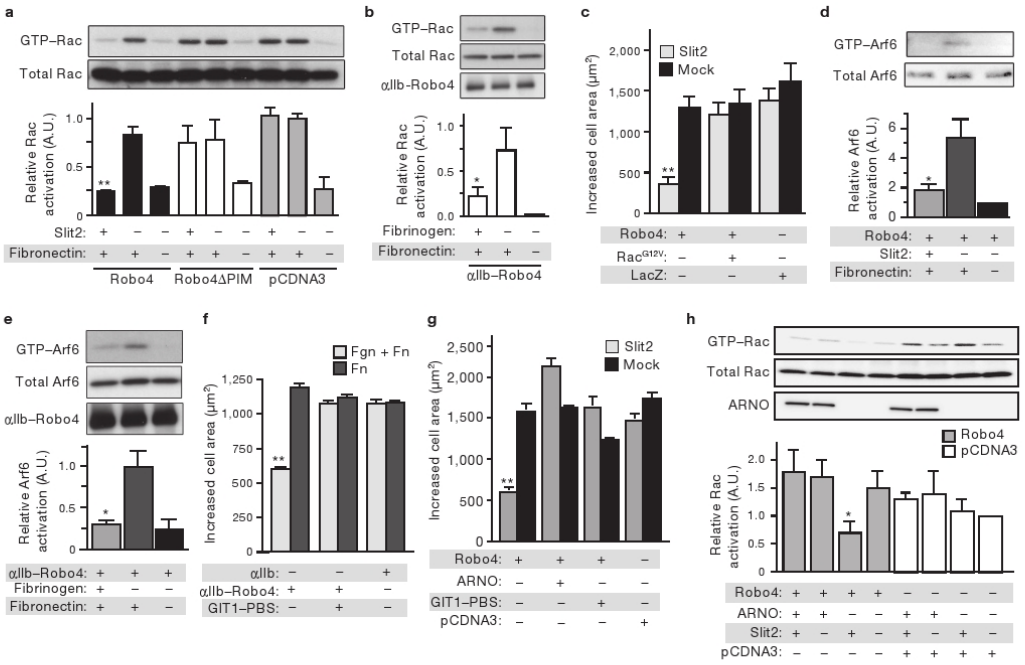

Figure 3 Robo4 blocks Rac-dependent protrusive activity through inhibition of Arf6. (**a**) Lysates from HEK 293 cells expressing the indicated constructs, plated on fibronectin and mock or Slit2, were precipitated with GST–PBD and immunblotted with Rac antibodies ($n = 3$). (**b**) Lysates from CHO-K1 cells expressing αIIb-Robo4 were precipitated with GST–PBD and immunoblotted with Rac antibodies ($n = 3$). (**c**) HEK 293 cells expressing Robo4 and Rac^{G12V} or LacZ were subjected to spreading assays on fibronectin and mock or Slit2. (**d**, **e**) Lysates from HEK 293 cells expressing full-length Robo4 (**d**) and CHO-K1 cells expressing αIIb integrin–Robo4 cytoplasmic tail (**e**), plated on the indicated matrix, were precipitated with GST–GGA3 and immunoblotted with Arf6 antibodies ($n = 3$). (**f**) CHO-K1 cells stably expressing αIIb or αIIb integrin–Robo4 cytoplasmic tail were co-transfected with GFP and either an empty vector or GIT1–PBS, and were subjected to spreading assays on the indicated matrix. (**g**) HEK 293 cells expressing GFP and the indicated constructs were subjected to spreading assays on fibronectin and Mock or Slit2. Expression of Robo4 and ARNO was verified by immunoblotting (data not shown). (**h**) Lysates from HEK 293 cells expressing the indicated constructs, plated on fibronectin and mock or Slit2, were precipitated with GST–PBD and immunoblotted with Rac antibodies ($n = 3$). For spreading assays, the area of GFP-positive cells was determined using ImageJ software ($n = 3$, 150 cells per experiment). Expression of Robo4 constructs was verified by western blotting (data not shown). $^*P < 0.05$; $^{**}P < 0.005$. Error bars indicate the mean ± s.e.m. Full scans of blots are shown in Supplementary Information, Fig. S7. αIIb–Robo4 indicates αIIb integrin–Robo4.

Cells expressing Ch-paxillinΔLim4 spread normally in the presence of Slit2, whereas cells expressing Ch-paxillin showed a reduction in cell area characteristic of Slit2–Robo4 signalling (Fig. 2i).

The ability of a cell to spread and migrate on an extracellular matrix protein, such as fibronectin, is regulated by the activation of Rho family GTPases, which include Rho, Cdc42 and Rac[18]. Of these proteins, Rac has an essential role in promoting the actin polymerization that leads to lamellipodial extension and cell spreading during migration[18,19]. To examine whether Slit2–Robo4 signalling inhibits adhesion-dependent Rac activation, cells expressing Robo4, Robo4ΔPIM or pcDNA3 alone were plated on fibronectin in the absence and presence of Slit2, and Rac–GTP levels were analysed. Additionally, cells expressing αIIb integrin–Robo4:β3 were plated on fibronectin in the absence and presence of fibrinogen, and Rac–GTP levels were analysed. Cells expressing Robo4 or αIIb integrin–Robo4:β3 showed significantly less adhesion-stimulated Rac activation when plated on Slit2 and fibrinogen, respectively (Fig. 3a, b). When this experiment was repeated with Robo4ΔPIM, we found that cells expressing this mutant receptor were refractory to Slit2 treatment (Fig. 3a).

To confirm that Robo4-dependent inhibition of cell spreading is principally due to suppression of Rac activation, we subjected cells co-expressing Robo4 and a dominant-active form of Rac, Rac^{G12V}, to spreading assays. Cells expressing Rac^{G12V} were refractory to Slit2 treatment (Fig. 3c), providing additional evidence that Slit2–Robo4 signalling blocks protrusive activity by inhibiting Rac.

We previously demonstrated that the interaction of α4 integrin with a paxillin–GIT1 complex enables α4 integrin to control Rac-dependent changes in protrusive activity by modulating the activity of the small GTPase Arf6 (ref. 20). Our finding that Robo4 interacts with paxillin and inhibits protrusive activity prompted us to determine whether Robo4 signalling impinges on the Arf6 pathway. Cells expressing full-length Robo4 were plated on fibronectin in the absence and presence of Slit2, while those expressing αIIb integrin–Robo4:β3 were plated on fibronectin in the absence and presence of fibrinogen, and Arf6–GTP levels were analysed. Whereas fibronectin alone stimulated an increase in Arf6–GTP, both Slit2 and fibrinogen reduced Arf6–GTP levels in cells expressing Robo4 or αIIb integrin–Robo4:β3, respectively (Fig. 3d, e).

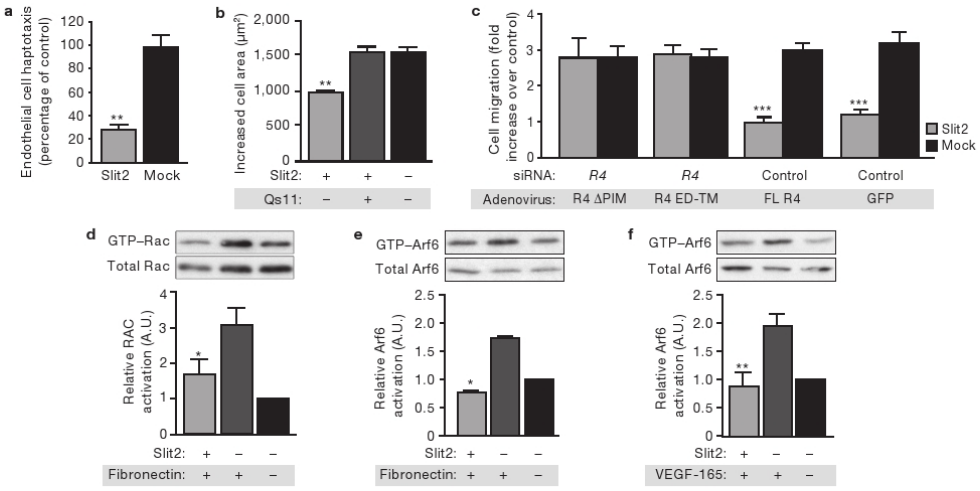

Figure 4 Slit2–Robo4 signalling inhibits endothelial cell protrusive activity through paxillin and Arf-GAPs. (**a**) Endothelial cells were subjected to haptotaxis migration assays on fibronectin and mock or Slit2. Cells on the underside of the filter were counted and migration on fibronectin/mock membranes was set at 100% ($n = 3$, in triplicate). (**b**) Endothelial cells were subjected to spreading assays on fibronectin and mock or Slit2, in the absence and presence of Qs11 ($n = 3$, 150 cells per experiment). Cell area was determined using ImageJ software. (**c**) Robo4 was depleted in endothelial cells using siRNA. Cells were then infected with an adenovirus expressing the indicated constructs, and were subjected to migration assays ($n = 5$, in triplicate). (**d**, **e**) Lysates from endothelial cells plated on fibronectin and either mock or Slit2, were precipitated with GST–PBD and immunoblotted with Rac antibodies (**d**) or GST-GGA3 and immunoblotted with Arf6 antibodies (**e**; $n = 3$ in **e** and **f**). (**f**) Lysates from endothelial cells plated on VEGF-165 and mock or Slit2 were precipitated with GST–GGA3 and immunoblotted with Arf6 antibodies ($n = 3$). $^*P < 0.05$, $^{**}P < 0.005$ and $^{***}P < 0.0005$. Error bars indicate the mean ± s.e.m. Full scans of blots are shown in Supplementary Information, Fig. S8. R4, Robo4. FL, full-length.

We analysed the requirement for a paxillin–GIT1 complex in Robo4-dependent inhibition of protrusive activity. The GIT1 paxillin-binding sequence (PBS) is at the C terminus of the protein, and ectopic expression of this fragment blocks interaction between GIT1 and paxillin[20]. Cells were transfected with αIIb integrin–Robo4:β3 and an empty vector or GIT1–PBS, and subjected to spreading assays on fibronectin in the absence and presence of fibrinogen. Cells expressing αIIb integrin–Robo4:β3 showed a decrease in cell area when plated on fibronectin and fibrinogen, but this effect was lost in cells expressing GIT1–PBS (Fig. 3f). Similarly, in full-length Robo4-expressing cells plated on fibronectin and Slit2, GIT1–PBS prevented a decrease in cell area (Fig. 3g).

To determine whether Slit2–Robo4 signalling inhibits protrusive activity by inactivating Arf6, we co-expressed the Arf6 guanine nucleotide exchange factor (GEF) ARNO with Robo4 and performed spreading assays. Overexpression of ARNO blocked the ability of Slit2 to reduce cell area, indicating that a principal effect of Slit2–Robo4 signalling is to prevent GTP-loading of Arf6 (Fig. 3g). If ARNO restores the ability of Robo4-expressing cells to spread on fibronectin and Slit2, it should similarly re-establish Rac activation on this matrix. Indeed, overexpression of ARNO led to normal levels of Rac–GTP in cells plated on fibronectin and Slit2 (Fig. 3h).

To assess the effect of Slit2–Robo4 signalling on the subcellular distribution of paxillin, cells were plated on fibronectin in the absence and presence of Slit2, and stained for endogenous paxillin. In the absence of Slit2, cells expressing full-length Robo4 spread normally and formed abundant, paxillin-stained focal adhesions near the cell periphery (Supplementary Information, Fig. S3a, top panel). In the presence of Slit2, however, cells showed reduced spreading, contained less F-actin and formed fewer and smaller paxillin-stained focal adhesions (Supplementary Information, Fig. S3a, bottom panel). Control cells (cells not expressing Robo4) showed similar morphology when adhered on fibronectin alone or on fibronectin and Slit2 (data not shown), indicating that the effect of Slit2 is Robo4-dependent.

We repeated this assay using bovine aortic endothelial (BAE) cells, which endogenously express Robo4. On substrata coated with fibronectin and Slit2, BAE cells showed reduced spreading compared with cells adhered to fibronectin alone (Supplementary Information, Fig. S3b). In addition, BAE cells adhered to fibronectin and Slit2 formed small paxillin-stained structures, which were inconsistent with the mature focal adhesions observed in cells adhered to fibronectin alone (Supplementary Information, Fig. S3b; see arrows). The inhibitory effect of Slit2 on cell spreading seems to be transient, as cells adhered for extended intervals showed similar morphology and focal adhesion formation irrespective of Slit2 treatment (data not shown).

Our data suggest that in Robo4-expressing cells, Slit2 redistributes paxillin from focal adhesions to the cell surface, where it co-localizes with Robo4. To test this hypothesis, we analysed the subcellular distribution of paxillin and Robo4 in the absence and presence of Slit2. Because Slit2 blocks cell spreading and prevents clear visualization of the plasma membrane, we performed these experiments in endothelial cells pre-spread on fibronectin. In the absence of Slit2, paxillin was found almost exclusively in focal adhesions, whereas Robo4 was localized to the cell surface (Supplementary Information, Fig. S3c, top panel). In the presence of Slit2, however, a significant portion of paxillin appeared at the cell surface, co-localized with Robo4; this alteration in localization was coincident with a reduction of paxillin in focal adhesions (Supplementary Information, Fig. S3c, middle panel).

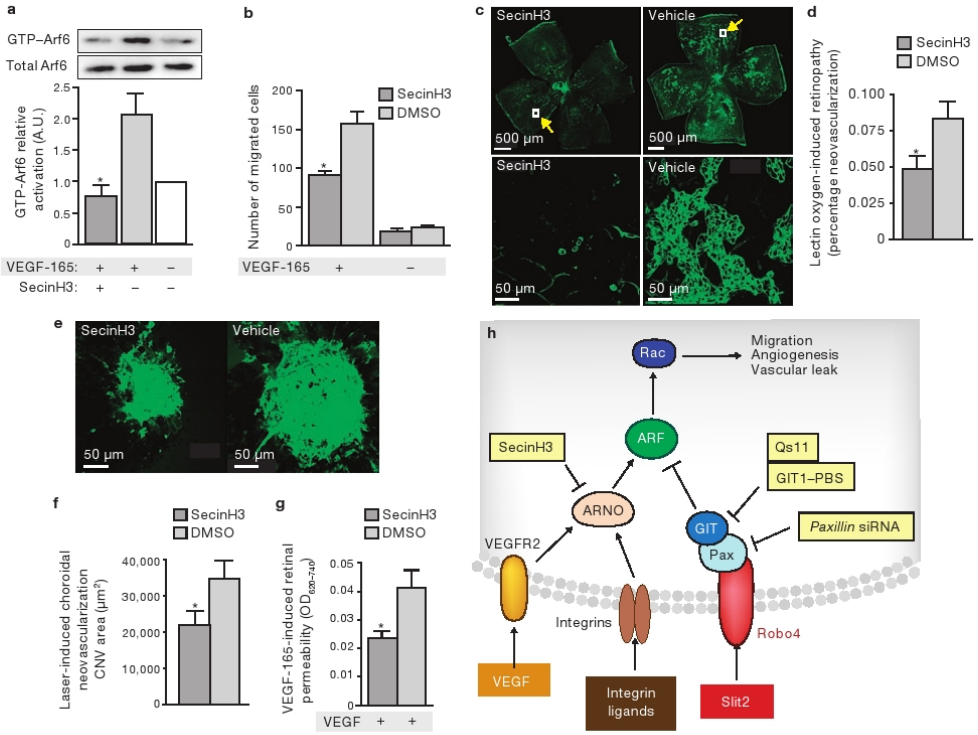

Figure 5 SecinH3 blocks Arf6 activation and inhibits pathologic angiogenesis and endothelial hyperpermeability in animal models of vascular eye disease. (**a**) Lysates from endothelial cells, pre-treated with SecinH3 or DMSO and then stimulated with VEGF-165, were precipitated with GST–GGA3 and immunoblotted with Arf6 antibodies. (**b**) Endothelial cells, pre-treated with SecinH3 or DMSO, were subjected to migration assays using VEGF-165. (**c**, **e**, **g**) SecinH3 or DMSO were injected into contralateral eyes of wild-type mice, which were then subjected to oxygen-induced retinopathy (**c**), laser-induced choroidal neovascularization (**e**) or VEGF-165-induced retinal hyperpermeability (**g**). (**c**) Retinal flatmounts prepared from neonatal mice subjected to oxygen-induced retinopathy were stained with fluorescent isolectin and analysed by fluorescence microscopy. Top panels are low magnification images, and bottom panels, high magnification images of the outlined areas, which emphasize the pathologic neovascular tufts. (**d**) Quantification of pathologic neovascularization shown in **c** ($n = 14$ animals). (**e**) Choroidal flatmounts prepared from 2–3- month-old mice subjected to laser-induced choroidal neovascularization were stained with fluorescent isolectin and analysed by confocal microscopy. (**f**) Quantification of pathologic angiogenesis observed in **e** ($n = 15$ animals) . (**g**) Quantification of retinal permeability following intravitreal injection of VEGF-165 ($n = 6$ animals). Vehicle is DMSO. $^*P < 0.05$. Error bars indicate the mean ± s.e.m. (**h**) VEGFR and integrin signalling promote sequential activation of Arf6 and Rac, leading to cellular protrusive activity. Concomitant initiation of Robo4-signalling by Slit2 stimulates recruitment of a paxillin–Arf–GAP complex to the cytoplasmic tail of the receptor, which causes local inactivation of Arf6 and Rac, thereby blocking the protrusive activity necessary for angiogenesis and vascular leak. Full scans of blots are shown in Supplementary Information, Fig. S9. CNV, choroidal neovascularization.

Thus far, our experiments had used model cell systems to decipher signal transduction downstream of Robo4. To determine whether this pathway is important for Robo4 function in primary cells, we first subjected human endothelial cells to haptotaxis assays and, analogous to the model cell system, Slit2 blocked fibronectin-driven cell motility (Fig. 4a). We also performed spreading assays on coverslips coated with the 9–11 fragment of fibronectin (a ligand for α5β1 integrin) and Slit2, and again found that Slit2 suppressed cellular protrusive activity stimulated by integrin ligation (Fig. 4b). To analyse a potential role for GIT1 in Slit2-dependent inhibition of cell protrusion, we pre-treated endothelial cells with a small-molecule inhibitor of Arf-GAPs, Qs11 (ref. 21), and subjected them to spreading assays on the 9–11 fibronectin fragment and Slit2. Arf–GAP-inhibition prevented the reduction in cell area elicited by Slit2 (Fig. 4b).

Next, we determined the requirement for paxillin binding to Robo4 in Slit2-dependent inhibition of cell migration. We depleted endogenous Robo4 in human endothelial cells using siRNA, and reconstituted the receptor using adenoviral vectors expressing full-length murine Robo4, Robo4 ED–TM or Robo4ΔPIM, and subjected these cells to migration assays in the absence and presence of Slit2. The migration of control cells and *Robo4*-knockdown cells reconstituted with full-length Robo4 was inhibited by Slit2 , but Slit2 had no effect on Robo4-knockdown cells reconstituted with either Robo4 ED–TM or Robo4ΔPIM (Fig. 4c).

These cell biological data suggest that Slit2–Robo4 signalling in endothelial cells blocks Rac and Arf6 activation in response to integrin ligation. To test this idea, we plated endothelial cells on fibronectin in the absence and presence of Slit2, and analysed Rac–GTP and Arf6–GTP levels. Consistent with results from the model cell systems, Slit2 blocked the

fibronectin-induced increase in Rac–GTP (Fig. 4d) and Arf6–GTP levels (Fig. 4e). In addition to fibronectin, the angiogenic and permeability-inducing factor VEGF-165 exists *in vivo* as an extracellular matrix component, and has been suggested to stimulate Arf6 activation[22]. Consequently, we plated endothelial cells on VEGF-165 in the absence and presence of Slit2, and analysed Arf6–GTP levels. Whereas VEGF-165 induced Arf6 activation, addition of Slit2 prevented this stimulatory event (Fig. 4f).

We previously demonstrated that the effect of Slit2 on endothelial cell biology is Robo4-dependent[6]. To determine whether this relationship exists for the biochemical regulation of Arf6, we plated endothelial cells from *Robo4*$^{+/+}$ and *Robo4*$^{AP/AP}$ mice[6] on fibronectin, in the absence and presence of Slit2, and analysed Arf6–GTP levels. Slit2 decreased activated Arf6 in *Robo4*$^{+/+}$, but not *Robo4*$^{AP/AP}$, endothelial cells (Supplementary Information, Fig. S4).

In addition to Arf6 and Rac, Rho and Cdc42 have known roles in cellular protrusion[18]. To gain insight into the regulation of these small GTPases by Slit2, we plated endothelial cells on fibronectin in the absence and presence of Slit2, and analysed Rho–GTP and Cdc42–GTP levels. Whereas Rho activation was unaltered by Slit2, Cdc42 activation was significantly reduced (Supplementary Information, Fig. S5a, b). This latter effect was surprising given that Robo4 does not interact with the Robo1-binding protein srGAP1, a known Cdc42 GTPase-activating protein (Supplementary Information, Fig. S5c).

Recently, we showed that Robo4 mediates Slit2-dependent inhibition of neovascular tuft formation and endothelial hyperpermeability[6], processes that are initiated and perpetuated by endothelial integrins and growth factor receptors. The ability of Slit2 to block Arf6 activation in response to fibronectin and VEGF-165 (which are ligands for these angiogenic and permeability-inducing receptors) led us to speculate that Arf6 is a critical nexus in signalling pathways regulating pathologic angiogenesis and vascular leak[22]. To test this hypothesis, we used a recently developed small-molecule inhibitor of cytohesin Arf–GEFs, SecinH3, which blocks insulin-induced Arf6 signalling[23]. SecinH3, but not DMSO, prevented both VEGF-induced Arf6 activation and VEGF-induced endothelial cell migration (Fig. 5a, b). Furthermore, injection of SecinH3 into the eyes of wild-type mice inhibited neovascular tuft formation in oxygen-induced retinopathy (Fig. 5c, d) and choroidal neovascularization (Fig. 5e, f), as well as retinal hyperpermeability caused by VEGF-165 (Fig. 5g).

Cumulatively, these data demonstrate the importance of paxillin and GIT1 in mediating Slit2–Robo4-dependent inhibition of endothelial-cell protrusive activity, and suggest that blocking activation of Arf6 is a potential therapy for human diseases characterized by pathologic angiogenesis and vascular leak (Fig. 5h). □

METHODS

Methods and any associated references are available in the online version of the paper at http://www.nature.com/naturecellbiology/.

Note: Supplementary Information is available on the Nature Cell Biology website.

ACKNOWLEDGEMENTS

We thank J. Wythe for critical reading of the manuscript, and D. Lim for expert graphical assistance. J. Bonafacino provided the GST–GGA3 expression plasmid. This work was funded by grants from the H.A. and Edna Benning Foundation, the Juvenile Diabetes Research Foundation, the American Heart Association, the Burroughs Wellcome Fund and the Department of Defense (D.Y.L.); the National Heart Lung and Blood Institute (D.Y.L. and M.H.G.); the National Eye Institute (K.Z.); the Deutsche Forschungsgemeinschaft SFB 704 (M.F.); the National Institute of Arthritis and Musculoskeletal and Skin Diseases (M.H.G.); the National Institute of Allergy and Disease AI065357 (D.Y.L.) and by the US National Institutes of Health, Ruth L. Kirschstein National Research Service Award (N.R.L.) and training grant T32-GM007464 (A.C.C.).

AUTHOR CONTRIBUTIONS

C.A.J., N.N., N.R.L., M.H.G. and D.Y.L. were responsible for project conceptualization and planning, experimental design, data analysis, and manuscript preparation. M.H.G. and D.Y.L. were responsible for funding the project. C.A.J., N.N. and N.R.L were responsible for performing all experiments or coordinating experimental design and work of others. W.Z., L.K.S., A.C., C.J.L. and K.R.T. performed specific and necessary experiments presented in the paper or in our response to reviewers. Q.Z., P.G.S., A.M.H., M.F. and K.Z. provided expertise, reagents or assays.

COMPETING FINANCIAL INTERESTS

The authors declare competing financial interests. The University of Utah has filed patents covering the technology described in this manuscript with the intent of commercializing this technology.

Published online at http://www.nature.com/naturecellbiology/.
Reprints and permissions information is available online at http://npg.nature.com/reprintsandpermissions/.

1. Seeger, M., Tear, G., Ferres-Marco, D. & Goodman, C. S. Mutations affecting growth cone guidance in *Drosophila*: genes necessary for guidance toward or away from the midline. *Neuron* **10,** 409–426 (1993).
2. Brose, K. *et al.* Slit proteins bind Robo receptors and have an evolutionarily conserved role in repulsive axon guidance. *Cell* **96,** 795–806 (1999).
3. Kidd, T., Bland, K. S. & Goodman, C. S. Slit is the midline repellent for the robo receptor in *Drosophila*. *Cell* **96,** 785–794 (1999).
4. Kidd, T. *et al.* Roundabout controls axon crossing of the CNS midline and defines a novel subfamily of evolutionarily conserved guidance receptors. *Cell* **92,** 205–215 (1998).
5. Li, H. S. *et al.* Vertebrate slit, a secreted ligand for the transmembrane protein roundabout, is a repellent for olfactory bulb axons. *Cell* **96,** 807–818 (1999).
6. Jones, C. A. *et al.* Robo4 stabilizes the vascular network by inhibiting pathologic angiogenesis and endothelial hyperpermeability. *Nature Med.* **14,** 448–453 (2008).
7. Park, K. W. *et al.* Robo4 is a vascular-specific receptor that inhibits endothelial migration. *Dev. Biol.* **261,** 251–267 (2003).
8. Seth, P. *et al.* Magic roundabout, a tumor endothelial marker: expression and signaling. *Biochem. Biophys. Res. Comm.* **332,** 533–541 (2005).
9. Ridley, A. J. *et al. Cell* migration: integrating signals from front to back. *Science* **302,** 1704–1709 (2003).
10. Pollard, T. D. & Borisy, G. G. Cellular motility driven by assembly and disassembly of actin filaments. *Cell* **112,** 453–465 (2003).
11. Etienne-Manneville, S. & Hall, A. Rho GTPases in cell biology. *Nature* **420,** 629–635 (2002).
12. Turner, C. E. Paxillin and focal adhesion signalling. *Nature cell Biol.* 2, E231–236 (2000).
13. Yuminamochi, T. *et al.* Expression of the LIM proteins paxillin and Hic-5 in human tissues. *J. Histochem. Cytochem.* **51,** 513–521 (2003).
14. Hohenester, E., Hussain, S. & Howitt, J. A. Interaction of the guidance molecule Slit with cellular receptors. *Biochem. Soc. Trans.* **34,** 418–421 (2006).
15. Jones, C. A. *et al.* Robo4 stabilizes the vascular network by inhibiting pathologic angiogenesis and endothelial hyperpermeability. *Nature Med.* (2008).
16. Bashaw, G. J., Kidd, T., Murray, D., Pawson, T. & Goodman, C. S. Repulsive axon guidance: Abelson and Enabled play opposing roles downstream of the roundabout receptor. *Cell* **101,** 703–715 (2000).
17. Turner, C. E. Paxillin interactions. *J. Cell Sci.* **113 (Pt 23),** 4139–4140 (2000).
18. Nobes, C. D. & Hall, A. Rho, rac, and cdc42 GTPases regulate the assembly of multimolecular focal complexes associated with actin stress fibers, lamellipodia, and filopodia. *Cell* **81,** 53–62 (1995).
19. Nobes, C. D. & Hall, A. Rho GTPases control polarity, protrusion, and adhesion during cell movement. *J. Cell Biol.* **144,** 1235–1244 (1999).
20. Nishiya, N., Kiosses, W. B., Han, J. & Ginsberg, M. H. An alpha4 integrin-paxillin-Arf-GAP complex restricts Rac activation to the leading edge of migrating cells. *Nature Cell Biol.* **7,** 343–352 (2005).
21. Zhang, Q. *et al.* Small-molecule synergist of the Wnt/ -catenin signaling pathway. *Proceedings of the National Academy of Sciences of the United States of America* **104,** 7444–7448 (2007).
22. Ikeda, S. *et al.* Novel role of ARF6 in vascular endothelial growth factor-induced signaling and angiogenesis. *Circ. Res.* **96,** 467–475 (2005).
23. Hafner, M. *et al.* Inhibition of cytohesins by SecinH3 leads to hepatic insulin resistance. *Nature* **444,** 941–944 (2006).

DOI: 10.1038/ncb1976

METHODS

Reagents. HEK 293 and COS-7 cells, and all IMAGE clones were from ATCC. SP6 and T7 Message Machine kits were from Ambion. Glutathione-Sepharose 4B, parental pGEX-4T1 and ECL PLUS were from Amersham-Pharmacia. Human fibronectin was from Biomedical Technologies and Invitrogen. Coomassie blue and PVDF (polyvinyldifluoride) were from BioRad. Yeast two-hybrid plasmids and reagents were from Clontech. Costar Transwells and Amicon Ultra-15 Concentrator Columns were from Fisher. FBS was from Hyclone. Anti-V5 antibody, DAPI, DMEM, Lipofectamine 2000, Penicillin-Streptomycin, Prolong Gold, Superscript III kit, Trizol and TrypLE Express were from Invitrogen. Goat Anti-Mouse-HRP and Goat Anti-Rabbit-HRP secondary antibodies were from Jackson ImmunoResearch. 3D Blind Deconvolution algorithm of AutoQuantX was from Media Cybernetics. HMVEC, HUVEC, EBM-2 and bullet kits were from Lonza. Alexa564-Phalloidin, Anti-GFP and Goat Anti-Rabbit Alex488 were from Molecular Probes. Rosetta2 *Escherichia coli* was from Novagen. Low melt agarose was from NuSieve. T7 *in vitro* transcription/translation kit was form Promega. Anti-HA affinity matrix, Fugene6 and protease inhibitor cocktail were from Roche. Arf6 antibody and normal Rat IgG-agarose conjugate was from Santa Cruz. Anti-Flag M2, phosphatase inhibitor cocktails, soybean trypsin inhibitor and fatty acid-free bovine serum albumin (BSA) were from Sigma. Nikon Eclipse TE2000-U microscope was from Semrock. Quick change site-directed mutagenesis kit was from Stratagene. Oligonucleotides for PCR were from the University of Utah Core Facility.

Molecular biology. The Robo4–HA, Slit2–Myc–His and chicken paxillin plasmids have been described previously[2,7,20]. Robo4–NH2 was amplified from Robo4–HA and cloned into *Eco*RV/*Not*I of pcDNA3-HA. Robo4–COOH was amplified from Robo4–HA by overlap-extension PCR and cloned into *Eco*RV/*Not*I of pcDNA3-HA. The N-terminal half of the human Robo4 cytoplasmic tail (amio-acids 465–723) was amplified by PCR and cloned into (*Eco*RI/*Bam*HI) of pGBKT7. Murine Robo4 fragments were amplified by PCR and cloned into *Bam*HI/*Eco*RI of pGEX-4T1. Murine Hic-5, Mena and paxillin (including deletions) were amplified from IMAGE clones by PCR and cloned into *Eco*RV/*Not*I of pcDNA3-V5. GST–Robo4ΔPIM and full-length Robo4ΔPIM were generated by site-directed mutagenesis of relevant wild-type constructs using Quick Change. The integrity of all constructs was verified by sequencing at the University of Utah Core Facility.

Cell culture. HEK 293 and COS-7 cells were cultured in DMEM supplemented with 10% FBS and 1% penicillin/streptomycin. Human microvascular endothelial cells (HMVEC) were cultured in EGM-2 MV and human umbilical vein endothelial cells (HUVEC) were cultured in EGM-2 supplemented with 10% FBS. Cells were used between passages 2 and 5.

Transfection. HEK293 and COS-7 cells were transfected with Fugene6 or Lipofectamine 2000 according to the manufacturer's protocol.

Preparation of concentrated recombinant Slit2 protein. Slit2 and mock were prepared as described previously[6]. Mock is sham preparation of Slit2, and was used as a control in all experiments analysing the effect of Slit2.

Haptotaxis migration assay. Cells were removed from tissue culture dishes with TrypLE Express, washed once with 0.1% trypsin inhibitor, 0.2% fatty acid-free BSA in DMEM or EBM-2, and twice with 0.2% BSA in the relevant media. The washed cells were counted, resuspended, and 1.5×10^5 (HEK) or 0.2×10^5 (HMVEC) cells were loaded into the upper chamber of 12-μm (HEK) or 8-μm (HMVEC) Costar transwells pre-coated on the lower surface with fibronectin (5 μg ml^{-1}). The effect of Slit2 on haptotaxis was analysed by co-coating with Slit2 (5 μg ml^{-1}) or an equivalent amount of mock. After 6 h (HEK) or 3 h (HMVEC), cells on the upper surface of the transwell were removed with a cotton swab. The cells on the lower surface were fixed with 4% formaldehyde, washed three times with PBS and mounted in Vectashield with DAPI. The number of GFP-positive (HEK) and DAPI-positive (HMVEC) cells on the lower surface was determined by counting six 10× fields on an inverted fluorescence microscope. The number of migrated cells on fibronectin/mock-coated membranes was set at 100%. Experiments were performed at least three times in triplicate.

Yeast two hybrid assay. pGBKT7::hRobo4 465-723 was transformed into the yeast strain PJ694A, creating PJ694A-Robo4. A human aortic cDNA library was cloned into the prey plasmid pACT2 and then transformed into PJ694A-Robo4. Co-transformed yeast strains were plated onto SD-Leu-Trp (-LT) to analyse transformation efficiency and SD-Leu-Trp-His-Ade (-LTHA) to identify putative interacting proteins. Yeast strains competent to grow on SD–LTHA were then tested for expression of β-galactosidase by a filter lift assay. Prey plasmids were isolated from yeast strains capable of growing on SD–LTHA and expressing β-galactosidase, and sequenced at the University of Utah Core Facility.

Immunoprecipitation. Cell lysates were prepared in 50 mM Tris-Cl at pH 7.4, 50 mM NaCl, 1 mM DTT, 0.5% Triton X-100, phosphatase and protease inhibitors, centrifuged at 16,000*g* for 20 min, cleared with normal IgG coupled to agarose beads for 60 min, and incubated for 2 h at 4 °C with relevant antibodies coupled to agarose beads. The precipitates were washed extensively in lysis buffer and resuspended in 2× sample buffer (125 mM Tris-Cl at pH 6.8, 4% SDS, 20% Glycerol, 0.04% bromophenol blue and 1.4 M 2-mercaptoethanol).

GST pulldown assay. Rosetta2 *E. coli* cells harbouring pGEX-4T1::mRobo4 were grown to an optical density at 600 nm (OD_{600}) of 0.6 and induced with IPTG (0.3 mM). After 3–4 h at 30 °C, cells were centrifuged at 2,800*g* for 5 min, cells were lysed by sonication in 20 mM Tris-Cl at pH 7.4, 1% Triton X-100, lysozyme (1 μg ml^{-1}), DTT (1 mM) and protease inhibitors. The GST fusion proteins were captured on glutathione-Sepharose 4B, washed once with lysis buffer without lysozyme and then twice with binding/wash buffer (50 mM Tris-Cl at pH 7.4, 150 mM NaCl, 1 mM DTT, 1% Triton X-100, 0.1% BSA and protease inhibitors). The GST fusion proteins were incubated with purified recombinant paxillin (60 nM) overnight at 4 °C, washed extensively in binding/wash buffer, and resuspended in 2× sample buffer.

Immunoblotting. Protein samples were incubated for 2 min at 100 °C, separated by SDS–PAGE and transferred to a PVDF membrane. PVDF membranes were incubated with 5% non-fat dry milk in PBS + 0.1% Tween 20 (PBST; PBST-M) for 60 min at 25 °C. Blocked membranes were incubated with primary antibodies (against Arf6, Cdc42, Flag M2, Hic-5, paxillin, Rac and Rho) in PBST-M for 60 min at 25 °C, or overnight at 4 °C. Membranes were washed for 10 min, three times, in PBST and then incubated with a secondary antibody (goat anti-mouse or goat anti-rabbit horseradish peroxidase) for 60 min at 25 °C. Membranes were washed for 10 min, three times, in PBST and visualized with ECL PLUS. Primary antibodies were used at the following dilutions: antibodies against GTPases, 1:1,000; Flag, 1:1,000; Hic-5, 1:500 and paxillin, 1:10,000.

***In vitro* transcription/translation.** Mena-V5 was synthesized with the T7 Quick Coupled *in vitro* Transcription/Translation system according to the manufacturer's protocol.

Spreading assay. Cell spreading was analysed as described previously[20]. The cell area from at least 150 cells, from three independent experiments, was measured using ImageJ (NIH).

Depletion and reconstitution of paxillin. HEK 293 cells were transfected with 100 nM of siRNA duplexes (5′-CCCUGACGAAAGAGAAGCCUAUU-3′ and 5′-UAGGCUUCUCUUUCGUCAGGGUU-3′) using Lipofectamine 2000, according to the manufacturer's instructions. At 48 h after transfection, cells were processed for biochemical analysis or cell spreading assays. Paxillin reconstitution was accomplished by transfection with an expression vector encoding chicken paxillin, which has the nucleotide sequence 5′-CCCCTACAAAAGAAAAACCAA-3′ within the siRNA target site. Knockdown and reconstitution were analysed by immunoblotting with paxillin antibodies, and quantified by densitometry.

GTPase activation assays. GTPase activation was analysed as described previously[20]. Experiments were performed at least three times.

Adenoviral preparation. Murine full-length Robo4, Robo4ΔPIM, and Robo4 ED–TM were subcloned into pShuttle-IRES-hrGFP-2 (Stratagene). Independently, these vectors were used with pAdEasy to cotransform BJ5183 cells (Stratagene). Recombinant plasmids were linearized by *Pac*I digestion and transfected into 293 cells for packaging. The adenovirus was then amplified and titered for plaque forming units (PFU).

DOI: 10.1038/ncb1976

Depletion and reconstitution of Robo4. hu*Robo4* siRNA duplex (Hs_ROBO4_1_HP #1919431, Qiagen) or, alternatively, equimolar AllStars Negative Control siRNA (#1027280, Qiagen) was diluted to 480 nM in OptiMEM (Invitrogen). To form transfection complexes, siRNAs were premixed for 5–15 minutes at room temperature with HiPerfect Transfection Reagent (70 µl; Qiagen) and added to human microvascular endothelial cells. After an overnight incubation, cells were re-transfected with siRNA according to the same protocol. Adenoviral constructs were also added at a concentration of 1×10^6 PFU ml^{-1} and allowed to incubate overnight.

Immunofluorescence imaging. Glass coverslips were coated sequentially with human plasma fibronectin (5 µg ml^{-1}) and Slit2 or Mock (5 µg ml^{-1}), and blocked with 1% BSA. HEK Robo4 and bovine aortic endothelial (BAE) cells were then adhered for 30 min in serum-free DMEM supplemented with 1% BSA, and fixed with 3.7% formaldehyde in PBS. Cells were permeabilized in 0.1% Triton X-100 for 5 min, blocked and stained for Paxillin using either a rabbit polyclonal antibody or a mouse monoclonal antibody and counterstained with a FITC-conjugated secondary antibody. When indicated, cells were co-stained for F-actin with rhodamine-phalloidin. Coverslips were subsequently mounted in Prolong Gold antifade reagent on slides. Epi-fluorescent images of cells were acquired with a 60× oil immersion objective on a Nikon Eclipse TE2000-U microscope. Images as shown are maximal projections of deconvolved images that were acquired at 0.1-µm *z*-section intervals. Images were deconvolved using the 3D Blind Deconvolution algorithm of AutoQuantX. Additional post-acquisition processing of images was performed using ImageJ and Adobe Photoshop.

Retinal permeability. Retinal permeability was assessed as described previously[15]. Data are presented as mean ± s.e.m. for six wild-type mice.

Oxygen-induced retinopathy. Oxygen-induced retinopathy was induced as described previously[15]. Data are presented as mean ± s.e.m. for 14 wild-type mice.

Laser-induced choroidal neovascularisation. Laser-induced choroidal neovascularization was induced as described previously[15]. Data are presented as mean ± s.e.m. for at least 15 wild-type mice.

Statistical analysis. Student's *t*-test or ANOVA was used to determine statistical significance, where appropriate. All *P* values were derived from at least three independent experiments.

nature cell biology

SUPPLEMENTARY INFORMATION

DOI: 10.1038/ncb1976

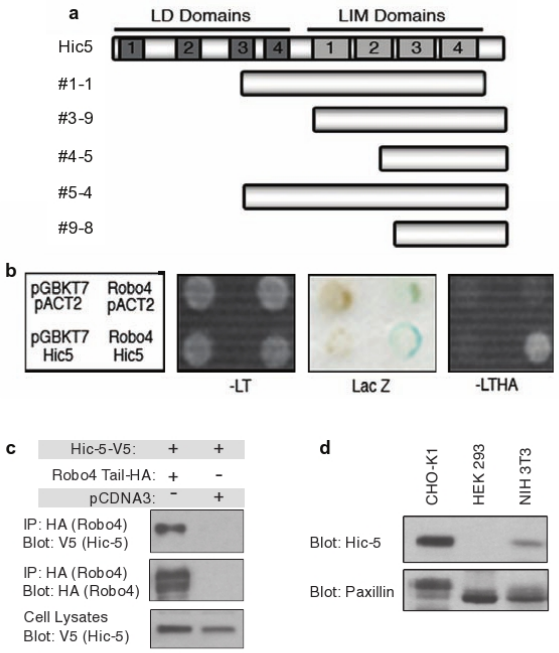

Figure S1 Hic-5 is a Robo4-interacting protein. (**a**) Schematic representation of full-length Hic-5 and the cDNA clones recovered from the yeast two-hybrid screen. (**b**) *S. cerevisiae* strain PJ694-A was transformed with the indicated plasmids and plated to synthetic media lacking Leucine and Tryptophan, or Leucine, Tryptophan, Histidine and Alanine. Colonies capable of growing on nutrient deficient media were spotted onto the same media, replica plated, and either photographed or used for the beta-galactosidase assay. (**c**) Lysates from HEK 293 cells expressing Robo4 cytoplasmic tail-HA and Hic-5-V5, or empty vector (pcDNA3) and Hic-5-V5 were immunoprecipitated with HA antibodies and immunoblotted with V5 antibodies. (**d**) Total cell lysates from Cho-K1, HEK 293 and NIH 3T3 cells were immunoblotted with antibodies to Hic-5 and paxillin.

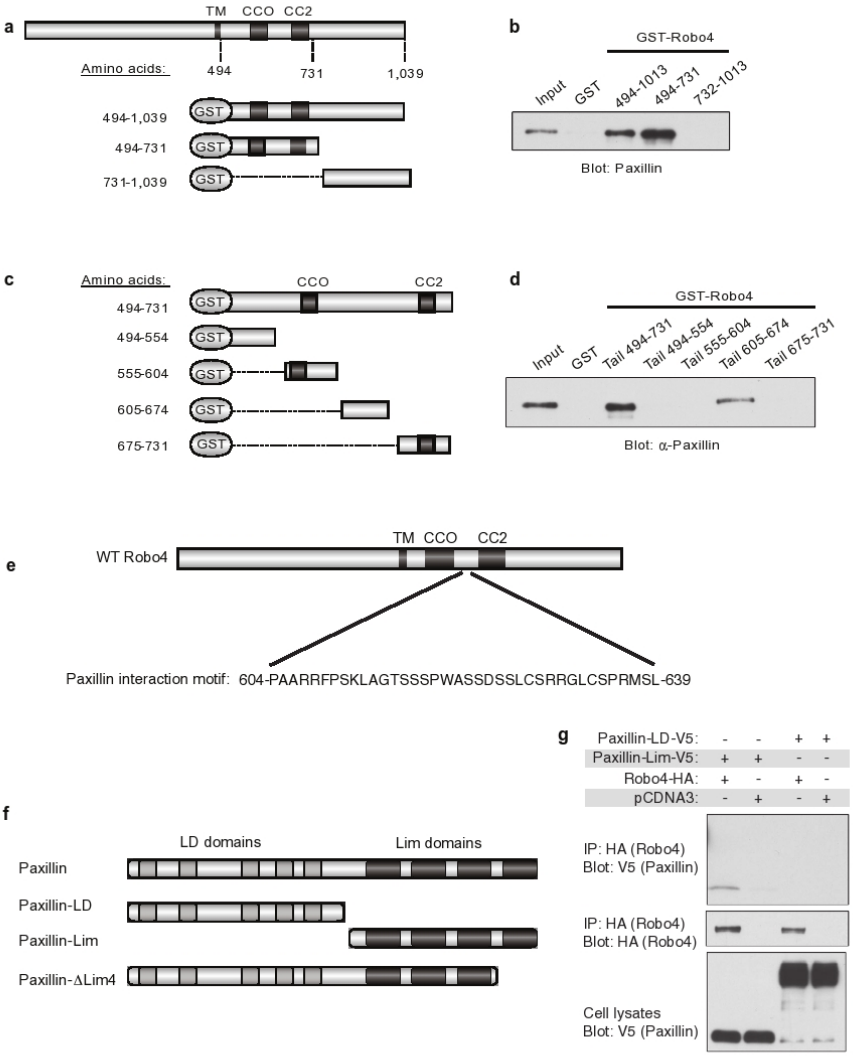

Figure S2 Identification of the Robo4 – paxillin interaction interface. (**a**, **c**) Schematic representation of GST-Robo4 fusion proteins used in pull down assays in **b** and **d**. (**b**, **d**) Purified GST-Robo4 fusion proteins were incubated with recombinant purified paxillin, precipitated with glutathione agarose and immunoblotted with paxillin antibodies. **(e)** A schematic representation of the murine Robo4 protein and illustration of the amino acids comprising the paxillin interaction motif (PIM). **(f)** Schematic representation of paxillin constructs. (**g**) Lysates of HEK 293 cells expressing Robo4 cytoplasmic tail-HA and the indicated paxillin constructs were immunoprecipitated from with HA antibodies and immunoblotted with V5 antibodies

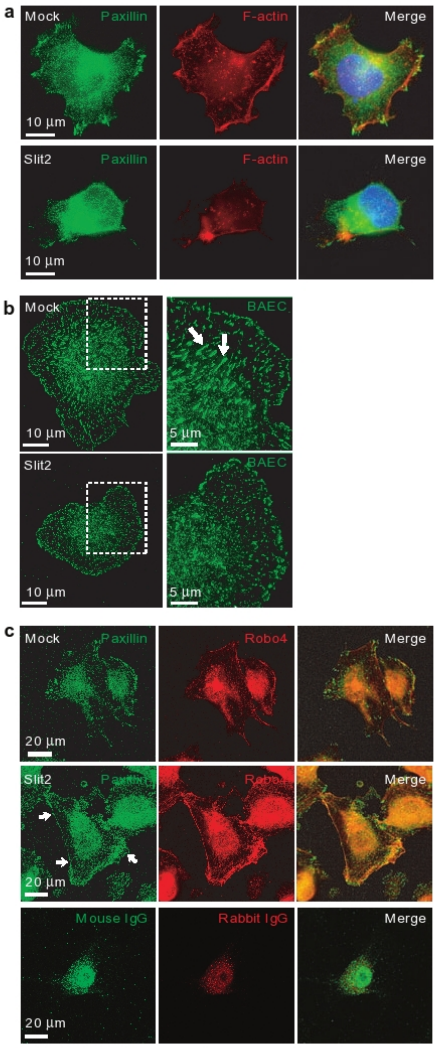

Figure S3 Slit2 redirects paxillin from focal adhesions to the cell surface. (**a**) HEK 293 cells expressing Robo4 were plated on fibronectin in the absence and presence of Slit2, and processed for indirect immunofluorescence using paxillin antibodies. (**b**) Bovine aortic endothelial (BAE) cells were plated on fibronectin in the absence and presence of Slit2, and processed for indirect immunofluorescence using paxillin antibodies. Arrows indicate mature focal adhesion complexes. (**c**) EAHY endothelial cells expressing Robo4 were plated on fibronectin incubated in the absence and presence of Slit2, and processed for indirect immunofluorescence using paxillin and Robo4 antibodies. Arrows indicate paxillin localized at the cell surface.

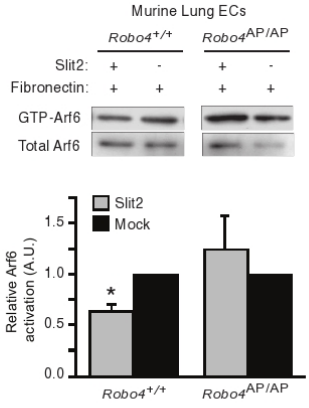

Figure S4 Robo4 is required for Slit2-mediated inhibition of Arf6 activity. Lysates from murine lung endothelial cells plated on fibronectin, in the absence and presence of Slit2, were precipitated with GST-GGA3 and immunoblotted with Arf6 antibodies ($n = 4$). *p<0.05.

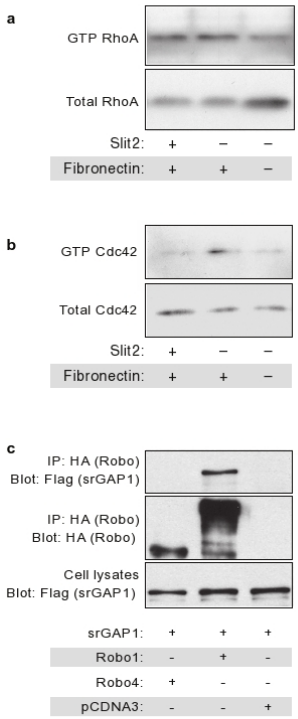

Figure S5 Robo4 inhibits Cdc42 activation but does not interact with srGAP1. (**a**, **b**) Lysates from endothelial cells plated on fibronectin, in the absence and presence of Slit2, were precipitated with (**a**) GST-RBD and immunoblotted with RhoA antibodies, or (**b**) GST-PBD and immunoblotted with Cdc42 antibodies. (**c**) Lysates from HEK 293 cells expressing the indicated plasmids were immunoprecipitated with HA antibodies and immunoblotted with Flag antibodies.

SUPPLEMENTARY INFORMATION

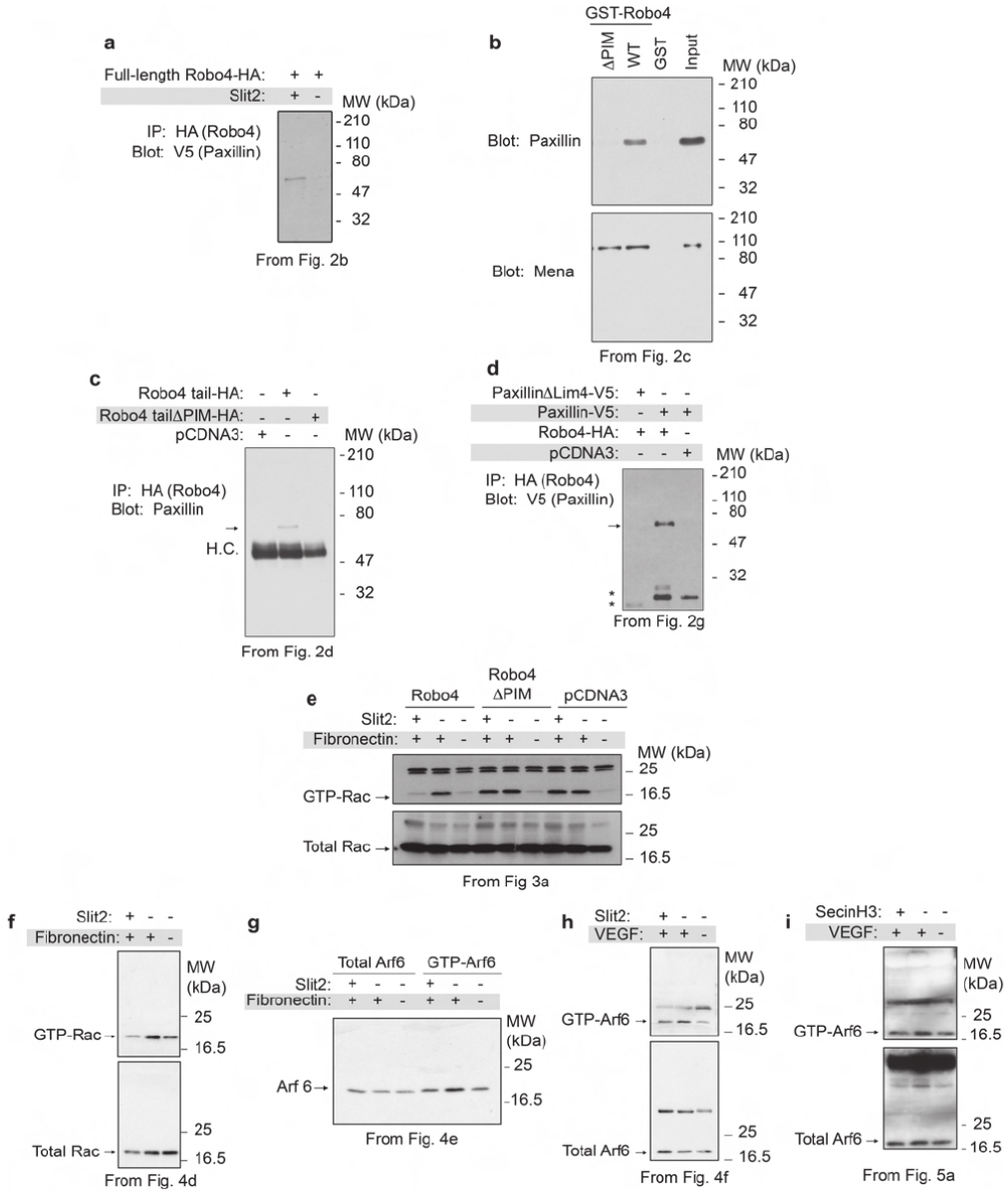

Figure S6 Selected representative full scans. (**a**) Figure 2b, Slit2 enhances Robo4-paxillin interaction. (**b**, **c**) Figure 2c and 2d, deletion of the paxillin interaction motif (PIM) results in loss of Robo4-paxillin interaction in vitro (**c**) and in mammalian cells (**d**). Figure 2g, deletion of Lim4 abrogates binding between paxillin and Robo4. (**e**) Figure 3a, the Robo4 PIM is necessary for Slit2-mediated inhibition of Rac activity. (**f**, **g**) Figure 4d and 4e, Slit2 blocks fibronectin-induced Rac (**f**) and Arf6 activation (**g**) in endothelial cells. (**h**) Figure 4f, Slit2 blocks VEGF-induced Arf6 activation in endothelial cells. (**i**) Figure 5a, SecinH3 blocks VEGF-induced Arf6 activation in endothelial cells. Arrows indicate relevant band. Asterisks indicate V5-tagged paxillin degradation products.

CHAPTER 4

CONCLUDING REMARKS

The findings presented in this dissertation add two major contributions. First, these data provide proof of principle that survival can be enhanced in sepsis and pandemic influenza by specifically blunting the vascular response to hypercytokinemia[1]. This was achieved without significantly dampening the cytokine immune response and without directly affecting the inflammatory cells, both likely important mediators in clearing an infection. The vascular stabilizing effect of Slit *in vivo* was lost in Robo4$^{AP/AP}$ mice or in the presence of a VE-cadherin blocking antibody, further demonstrating the vascular specific effect of Slit. Therefore, blunting the vascular response of the host to hypercytokinemia may provide a broad platform for treating multiple infectious threats characterized by an exuberant cytokine response.

Current medical therapies target individual pathogens using vaccines and anti-microbial agents. These approaches have proven very effective. However, vaccines for example take time to generate after isolating the pandemic agent and infectious agents are prone to developing resistance to current anti-microbial drugs[2,3]. Thus the need for generating a broad approach is real. One would imagine that instead of replacing current medical therapies, that the approach defined in this dissertation would be used in combination. Perhaps the combination of these two approaches would result in

synergistic therapeutic efficacy, a hypothesis that still needs to be validated in animal models.

In moving forward, it is important to note that additional endogenous vascular stabilizing systems have been defined including Angiopoietin/Tie2, Delta-like 4/Notch, and Sphingosine 1-phosphate/Sphingosine 1-phosphate receptor[4,5]. The conclusions defined in this dissertation suggest that in addition to Robo4-dependent Slit signaling, these other systems warrant further investigation as therapeutics for pandemic infection characterized by hypercytokinemia. Indeed, efficacy of Angiopoietin has already been demonstrated in endotoxic shock[6]. In utilizing these various pathways, one may predict varying degrees of potency and efficacy, thus it will be important to determine which is most efficacious in developing a target for future clinical application. This investigation should entail infectious settings such as hemorrhagic fever, cerebral malaria, and severe acute respiratory syndrome (SARS). It would be interesting to see if these other stabilizing cues utilize similar signaling mechanisms as Robo4.

Although hypercytokinemia can be a significant source of pathologic damage, the exact number of patients that are hospitalized or die from the indirect effects of cytokine storm is unknown. This is an interesting point on which to speculate. For example, sepsis, acute lung injury/acute respiratory distress syndrome, and multiple organ dysfunction syndrome are characterized by cytokine storm and are significant sources of morbidity and mortality[7]. The exaggerated cytokine response destabilizes the vasculature resulting in increased vascular permeability, organ failure, and ultimately death. Perhaps through blunting the host vascular response to cytokines a significant advance in combating these diseases may be made.

The second contribution is to our understanding of signaling events downstream of Robo4 activation. We found that administration of Slit to endothelial cells *in vitro* significantly increased VE-cadherin and p120-catenin cell surface localization as measured by immunofluoresence and membrane fractionation[1]. Slit enhanced a p120-catenin/VE-cadherin interaction, an interaction important in preventing internalization of VE-cadherin and its removal from the cell surface. This interaction was maintained in the presence of interleukin-1β (IL-1β) and Slit administration did indeed inhibit IL-1β-induced internalization of VE-cadherin. Since one of the ultimate endpoints of cytokine-induced permeability is the dissolution of VE-cadherin cell-cell interactions, Robo4 activation provides a broad vascular stabilizing signal against multiple permeability inciting agents.

Previous experiments performed in our lab by Chris Jones or in collaboration with Naoyuki Nishiya defined the immediate proximal signaling events that result from Robo4 activation[8]. First, paxillin is recruited to a small fragment of the Robo4 cytoplasmic domain known as the paxillin interaction motif. Paxillin binds via the Lim4 domain and recruits GIT1, an Arf GTPase activating protein (Arf-GAP). GIT1 recruitment accelerates the conversion of Arf6-GTP to Arf6-GDP resulting in the inactivation of Arf6. While Arf6 is known to regulate epithelial cadherin (E-cadherin) cell surface localization, a role in VE-cadherin cell surface localization has yet to be fully defined. Additional experiments conducted by Weiquan Zhu in our lab have cemented this relationship. Knockdown of Arf6 expression by siRNA in endothelial cells results in increased cell surface localization of VE-cadherin. Conversely, siRNA knockdown of GIT1 results in decreased cell surface localization of VE-cadherin and increased

permeability. Interestingly, these findings demonstrate that there is basal, tonic control of VE-cadherin localization in the cell and that this is controlled by GIT1 and Arf6. Taken together, these data define a critical link between proximal signaling events of Robo4 activation such as paxillin and GIT1 recruitment all the way to VE-cadherin cell surface presentation.

In moving towards applying what we have learned into a clinical application, it is important to note that protein therapeutics are difficult and expensive to both produce and administer. A small molecule inhibitor approach may be simpler and more effective. Having fully characterized the signaling cascade downstream of Robo4 activation we have identified Arf6 as a candidate target. Previous work has defined a small molecule inhibitor of Arf guanine nucleotide exchange factors (Arf-GEFs) known as secinH3[9]. Inhibition of Arf-GEFs results in the inactivation of Arf6, similar to Robo4-dependent Slit signaling. To validate such an approach one needs to corroborate a previously demonstrated effect of Slit *in vivo*. We previously demonstrated that Robo4-dependent Slit signaling limits retinal and choroidal vascular disease in mouse models of proliferative retinopathy and wet macular degeneration[10]. In this dissertation, we have found that secinH3 is also effective at reducing neovascularization in these models, thus phenocopying the effect of Robo4-dependent Slit signaling[8]. Therefore, using a small molecule inhibitor approach targeting Arf6 activation may prove effective in clinical settings of retinal and choroidal vascular disease and infectious disease characterized by hypercytokinemia.

REFERENCES

1. London, N.R., *et al.* Targeting Robo4-dependent slit signaling to survive the cytokine storm in sepsis and influenza. *Sci Transl Med* **2**, 23ra19 (2010).

2. De Jong, J.C., Rimmelzwaan, G.F., Fouchier, R.A. & Osterhaus, A.D. Influenza virus: a master of metamorphosis. *J Infect* **40**, 218-228 (2000).

3. Morse, S.S., Garwin, R.L. & Olsiewski, P.J. Public health. Next flu pandemic: what to do until the vaccine arrives? *Science* **314**, 929 (2006).

4. London, N.R., Whitehead, K.J. & Li, D.Y. Endogenous endothelial cell signaling systems maintain vascular stability. *Angiogenesis* (2009).

5. Mochizuki, N. Vascular integrity mediated by vascular endothelial cadherin and regulated by sphingosine 1-phosphate and angiopoietin-1. *Circ J* **73**, 2183-2191 (2009).

6. Witzenbichler, B., Westermann, D., Knueppel, S., Schultheiss, H.P. & Tschope, C. Protective role of angiopoietin-1 in endotoxic shock. *Circulation* **111**, 97-105 (2005).

7. Wang, H. & Ma, S. The cytokine storm and factors determining the sequence and severity of organ dysfunction in multiple organ dysfunction syndrome. *Am J Emerg Med* **26**, 711-715 (2008).

8. Jones, C.A., *et al.* Slit2-Robo4 signalling promotes vascular stability by blocking Arf6 activity. *Nat Cell Biol* **11**, 1325-1331 (2009).

9. Hafner, M., *et al.* Inhibition of cytohesins by SecinH3 leads to hepatic insulin resistance. *Nature* **444**, 941-944 (2006).

10. Jones, C.A., *et al.* Robo4 stabilizes the vascular network by inhibiting pathologic angiogenesis and endothelial hyperpermeability. *Nat Med* **14**, 448-453 (2008).